The Pennsylvania State University

The Graduate School

DEVELOPMENT OF VERSATILE MIXED FINITE ELEMENT METHODS FOR THE NON-ISOTHERMAL INCOMPRESSIBLE AND COMPRESSIBLE NAVIER-STOKES EQUATIONS

A Dissertation in

Mechanical Engineering

by

Edward Miller

©2024 Edward Miller

Submitted in Partial Fulfillment

of the Requirements

for the Degree of

Doctor of Philosophy

May 2024

The dissertation of Edward Miller was reviewed and approved by the following:

David Williams

Assistant Professor of Mechanical Engineering Dissertation Advisor

Chair of Committee

Robert Kunz

Professor of Mechanical Engineering Professor in Charge

Xiang Yang

Assistant Professor of Mechanical Engineering

Stephen Lynch

Associate Professor of Mechanical Engineering

James Coder

Associate Professor of Aerospace Engineering

Abstract

The ever increasing demand for accurate numerical methods has led to the development of more and more sophisticated methods for simulating fluid flow. These methods are often designed to handle a specific flow regime or be valid under specific circumstances. What is needed in the field is a method that is accurate and robust over a wide range of conditions. Here, we propose a finite element method designed to work over a broad range of flow regimes and remain consistent and accurate in each regime. This is accomplished utilizing a mixed finite element method whose properties are rigorously analyzed to demonstrate the method's effectiveness at handling these different flow regimes. We first use standard mathematical techniques to prove that the method is stable and obtains optimal error estimates for the non-isothermal incompressible Navier-Stokes equations. We then demonstrate on a series of test cases that the method accurately captures the physics of the non-isothermal incompressible Navier-Stokes equations. Next, we extend our method to the compressible Navier-Stokes equations where again the order of accuracy is demonstrated, this time using a series of numerical experiments. Finally, we present a series of compressible flow test cases to prove that the method can capture the physics of this regime.

Table of Contents

List of Tables

List of Figures

List of Appendices

1 Introduction

The accurate simulation of fluid flows is a critical area of engineering. Often times, before designs of parts are finalized they are run through a gauntlet of CFD (computational fluid dynamics) to gauge performance. It is then critical that the methods used in these simulations are as accurate and robust as possible. Finite element methods (FEM) represent a class of methods that are capable of this accuracy and robustness if one selects a FEM appropriate to their problem. This highlights a pitfall for widespread adoption of these methods since one requires a high degree of knowledge beforehand to select a FEM appropriate for their problem. For some methods, like discontinuous Galerkin (DG) methods, this might come in the form of knowing you may need a post-processing procedure to ensure that mass is being conserved. For other methods, such as a continuous Galerkin (CG) method, one may not realize that issues can arise for convection-dominated flows. This class of flows is common at high Mach (Ma) numbers. What is lacking is a method that is well-suited for a variety of flow regimes that can be applied without extensive background knowledge on these different methods or, in other words, a method that is versatile enough to handle a range of flows without special consideration on the part of the user.

The goal of this thesis is the development and analysis of such a class of methods. What we propose is a method well-suited for both incompressible and compressible flows. To this end, we rigorously analyze the behavior and properties of the method for incompressible non-isothermal flows. This flow regime is modeled via the Oberbeck-Boussinesq approximation which adds an additional term to the incompressible Navier-Stokes equations. This new term couples the temperature and momentum equations together. This means that the two equations cannot be solved independently using an equation-splitting approach, as is often the case for methods designed exclusively for the incompressible *isothermal* Navier-Stokes equations. In addition, this means that any analysis done on the non-isothermal incompressible equations has a much more natural extension to the compressible Navier-Stokes equations. Our approach of analyzing the method's characteristics on a more complicated equation, and thereafter extending this method to compressible flows runs contrary to other efforts in the field. In fact, the standard practice is to analyze the method of interest on simple advection-diffusion style equations and extrapolate to compressible flow. We believe that the procedure that we propose is much more rigorous than previous efforts, as well as it highlights the usefulness of our method for non-isothermal flows.

The document is formatted as follows. In chapter 2, our analysis of the versatile finite element methods for non-isothermal flows is presented. It begins with an introduction on the non-isothermal flow problem and the previous work that has been done to simulate this type of flow. Then the formulation of the methods and notation is introduced. The methods are then analyzed to demonstrate their stability and provide error estimates. Thereafter, numerical experiments are performed to demonstrate the methods' ability to capture the physics of non-isothermal, incompressible flows. In chapter 3, the versatile mixed methods are extended to *compressible* flows. We use numerical experiments to demonstrate the excellent performance of the methods on weakly- and fully-compressible flows. We note that a detailed study of the methods, and their ability to handle supersonic, and high-Reynolds number flows remains an open area of research.

2 Versatile Mixed Methods for Non-Isothermal Incompressible Flows

2.1. Motivation

The motion of a non-isothermal incompressible fluid is frequently induced by buoyancy forces, viscous forces, and pressure fields. In accordance with standard practices, we refer to the motion that is induced solely by buoyancy forces as *natural* or *free* convection, the motion that is induced solely by viscous forces and pressure fields as *forced* convection, and the motion that is induced by all three factors as *mixed* convection. In order to characterize the various types of convection, one may solve the incompressible Navier-Stokes equations for mass and momentum conservation, in conjunction with a temperature equation (usually obtained from the internal energy or enthalpy equations). In addition, one may couple the momentum and temperature equations via the approach of Oberbeck [4] and Boussinesq [5] by adding a temperature-dependent buoyancy term to the right hand side (RHS) of the momentum equation. The buoyancy term is assumed to be directly proportional to changes in the temperature field, and these changes are assumed to be small enough such that the density remains constant. This approximation is frequently referred to as the Boussinesq model [6], or (less commonly) the Oberbeck-Boussinesq model [7]. For practical applications, it is usually necessary to solve the Boussinesq model in the vicinity of complicated geometries, using unstructured meshes. As a result, our preference is to use finite element methods for solving the model because of their ability to operate on both structured and unstructured meshes, while simultaneously achieving high-order accuracy, stability, and robustness.

In what follows, we briefly review some previous efforts to apply finite element methods to the Boussinesq model. Some of the earliest work in this area was performed by Laskaris [8] who used a high-order continuous Galerkin (CG) method to simulate channel flows with heated walls. In addition, Young et al. [9] and Tabarrok and Lin [10] used a similar approach to study natural convection in heated cavities. Next, Gartling [11] used a CG method to simulate a thin-walled tube with wall heat transfer, a rectangular heat exchanger, and a heated hexagonal cylinder in a cooled cavity. Thereafter, Marshall et al. [12] used a high-order CG method with a penalty function (for enforcement of the dilatational constraint) to simulate a heated cavity. This was the first time that a finite element method was successfully applied to natural convection problems for a wide range of Rayleigh numbers ($10^4 - 10^7$). Based on this work, Reddy and Satake [13] formulated an alternative CG method, and used it to simulate heated, non-convex, straight-sided cavities.

It is important to note that all of the early work described above was limited to two-dimensional geometries. Fortunately, with the advent of more powerful computers and more advanced stabilization strategies, such as the Galerkin Least Squares (GLS) approach [14–16], the solutions to three-dimensional problems became possible. Some of the early work in this area was performed by Tang and Tsang [17, 18], who used least-square finite element methods to simulate three-dimensional heated cavities, and accurately reproduce the dynamics of Rayleigh-Bénard convection cells. A detailed review of the latest efforts to apply finite element methods to natural and mixed convection problems is beyond the scope of the present work. However, the interested reader may consult [1, 19] for an extensive collection of references on this topic.

Despite the many applications of finite element methods to the Boussinesq model, there have been a relatively small number of efforts to rigorously analyze the existing methods, or to develop new mixed methods which maintain inf-sup stability. Some pioneering efforts in this area were undertaken by Boland and Layton [20, 21], as they derived stability and error estimates for CG methods for steady and unsteady natural convection problems. In addition, they analyzed low-order, non-conforming discontinuous Galerkin (DG) methods. Most notably, they were among the first researchers to recognize the importance of using a skew-symmetrizing procedure to stabilize the convective operator in the temperature equation. Subsequently, their work was expanded by Dorok et al. [22] and Bernardi et al. [23], who developed stability and error estimates for mixed methods. More recently, Codina et al. [24] and Löwe and Lube [25] developed variational multiscale (VMS) methods for problems with turbulent mixed convection. Within the VMS framework, they constructed rigorous stability estimates and (in the case of [25]) error estimates for the resulting schemes. In addition, DG methods and mixed methods were rigorously analyzed for the steady, isothermal case by Cockburn et al. [26, 27], and subsequently extended to the steady, non-isothermal case by Oyarzúa et al. [28]. Thereafter, Dallmann and Arndt [1, 7] developed a mixed method which was stabilized using a combination of local projection stabilization [29, 30], streamline-upwind stabilization [31–33], and grad-div stabilization [34]. For this method, they rigorously derived stability and error estimates, and produced accurate numerical results for a wide range of steady and unsteady convection problems. Next, Rebollo et al. [35] developed a mixed method which they stabilized using an interpolation-based operator that acts as a low-pass filter. We note that, although the performance of this method is quite adequate from an accuracy standpoint, it is only weakly consistent. Most recently, de Frutos et al. [36] derived an optimal set of stability and error estimates for grad-div stabilized, inf-sup stable mixed methods. These methods are effectively a subset of the methods constructed by Dallmann and Arndt in [1, 7]. Lastly, we note that there are ongoing efforts to analyze mixed methods for Boussinesq models with nonconstant, temperature-dependent parameters (cf. [37–40] for several examples).

Due to the limited number of efforts to develop mixed methods (see above), there are still opportunities to improve their robustness, accuracy, and flexibility. With this in mind, the goal of the present chapter is to extend the recently developed versatile mixed methods (see [41]) to solve the Boussinesq model with constant parameters. For the sake of completeness, let us briefly describe the underlying philosophy of versatile mixed methods: i) we begin with the compressible formulation of the governing equations and then enforce the assumption of constant density, ii) we maintain the presence of dilatational terms that would usually be neglected, and iii) we discretize the resulting formulation using standard, inf-sup stable, mixed methods. This approach has several advantages, as most importantly, it can be almost immediately applied to weakly-compressible flows, and furthermore, it ensures that the dilatational constraint is enforced in a consistent fashion in each of the governing equations. In [41], this philosophy was applied to the isothermal incompressible Navier-Stokes equations. There, we used the full compressible stress tensor (with the dilatational component) in the momentum conservation equation, and we rigorously proved the stability of the discrete velocity field. The resulting methods were successfully applied to isothermal Taylor-Green and Gresho vortex problems. In the present work, we apply the same methods to non-isothermal incompressible flows.

The format of this chapter is as follows. In section 2.2, we formally introduce the Boussinesq model equations for non-isothermal incompressible flows and we develop the notation and mathematical machinery for discretizing these equations. In sections 2.3 and 2.4, we introduce the versatile mixed methods, and construct stability and error estimates. In section 2.5, we introduce an expanded formulation of the versatile mixed methods which contains an additional viscous dissipation term. In section 2.6, we apply the original methods and the expanded formulation to a set of standard benchmark problems, and compare the results of both approaches. Finally, in section 2.7, we conclude with a summary of our work and a few final remarks.

2.2. Preliminaries

Let us start by introducing a domain $\Omega_t = (t_0, t_n) \times \Omega$, where $\Omega \in \mathbb{R}^d$ is a spatial domain and $(t_0, t_n) \in \mathbb{R}$ is a temporal domain. In a natural fashion, we denote the spatial and temporal coordinates by $\boldsymbol{x}$ and t, and we denote the spatial and temporal derivatives by $\nabla(\cdot)$ and $\partial_t(\cdot)$, respectively. We assume $d = 2$ or 3, and that the domain boundary $\partial\Omega$ is composed from straight line segments (for the case of $d = 2$) and planar faces (for the case of $d = 3$). Inside the domain Ω_t, we are interested in simulating the motion of a homogeneous, non-isothermal, incompressible fluid with a constant density ρ_0, and non-constant velocity, temperature, and pressure fields $\boldsymbol{u} = \boldsymbol{u}(t, \boldsymbol{x})$, $T = T(t, \boldsymbol{x})$, and $P = P(t, \boldsymbol{x})$. Since the density is constant, we find it convenient to divide the governing equations by ρ_0, and then introduce density-weighted quantities, such as the kinematic pressure, $p = P/\rho_0$. Now, having established the necessary background, we present the Boussinesq model for non-isothermal flows

$$\nabla \cdot \boldsymbol{u} = 0, \qquad \text{in } \Omega_t \tag{2.2.1}$$

$$\partial_t \boldsymbol{u} + \nabla \cdot (\boldsymbol{u} \otimes \boldsymbol{u} + p\,\mathbb{I}) - \nabla \cdot \boldsymbol{\tau} = -\beta T \boldsymbol{g} + \boldsymbol{f}_u, \qquad \text{in } \Omega_t \tag{2.2.2}$$

$$\partial_t T + \nabla \cdot (T\boldsymbol{u}) - \nabla \cdot (\alpha\gamma\nabla T) = -(\gamma - 1)\, T\, (\nabla \cdot \boldsymbol{u}) + f_T, \qquad \text{in } \Omega_t \tag{2.2.3}$$

These equations are subject to the following boundary and initial conditions

$$\boldsymbol{u} = 0, \quad T = 0, \qquad \text{on } \partial\Omega_t, \tag{2.2.4}$$

$$\boldsymbol{u}(t_0, \boldsymbol{x}) = \boldsymbol{u}_0(\boldsymbol{x}), \quad T(t_0, \boldsymbol{x}) = T_0(\boldsymbol{x}), \qquad \text{in } \Omega. \tag{2.2.5}$$

Furthermore, in order to close the equations, we define $\boldsymbol{\tau}$ as the stress tensor

$$\boldsymbol{\tau} = \nu \left(\nabla \boldsymbol{u} + \nabla \boldsymbol{u}^T - \frac{2}{3} \left(\nabla \cdot \boldsymbol{u} \right) \mathbb{I} \right), \tag{2.2.6}$$

$\boldsymbol{g}$ as the gravitational acceleration (where $g_i = -g\delta_{id}$ with $g = const$), $\boldsymbol{f}_u$ as a source term for the linear momentum, f_T as a source term for the temperature, $\gamma = C_p/C_v$ as the ratio of specific heats, C_v as the specific heat at constant volume, C_p as the specific heat at constant pressure, $\alpha = \kappa / \left(C_p \, \rho_0 \right)$ as the thermal diffusivity coefficient, β as the thermal expansion coefficient, κ as the thermal conductivity coefficient, $\nu = \mu/\rho_0$ as the kinematic viscosity coefficient, and μ as the dynamic viscosity coefficient.

Before proceeding further, it is important to note that our equations for the temperature and the stress tensor (Eqs. (2.2.3) and (2.2.6)) are unconventional. In particular, it is common practice to neglect the temperature-scaled divergence term on the RHS of Eq. (2.2.3), such that

$$\partial_t T + \nabla \cdot (T\boldsymbol{u}) - \nabla \cdot (\alpha \gamma \nabla T) = f_T. \tag{2.2.7}$$

In addition, most researchers neglect the divergence and gradient transpose terms on the RHS of Eq. (2.2.6), as follows

$$\boldsymbol{\tau} = \nu \nabla \boldsymbol{u}. \tag{2.2.8}$$

However, we prefer to use Eqs. (2.2.3) and (2.2.6) due to their superior physical accuracy, flexibility, and discrete consistency. We refer the interested reader to [41] for a detailed discussion of our motivation for using the full stress tensor (Eq. (2.2.6)). In what follows, we will only discuss our motivation for using the augmented temperature equation (Eq. (2.2.3)).

1. The formulation in Eq. (2.2.3) follows immediately from a careful asymptotic analysis of the compressible Navier-Stokes equations. In particular, one can show that Eq. (2.2.3) can be derived from the compressible equation for internal energy if one assumes that the Mach number approaches zero, and the density approaches a constant value. Please see the analysis in section A of the Appendix for more details.

2. In accordance with point 1, the formulation in Eq. (2.2.3) is more suitable for adaptation to *compressible* flows, as it retains the temperature-scaled divergence term which becomes increasingly important in these types of flows. Retaining this term helps facilitate flexibility of the resulting methods, and encourages code-reuse between incompressible and compressible CFD codes.

3. The formulation in Eq. (2.2.3) is more 'consistent', as it enables consistent enforcement of the dilatational constraint. Evidently, the temperature-scaled

divergence term contains the divergence of the velocity field, which is guaranteed to vanish at the continuous level (by Eq. (2.2.1)), but may or may not vanish at the discrete level. Of course, for pointwise divergence-free methods, this term vanishes in both cases, but for more general methods, the dilatation term typically only vanishes in the weak sense, and the temperature-scaled divergence term is non-zero. Therefore, neglecting the temperature-scaled divergence term *a priori* is inconsistent, as this effectively forces the dilatation contribution to vanish pointwise in the temperature equation, even though it may only vanish weakly in the mass conservation equation. Naturally, we prefer to use Eq. (2.2.3), as it avoids this inconsistency.

In summary, we have introduced a 'versatile' approach in which we solve Eqs. (2.2.1)–(2.2.3) in conjunction with the stress tensor in Eq. (2.2.6). In what follows, we will introduce the analytical machinery for discretizing these equations.

In accordance with standard practices, we tessellate the spatial domain Ω with a mesh $\mathcal{T}_h$. The mesh is composed from straight-sided, d-dimensional simplicial elements K, with characteristic size h. The faces of elements on the perimeter of the mesh are required to exactly conform to the domain boundaries, and the union of all the elements is required to cover the domain. In addition, for the sake of simplicity the elements are required to be non-overlapping, and the mesh is required to be devoid of hanging nodes. The boundary of each element K is denoted by ∂K and the outward-pointing unit normal vector on this boundary is denoted by $\boldsymbol{n}$. Elements are considered to be 'face neighbors' if they share a $(d-1)$-dimensional face F. We denote the unit normal vector that points from the positive side to the negative side of the shared face as $\boldsymbol{n}_+$, and naturally $\boldsymbol{n}_- = -\boldsymbol{n}_+$. The total collection of faces in the mesh is denoted by $\mathcal{F}_h$, and the faces of a single element K are denoted by $\mathcal{F}_K = \{F \in \mathcal{F}_h : F \subset \partial K\}$. The set of interior faces is denoted by $\mathcal{F}_h^i = \{F \in \mathcal{F}_h : F \cap \partial\Omega = \emptyset\}$ and the set of boundary faces by $\mathcal{F}_h^\partial = \{F \in \mathcal{F}_h : F \cap \partial\Omega \neq \emptyset\}$. Finally, for a given face F, we can define a normal vector $\boldsymbol{n}_F = \boldsymbol{n}_+$ which points from the positive to the negative side of the face.

Next, one may define jump $[\![\cdot]\!]$ and average $\{\{\cdot\}\}$ operators for an interior face $F \in \mathcal{F}_h^i$ as follows

$$[\![\phi]\!] = \phi_+ - \phi_-, \qquad [\![\phi \boldsymbol{n}]\!] = \phi_+ \boldsymbol{n}_+ + \phi_- \boldsymbol{n}_-, \qquad \{\{\phi\}\} = \frac{1}{2}\left(\phi_+ + \phi_-\right),$$

$$[\![\boldsymbol{v}]\!] = \boldsymbol{v}_+ - \boldsymbol{v}_-, \qquad [\![\boldsymbol{v} \otimes \boldsymbol{n}]\!] = \boldsymbol{v}_+ \otimes \boldsymbol{n}_+ + \boldsymbol{v}_- \otimes \boldsymbol{n}_-, \qquad \{\{\boldsymbol{v}\}\} = \frac{1}{2}\left(\boldsymbol{v}_+ + \boldsymbol{v}_-\right),$$

where ϕ is a generic scalar function, and $\boldsymbol{v}$ is a generic vector function. Similarly, for all boundary faces $F \in \mathcal{F}_h^\partial$, one may define

$$[\![\phi]\!] = \phi, \qquad [\![\phi \boldsymbol{n}]\!] = \phi \boldsymbol{n}, \qquad \{\{\phi\}\} = \phi,$$

$$[\![\boldsymbol{v}]\!] = \boldsymbol{v}, \qquad [\![\boldsymbol{v} \otimes \boldsymbol{n}]\!] = \boldsymbol{v} \otimes \boldsymbol{n}, \qquad \{\{\boldsymbol{v}\}\} = \boldsymbol{v}.$$

In addition, it is convenient to introduce some standard notation for representing inner products. With this in mind, let us introduce a generic vector $\boldsymbol{w}$ and generic tensors $\boldsymbol{T}$ and $\boldsymbol{U}$. Note: here, we assume that $\boldsymbol{v}$, $\boldsymbol{w}$, $\boldsymbol{T}$, $\boldsymbol{U}$, and ϕ are sufficiently smooth, such that the associated integrations are possible. Based on this assumption, we can define

$$\begin{aligned}
(\boldsymbol{v}, \boldsymbol{w})_{\mathcal{T}_h} &:= \sum_{K \in \mathcal{T}_h} \int_K \boldsymbol{v} \cdot \boldsymbol{w} \, dV, & (\boldsymbol{T}, \boldsymbol{U})_{\mathcal{T}_h} &:= \sum_{K \in \mathcal{T}_h} \int_K \boldsymbol{T} : \boldsymbol{U} \, dV, \\
\langle \boldsymbol{v}, \boldsymbol{w} \rangle_{\partial \mathcal{T}_h} &:= \sum_{K \in \mathcal{T}_h} \int_{\partial K} \boldsymbol{v} \cdot \boldsymbol{w} \, dA, & \langle \boldsymbol{T}, \boldsymbol{U} \rangle_{\partial \mathcal{T}_h} &:= \sum_{K \in \mathcal{T}_h} \int_{\partial K} \boldsymbol{T} : \boldsymbol{U} \, dA, \\
\langle \boldsymbol{v}, \boldsymbol{w} \rangle_{\mathcal{F}_h} &:= \sum_{F \in \mathcal{F}_h} \int_F \boldsymbol{v} \cdot \boldsymbol{w} \, dA, & \langle \boldsymbol{T}, \boldsymbol{U} \rangle_{\mathcal{F}_h} &:= \sum_{F \in \mathcal{F}_h} \int_F \boldsymbol{T} : \boldsymbol{U} \, dA.
\end{aligned}$$

Using this notation, we can introduce the well-known integration by parts formulas

$$\begin{aligned}
\langle \phi \boldsymbol{v}, \boldsymbol{n} \rangle_{\partial K} &= (\phi, \nabla \cdot \boldsymbol{v})_K + (\boldsymbol{v}, \nabla \phi)_K \,, \\
\langle \boldsymbol{v}, \boldsymbol{T} \boldsymbol{n} \rangle_{\partial K} &= (\boldsymbol{v}, \nabla \cdot \boldsymbol{T})_K + (\boldsymbol{T}, \nabla \boldsymbol{v})_K \,.
\end{aligned}$$

In what follows, we will conclude this section by defining the standard function spaces for mixed finite element methods. We start by introducing the broken Sobolev space

$$\boldsymbol{W}^{m,p}(\mathcal{T}_h) := \left\{ \boldsymbol{w} \in \boldsymbol{L}^p(\Omega), \boldsymbol{w}|_K \in \boldsymbol{W}^{m,p}(K), \ \forall K \in \mathcal{T}_h \right\},$$

where $\boldsymbol{W}^{m,p}\left(\mathcal{T}_h\right) := \left(W^{m,p}\left(\mathcal{T}_h\right)\right)^d$. Next, we introduce the Hilbert spaces

$$\begin{aligned}
&\boldsymbol{H}_0(\mathrm{div};\Omega) := \left\{ \boldsymbol{w} : \boldsymbol{w} \in \boldsymbol{L}^2(\Omega), \ \nabla \cdot \boldsymbol{w} \in L^2(\Omega), \ \boldsymbol{w} \cdot \boldsymbol{n}|_{\partial\Omega} = 0 \right\}, \\
&\boldsymbol{H}_0^1(\Omega) := \left\{ \boldsymbol{w} : \boldsymbol{w} \in \boldsymbol{H}^1(\Omega), \ \boldsymbol{w}|_{\partial\Omega} = 0 \right\},
\end{aligned}$$

where $\boldsymbol{H}^1(\Omega) := \left(H^1(\Omega)\right)^d$. Having established these spaces, we can define scalar-valued polynomial spaces Q_h^{DC} and Q_h^C for the kinematic pressure, and R_h^C for the temperature

$$Q_h^{DC} := \left\{q_h : q_h \in L_*^2(\Omega), q_h|_K \in \mathcal{P}_k(K), \forall K \in \mathcal{T}_h\right\},$$

$$Q_h^{C} := \left\{q_h : q_h \in C^0(\Omega), q_h|_K \in \mathcal{P}_k(K), \forall K \in \mathcal{T}_h\right\} \cap L_*^2(\Omega),$$

$$R_h^{C} := \left\{r_h : r_h \in C^0(\Omega), r_h|_K \in \mathcal{P}_{k+1}(K), \forall K \in \mathcal{T}_h\right\} \cap H_0^1(\Omega),$$

where $\mathcal{P}_k(K)$ is the space of polynomials of degree $\leq k$, and $L_*^2(\Omega)$ is the space of L^2 functions with zero mean. Furthermore, we can define the vector-valued Raviart-Thomas and Taylor-Hood spaces for the velocity

$$\boldsymbol{W}_h^{RT} := \left\{\boldsymbol{w}_h : \boldsymbol{w}_h \in \boldsymbol{H}_0(\mathrm{div};\Omega), \boldsymbol{w}_h|_K \in \boldsymbol{RT}_k(K), \forall K \in \mathcal{T}_h\right\},$$

$$\boldsymbol{W}_h^{TH} := \left\{\boldsymbol{w}_h : \boldsymbol{w}_h \in \boldsymbol{C}^0(\Omega), \boldsymbol{w}_h|_K \in \left(\mathcal{P}_{k+1}(K)\right)^d, \forall K \in \mathcal{T}_h\right\} \cap \boldsymbol{H}_0^1(\Omega),$$

where $\boldsymbol{C}^0(\Omega) := \left(C^0(\Omega)\right)^d$, and

$$\boldsymbol{RT}_k(K) := \left(\mathcal{P}_k(K)\right)^d \oplus \mathcal{P}_k(K)\,\boldsymbol{x}.$$

Lastly, we can introduce $\boldsymbol{W}_h^{BDM}$, the Brezzi-Douglas-Marini space (see [42] for an explicit definition of this space).

2.3. Versatile Mixed Methods for the Incompressible Non-Isothermal Navier-Stokes Equations

In this section, we develop a general class of mixed methods for solving Eqs. (2.2.1) – (2.2.3). The methods can be constructed using the following steps: i) choose function spaces $\boldsymbol{W}_h \subset \boldsymbol{H}_0(\mathrm{div};\Omega)$, $R_h \subset H_0^1(\Omega)$, and $Q_h \subset L_*^2(\Omega)$, ii) identify test functions $(\boldsymbol{w}_h, r_h, q_h)$ that span $\boldsymbol{W}_h \times R_h \times Q_h$, and iii) find unknowns $(\boldsymbol{u}_h, T_h, p_h)$ in $\boldsymbol{W}_h \times R_h \times Q_h$ that satisfy

$$(\nabla \cdot \boldsymbol{u}_h, q_h)_{\mathcal{T}_h} = 0, \tag{2.3.1}$$

$$\begin{aligned}
&(\partial_t \boldsymbol{u}_h, \boldsymbol{w}_h)_{\mathcal{T}_h} - (\boldsymbol{u}_h \otimes \boldsymbol{u}_h, \nabla_h \boldsymbol{w}_h)_{\mathcal{T}_h} - (p_h, \nabla \cdot \boldsymbol{w}_h)_{\mathcal{T}_h} + \langle \widehat{\boldsymbol{\sigma}}_{\mathrm{inv}}\, \boldsymbol{n}, \boldsymbol{w}_h \rangle_{\partial\mathcal{T}_h} \\
&+ \nu \Bigg[\left(\nabla_h \boldsymbol{u}_h + \nabla_h \boldsymbol{u}_h^T - \frac{2}{3} (\nabla \cdot \boldsymbol{u}_h)\, \mathbb{I}, \nabla_h \boldsymbol{w}_h \right)_{\mathcal{T}_h} - \langle \widehat{\boldsymbol{\sigma}}_{\mathrm{vis}}\, \boldsymbol{n}, \boldsymbol{w}_h \rangle_{\partial\mathcal{T}_h} \\
&+ \left\langle \widehat{\boldsymbol{\varphi}}_{\mathrm{vis}} - \boldsymbol{u}_h, \left(\nabla_h \boldsymbol{w}_h + \nabla_h \boldsymbol{w}_h^T - \frac{2}{3} (\nabla \cdot \boldsymbol{w}_h)\, \mathbb{I} \right) \boldsymbol{n} \right\rangle_{\partial\mathcal{T}_h} \Bigg] - \frac{1}{2} \left((\nabla \cdot \boldsymbol{u}_h)\, \boldsymbol{u}_h, \boldsymbol{w}_h \right)_{\mathcal{T}_h} \\
&= - (\beta T_h \boldsymbol{g}, \boldsymbol{w}_h)_{\mathcal{T}_h} + (\boldsymbol{f}_u, \boldsymbol{w}_h)_{\mathcal{T}_h}\,,
\end{aligned} \tag{2.3.2}$$

$$
\begin{aligned}
&(\partial_t T_h, r_h)_{\mathcal{T}_h} - (T_h \boldsymbol{u}_h, \nabla_h r_h)_{\mathcal{T}_h} + \left\langle \widehat{\boldsymbol{\phi}}_{\text{inv}} \cdot \boldsymbol{n}, r_h \right\rangle_{\partial\mathcal{T}_h} \\
&+ \alpha\gamma \Bigg[(\nabla_h T_h, \nabla_h r_h)_{\mathcal{T}_h} - \left\langle \widehat{\boldsymbol{\phi}}_{\text{vis}} \cdot \boldsymbol{n}, r_h \right\rangle_{\partial\mathcal{T}_h} \\
&+ \left\langle \widehat{\lambda}_{\text{vis}} - T_h, \nabla_h r_h \cdot \boldsymbol{n} \right\rangle_{\partial\mathcal{T}_h} \Bigg] - \frac{1}{2} \left((\nabla \cdot \boldsymbol{u}_h)\, T_h, r_h \right)_{\mathcal{T}_h} \\
&= -(\gamma - 1) \Big[\left((\nabla \cdot \boldsymbol{u}_h)\, T_h, r_h \right)_{\mathcal{T}_h} + C_{\text{mod}} \left(|\nabla \cdot \boldsymbol{u}_h|\, \nabla_h T_h, \nabla_h r_h \right)_{\mathcal{T}_h} \Big] + (f_T, r_h)_{\mathcal{T}_h} .
\end{aligned}
\tag{2.3.3}
$$

Here, we observe that $C_{\text{mod}} \geq 0$ is a stabilizing coefficient, and the quantities with hats (for example $\widehat{\boldsymbol{\sigma}}_{\text{inv}}$) denote numerical fluxes. Some possible formulas for the fluxes are given below

$$
\begin{aligned}
\widehat{\boldsymbol{\sigma}}_{\text{inv}} &:= \{\{\boldsymbol{u}_h\}\} \otimes \{\{\boldsymbol{u}_h\}\} + \{\{p_h\}\}\, \mathbb{I} + \zeta\, |\boldsymbol{u}_h \cdot \boldsymbol{n}_F|\, [\![\boldsymbol{u}_h \otimes \boldsymbol{n}]\!] , \\
\widehat{\boldsymbol{\sigma}}_{\text{vis}} &:= \left\{\!\!\left\{ \nabla_h \boldsymbol{u}_h + \nabla_h \boldsymbol{u}_h^T - \frac{2}{3} (\nabla \cdot \boldsymbol{u}_h)\, \mathbb{I} \right\}\!\!\right\} - \frac{\eta}{h_F}\, [\![\boldsymbol{u}_h \otimes \boldsymbol{n}]\!] , \\
\widehat{\boldsymbol{\phi}}_{\text{inv}} &:= \{\{T_h\}\}\, \boldsymbol{u}_h + \delta\, |\boldsymbol{u}_h \cdot \boldsymbol{n}_F|\, [\![T_h\, \boldsymbol{n}]\!] , \\
\widehat{\boldsymbol{\phi}}_{\text{vis}} &:= \{\{\nabla_h T_h\}\} - \frac{\varepsilon}{h_F}\, [\![T_h\, \boldsymbol{n}]\!] , \\
\widehat{\boldsymbol{\varphi}}_{\text{vis}} &:= \{\{\boldsymbol{u}_h\}\} , \qquad \widehat{\lambda}_{\text{vis}} := \{\{T_h\}\} ,
\end{aligned}
$$

where ζ, η, δ, and ε are parameters which control the amount of dissipation introduced by the fluxes. By substituting these flux formulas into Eqs. (2.3.1) – (2.3.3), one may rewrite the equations in standard form as follows

$$b_h\left(\boldsymbol{u}_h, q_h\right) = 0, \tag{2.3.4}$$

$$\left(\partial_t\, \boldsymbol{u}_h, \boldsymbol{w}_h\right)_{\mathcal{T}_h} + c_h\left(\boldsymbol{u}_h; \boldsymbol{u}_h, \boldsymbol{w}_h\right) + \nu a_h\left(\boldsymbol{u}_h, \boldsymbol{w}_h\right) - b_h\left(\boldsymbol{w}_h, p_h\right)$$

$$= -\left(\beta T_h \boldsymbol{g}, \boldsymbol{w}_h\right)_{\mathcal{T}_h} + \left(\boldsymbol{f}_u, \boldsymbol{w}_h\right)_{\mathcal{T}_h}, \tag{2.3.5}$$

$$\left(\partial_t T_h, r_h\right)_{\mathcal{T}_h} + \underline{c}_h\left(\boldsymbol{u}_h; T_h, r_h\right) + \alpha\gamma\, \underline{a}_h\left(T_h, r_h\right)$$

$$= -\left(\gamma - 1\right)\Big[\left(\left(\nabla \cdot \boldsymbol{u}_h\right) T_h, r_h\right)_{\mathcal{T}_h} + C_{\mathrm{mod}}\left(\left|\nabla \cdot \boldsymbol{u}_h\right| \nabla_h T_h, \nabla_h r_h\right)_{\mathcal{T}_h}\Big] + \left(f_T, r_h\right)_{\mathcal{T}_h}. \tag{2.3.6}$$

Next, we must define the operators a_h, b_h, c_h, $\underline{a}_h$, and $\underline{c}_h$. In order to setup these definitions, we introduce functions $q_h \in Q_h$, r_h and $\theta_h \in R_h$, and $\boldsymbol{v}_h, \boldsymbol{w}_h$ and $\boldsymbol{\varrho}_h \in \boldsymbol{W}_h$. Thereafter, we expand the operators in Eqs. (2.3.4) and (2.3.5) as follows

$$b_h\left(\boldsymbol{v}_h, q_h\right) := \left(\nabla \cdot \boldsymbol{v}_h, q_h\right)_{\mathcal{T}_h}, \tag{2.3.7}$$

$$\begin{aligned} c_h\left(\boldsymbol{\varrho}_h; \boldsymbol{v}_h, \boldsymbol{w}_h\right) := {} & \left(\boldsymbol{\varrho}_h \cdot \nabla_h \boldsymbol{v}_h, \boldsymbol{w}_h\right)_{\mathcal{T}_h} + \frac{1}{2}\left(\left(\nabla \cdot \boldsymbol{\varrho}_h\right) \boldsymbol{v}_h, \boldsymbol{w}_h\right)_{\mathcal{T}_h} \\ & - \left\langle\left(\boldsymbol{\varrho}_h \cdot \boldsymbol{n}_F\right) [\![\boldsymbol{v}_h]\!], \{\{\boldsymbol{w}_h\}\}\right\rangle_{\mathcal{F}_h^i} + \zeta\left\langle\left|\boldsymbol{\varrho}_h \cdot \boldsymbol{n}_F\right| [\![\boldsymbol{v}_h]\!], [\![\boldsymbol{w}_h]\!]\right\rangle_{\mathcal{F}_h^i}, \end{aligned} \tag{2.3.8}$$

$$a_h\left(\boldsymbol{v}_h, \boldsymbol{w}_h\right) := \left(\nabla_h \boldsymbol{v}_h + \nabla_h \boldsymbol{v}_h^T - \frac{2}{3}\left(\nabla \cdot \boldsymbol{v}_h\right)\mathbb{I}, \nabla_h \boldsymbol{w}_h\right)_{\mathcal{T}_h} \tag{2.3.9}$$
$$- \left\langle \left[\!\left[\boldsymbol{v}_h\right]\!\right], \left\{\!\!\left\{\nabla_h \boldsymbol{w}_h + \nabla_h \boldsymbol{w}_h^T - \frac{2}{3}\left(\nabla \cdot \boldsymbol{w}_h\right)\mathbb{I}\right\}\!\!\right\} \boldsymbol{n}_F \right\rangle_{\mathcal{F}_h}$$
$$- \left\langle \left[\!\left[\boldsymbol{w}_h\right]\!\right], \left\{\!\!\left\{\nabla_h \boldsymbol{v}_h + \nabla_h \boldsymbol{v}_h^T - \frac{2}{3}\left(\nabla \cdot \boldsymbol{v}_h\right)\mathbb{I}\right\}\!\!\right\} \boldsymbol{n}_F \right\rangle_{\mathcal{F}_h} + \left\langle \frac{\eta}{h_F}\left[\!\left[\boldsymbol{v}_h\right]\!\right], \left[\!\left[\boldsymbol{w}_h\right]\!\right] \right\rangle_{\mathcal{F}_h}.$$

In addition, the operators in Eq. (2.3.6) can be expanded as follows

$$\underline{c}_h\left(\boldsymbol{\varrho}_h; \theta_h, r_h\right) := \left(\boldsymbol{\varrho}_h \cdot \nabla_h \theta_h, r_h\right)_{\mathcal{T}_h} + \frac{1}{2}\left(\left(\nabla \cdot \boldsymbol{\varrho}_h\right)\theta_h, r_h\right)_{\mathcal{T}_h} \tag{2.3.10}$$
$$- \left\langle \left(\boldsymbol{\varrho}_h \cdot \boldsymbol{n}_F\right)\left[\!\left[\theta_h\right]\!\right], \left\{\!\left\{r_h\right\}\!\right\} \right\rangle_{\mathcal{F}_h^i} + \delta \left\langle \left|\boldsymbol{\varrho}_h \cdot \boldsymbol{n}_F\right| \left[\!\left[\theta_h\right]\!\right], \left[\!\left[r_h\right]\!\right] \right\rangle_{\mathcal{F}_h^i},$$

$$\underline{a}_h\left(\theta_h, r_h\right) := \left(\nabla_h \theta_h, \nabla_h r_h\right)_{\mathcal{T}_h} - \left\langle \left[\!\left[\theta_h\right]\!\right], \left\{\!\left\{\nabla_h r_h\right\}\!\right\} \cdot \boldsymbol{n}_F \right\rangle_{\mathcal{F}_h} \tag{2.3.11}$$
$$- \left\langle \left[\!\left[r_h\right]\!\right], \left\{\!\left\{\nabla_h \theta_h\right\}\!\right\} \cdot \boldsymbol{n}_F \right\rangle_{\mathcal{F}_h} + \left\langle \frac{\varepsilon}{h_F}\left[\!\left[\theta_h\right]\!\right], \left[\!\left[r_h\right]\!\right] \right\rangle_{\mathcal{F}_h}.$$

We note that technically speaking, θ_h and r_h are $H_0^1(\Omega)$-conforming, and therefore the jump terms vanish in Eqs. (2.3.10) and (2.3.11), i.e. $[\![\theta_h]\!] = 0$ and $[\![r_h]\!] = 0$. Nevertheless, for the sake of completeness, we retain these terms in the subsequent analysis of $\underline{c}_h$ and $\underline{a}_h$. This enables some of this analysis to be applied to more general finite element methods, such as DG methods.

2.4. Analysis of Versatile Mixed Methods

In this section, we rigorously analyze the stability and accuracy of the versatile mixed methods which were introduced in section 2.3. In preparation for this analysis, we first introduce some important definitions, lemmas, and assumptions. Next, we use these results to establish the L2-stability of the discrete temperature, velocity, and kinematic pressure fields. Finally, we obtain error estimates for the discrete temperature, velocity, and kinematic pressure fields. Broadly speaking, the results in this section are most relevant for H1-conforming, non-pointwise divergence-free methods. The H(div)-conforming methods have been treated effectively elsewhere, (see for example [43–45]).

2.4.1 Definitions

Definition 2.4.1 (Gradient Norm)**.** Consider the scalar-valued function $r \in W^{1,p}\left(\mathcal{T}_h\right)$. Then,

$$\begin{aligned}
\|r\|_{\mathrm{grad},p} &:= \left[\|\nabla_h r\|^p_{\boldsymbol{L}^p(\Omega)} + \sum_{F \in \mathcal{F}_h} \frac{1}{h_F^{p-1}} \|[\![r]\!]\|^p_{L^p(F)} \right]^{1/p} \\
&= \left[\sum_{K \in \mathcal{T}_h} \int_K \left(\sum_j^d |\partial_j r|^p \right) dV + \sum_{F \in \mathcal{F}_h} \frac{1}{h_F^{p-1}} \int_F |[\![r]\!]|^p \, dA \right]^{1/p},
\end{aligned}$$

is a norm on Ω. In a similar fashion, for the vector-valued function $\boldsymbol{w} \in \boldsymbol{W}^{1,p}(\mathcal{T}_h)$, we have

$$\begin{aligned} \|\boldsymbol{w}\|_{\mathrm{grad},p} &:= \left[\|\nabla_h \boldsymbol{w}\|^p_{\boldsymbol{L}^p(\Omega)\times\boldsymbol{L}^p(\Omega)} + \sum_{F\in\mathcal{F}_h} \frac{1}{h_F^{p-1}} \|[\![\boldsymbol{w}]\!]\|^p_{\boldsymbol{L}^p(F)} \right]^{1/p} \\ &= \left[\sum_{K\in\mathcal{T}_h} \int_K \left(\sum_{i,j}^d |\partial_j w_i|^p \right) dV + \sum_{F\in\mathcal{F}_h} \frac{1}{h_F^{p-1}} \int_F \left(\sum_i^d |[\![w_i]\!]|^p \right) dA \right]^{1/p}. \end{aligned} \tag{2.4.1}$$

Definition 2.4.2 (Full Symmetric Gradient Norm)**.** Consider the vector-valued function $\boldsymbol{w} \in \boldsymbol{W}^{1,p}(\mathcal{T}_h)$. Then,

$$\begin{aligned} \|\boldsymbol{w}\|_{\mathrm{sym},p} &:= \left[\left\| \nabla_h \boldsymbol{w} + \nabla_h \boldsymbol{w}^T - \frac{2}{3} (\nabla_h \cdot \boldsymbol{w}) \mathbb{I} \right\|^p_{\boldsymbol{L}^p(\Omega)\times\boldsymbol{L}^p(\Omega)} + \sum_{F\in\mathcal{F}_h} \frac{1}{h_F^{p-1}} \|[\![\boldsymbol{w}]\!]\|^p_{\boldsymbol{L}^p(F)} \right]^{1/p} \\ &= \left[\sum_{K\in\mathcal{T}_h} \int_K \left(\sum_{i,j}^d \left| \partial_j w_i + \partial_i w_j - \frac{2}{3} \left(\sum_k^d \partial_k w_k \right) \delta_{ij} \right|^p \right) dV \right. \\ &\quad \left. + \sum_{F\in\mathcal{F}_h} \frac{1}{h_F^{p-1}} \int_F \left(\sum_i^d |[\![w_i]\!]|^p \right) dA \right]^{1/p}, \end{aligned} \tag{2.4.2}$$

is a norm on Ω.

Definition 2.4.3 (Error Decompositions)**.** The total error can be decomposed as follows

$$
\begin{aligned}
&\boldsymbol{\xi}_{u,h} := \boldsymbol{u} - \boldsymbol{u}_h, && \xi_{T,h} := T - T_h, && \xi_{p,h} := p - p_h, \\
&\boldsymbol{\eta}_{u,h} := \boldsymbol{u} - j_u \boldsymbol{u}, && \eta_{T,h} := T - j_T T, && \eta_{p,h} := p - j_p p, \\
&\boldsymbol{e}_{u,h} := j_u \boldsymbol{u} - \boldsymbol{u}_h, && e_{T,h} := j_T T - T_h, && e_{p,h} := j_p p - p_h.
\end{aligned}
$$

Here j_u, j_T, and j_p are bounded linear interpolation operators from the infinite-dimensional spaces $\boldsymbol{W} \times R \times Q$ on to the finite-dimensional spaces $\boldsymbol{W}_h \times R_h \times Q_h$.

Definition 2.4.4 (Local Reynolds and Péclet Numbers)**.** It is beneficial to introduce the following local quantities

$$
Re_K := \frac{\|\boldsymbol{u}_h\|_{L^\infty(K)}\, h_K}{\nu}, \quad Pe_K := \frac{\|\boldsymbol{u}_h\|_{L^\infty(K)}\, h_K}{\alpha}, \tag{2.4.3}
$$

where Re_K and Pe_K are local Reynolds and Péclet numbers, respectively.

2.4.2 Preliminary Results and Assumptions

In this section, we review some important results that govern the bilinear and trilinear forms and the associated norms which arise during the subsequent analysis of versatile mixed methods.

Lemma 2.4.5 (Grad-Div Inequality)**.** *The following inequality holds for piecewise-*

H1 vector fields

$$\|\nabla_h \cdot \boldsymbol{w}\|_{L^2(\Omega)} \le C_1 \|\boldsymbol{w}\|_{\text{grad},2}, \qquad \forall \boldsymbol{w} \in \boldsymbol{W}^{1,2}(\mathcal{T}_h). \tag{2.4.4}$$

Proof. The proof appears in Lemma 3.34 of [45]. □

Lemma 2.4.6 (Generalized Korn's Inequality)**.** *The following generalized Korn's inequality holds for piecewise-H2 vector fields*

$$\|\boldsymbol{w}\|_{\text{grad},2} \le C_2 \|\boldsymbol{w}\|_{\text{sym},2}, \qquad \forall \boldsymbol{w} \in \boldsymbol{W}^{2,2}(\mathcal{T}_h). \tag{2.4.5}$$

Proof. The proof for the $\boldsymbol{H}_0^1(\Omega)$-conforming case is relatively straightforward. We begin by applying integration by parts to the following expression

$$\begin{aligned}
&-\left(\nabla \cdot \left(\nabla \boldsymbol{w} + \nabla \boldsymbol{w}^T - \frac{2}{3}(\nabla \cdot \boldsymbol{w})\,\mathbb{I}\right), \boldsymbol{w}\right)_\Omega \\
&= -\left(\nabla \cdot (\nabla \boldsymbol{w}), \boldsymbol{w}\right)_\Omega - \left(\nabla \cdot \left(\nabla \boldsymbol{w}^T\right), \boldsymbol{w}\right)_\Omega + \frac{2}{3}\left(\nabla \cdot ((\nabla \cdot \boldsymbol{w})\,\mathbb{I}), \boldsymbol{w}\right)_\Omega \\
&= \|\boldsymbol{w}\|_{\text{grad},2}^2 + \frac{1}{3}\|\nabla \cdot \boldsymbol{w}\|_{L^2(\Omega)}^2 .
\end{aligned} \tag{2.4.6}$$

In a similar fashion, we have that

$$
\begin{aligned}
&-\left(\nabla \cdot \left(\nabla \boldsymbol{w} + \nabla \boldsymbol{w}^T - \frac{2}{3}\left(\nabla \cdot \boldsymbol{w}\right)\mathbb{I}\right), \boldsymbol{w}\right)_\Omega = \left(\nabla \boldsymbol{w} + \nabla \boldsymbol{w}^T - \frac{2}{3}\left(\nabla \cdot \boldsymbol{w}\right)\mathbb{I}, \nabla \boldsymbol{w}\right)_\Omega \\
&= \frac{1}{2}\left(\nabla \boldsymbol{w} + \nabla \boldsymbol{w}^T - \frac{2}{3}\left(\nabla \cdot \boldsymbol{w}\right)\mathbb{I}, \nabla \boldsymbol{w} + \nabla \boldsymbol{w}^T - \frac{2}{3}\left(\nabla \cdot \boldsymbol{w}\right)\mathbb{I}\right)_\Omega \\
&+ \frac{2(3-d)}{9}\left(\nabla \cdot \boldsymbol{w}, \nabla \cdot \boldsymbol{w}\right)_\Omega \\
&= \frac{1}{2}\left\|\boldsymbol{w}\right\|_{\mathrm{sym},2}^2 + \frac{2(3-d)}{9}\left\|\nabla \cdot \boldsymbol{w}\right\|_{L^2(\Omega)}^2. \qquad (2.4.7)
\end{aligned}
$$

Upon combining Eqs. (2.4.6) and (2.4.7), we obtain

$$
2\left\|\boldsymbol{w}\right\|_{\mathrm{grad},2}^2 + \left(\frac{2}{3} - \frac{4(3-d)}{9}\right)\left\|\nabla \cdot \boldsymbol{w}\right\|_{L^2(\Omega)}^2 = \left\|\boldsymbol{w}\right\|_{\mathrm{sym},2}^2.
$$

Here, the quantity in parenthesis is always positive for $d \geq 2$, and therefore

$$
\left\|\boldsymbol{w}\right\|_{\mathrm{grad},2} \leq \frac{1}{\sqrt{2}}\left\|\boldsymbol{w}\right\|_{\mathrm{sym},2}.
$$

We complete the proof for the $\boldsymbol{H}_0^1(\Omega)$-conforming case by setting $C_2 = 1/\sqrt{2}$. The proof for the more general case of piecewise-H1 and piecewise-H2 vector fields appears in Theorem 4.7 of [46] for $d = 3$. The $d = 2$ case remains to be shown. □

Lemma 2.4.7 (Inverse Generalized Korn's Inequality)**.** *The following inequality holds for piecewise-H1 vector fields*

$$
\left\|\boldsymbol{w}\right\|_{\mathrm{sym},2} \leq C_3\left\|\boldsymbol{w}\right\|_{\mathrm{grad},2}, \qquad \forall \boldsymbol{w} \in \boldsymbol{W}^{1,2}\left(\mathcal{T}_h\right). \qquad (2.4.8)
$$

Proof. The proof follows immediately from the fact that the trace of $\nabla_h \boldsymbol{w}$ is equivalent to $\nabla \cdot \boldsymbol{w}$. □

Lemma 2.4.8 (Coercivity of the Viscous Bilinear Form)**.** *The following inequality holds for piecewise-H1 vector fields*

$$a_h(\boldsymbol{w}, \boldsymbol{w}) \geq C_4 \|\boldsymbol{w}\|_{\text{sym},2}^2, \qquad \forall \boldsymbol{w} \in \boldsymbol{W}^{1,2}(\mathcal{T}_h). \tag{2.4.9}$$

Proof. The proof appears in Lemma 6.2 of [41]. □

Lemma 2.4.9 (Boundedness of the Viscous Bilinear Form)**.** *The following inequality holds for piecewise-H1 vector fields*

$$a_h(\boldsymbol{v}, \boldsymbol{w}) \leq C_5 \|\boldsymbol{v}\|_{\text{sym},2} \|\boldsymbol{w}\|_{\text{sym},2}, \tag{2.4.10}$$
$$\forall (\boldsymbol{v}, \boldsymbol{w}) \in \boldsymbol{W}^{1,2}(\mathcal{T}_h) \times \boldsymbol{W}^{1,2}(\mathcal{T}_h).$$

Proof. In order to prove the desired result, we will systematically analyze each term in the definition of a_h (Eq. (2.3.9)):

Term 1

$$
\begin{aligned}
&\frac{1}{2}\left(\nabla_h \boldsymbol{v} + \nabla_h \boldsymbol{v}^T - \frac{2}{3}\left(\nabla_h \cdot \boldsymbol{v}\right)\mathbb{I}, \nabla_h \boldsymbol{w} + \nabla_h \boldsymbol{w}^T - \frac{2}{3}\left(\nabla_h \cdot \boldsymbol{w}\right)\mathbb{I}\right)_{\mathcal{T}_h} \\
&+ \frac{2(3-d)}{9}\left(\nabla_h \cdot \boldsymbol{v}, \nabla_h \cdot \boldsymbol{w}\right)_\Omega \\
&\leq \frac{1}{2}\left\|\nabla_h \boldsymbol{v} + \nabla_h \boldsymbol{v}^T - \frac{2}{3}\left(\nabla_h \cdot \boldsymbol{v}\right)\mathbb{I}\right\|_{\boldsymbol{L}^2(\Omega)\times\boldsymbol{L}^2(\Omega)} \left\|\nabla_h \boldsymbol{w} + \nabla_h \boldsymbol{w}^T - \frac{2}{3}\left(\nabla_h \cdot \boldsymbol{w}\right)\mathbb{I}\right\|_{\boldsymbol{L}^2(\Omega)\times\boldsymbol{L}^2(\Omega)} \\
&+ \frac{2(3-d)}{9}\left\|\nabla_h \cdot \boldsymbol{v}\right\|_{L^2(\Omega)} \left\|\nabla_h \cdot \boldsymbol{w}\right\|_{L^2(\Omega)} \\
&\leq \left(\frac{1}{2} + \frac{2(3-d)}{9}(C_1 C_2)^2\right)\|\boldsymbol{v}\|_{\mathrm{sym},2}\|\boldsymbol{w}\|_{\mathrm{sym},2}.
\end{aligned}
\tag{2.4.11}
$$

Term 2

$$
\begin{aligned}
&\left\langle [\![\boldsymbol{v}]\!], \left\{\!\!\left\{\nabla_h \boldsymbol{w} + \nabla_h \boldsymbol{w}^T - \frac{2}{3}\left(\nabla_h \cdot \boldsymbol{w}\right)\mathbb{I}\right\}\!\!\right\} \boldsymbol{n}_F\right\rangle_{\mathcal{F}_h} \\
&\leq C_{\mathrm{tr}}\left\|\nabla_h \boldsymbol{w} + \nabla_h \boldsymbol{w}^T - \frac{2}{3}\left(\nabla_h \cdot \boldsymbol{w}\right)\mathbb{I}\right\|_{\boldsymbol{L}^2(\Omega)\times\boldsymbol{L}^2(\Omega)} \left(\sum_{F\in\mathcal{F}_h} h_F^{-1}\left\|[\![\boldsymbol{v}]\!]\right\|^2_{\boldsymbol{L}^2(F)}\right)^{1/2} \\
&\leq C_{\mathrm{tr}}\|\boldsymbol{v}\|_{\mathrm{sym},2}\|\boldsymbol{w}\|_{\mathrm{sym},2}.
\end{aligned}
\tag{2.4.12}
$$

Term 3: the same as Term 2 with $\boldsymbol{v}$ and $\boldsymbol{w}$ swapped.

Term 4

$$\left\langle \frac{\eta}{h_F} [\![\boldsymbol{v}]\!], [\![\boldsymbol{w}]\!] \right\rangle_{\mathcal{F}_h} \tag{2.4.13}$$
$$\leq \eta \left(\sum_{F \in \mathcal{F}_h} h_F^{-1} \left\| [\![\boldsymbol{v}]\!] \right\|^2_{\boldsymbol{L}^2(F)} \right)^{1/2} \left(\sum_{F \in \mathcal{F}_h} h_F^{-1} \left\| [\![\boldsymbol{w}]\!] \right\|^2_{\boldsymbol{L}^2(F)} \right)^{1/2}$$
$$\leq \eta \left\| \boldsymbol{v} \right\|_{\mathrm{sym},2} \left\| \boldsymbol{w} \right\|_{\mathrm{sym},2}.$$

In the equations above, we have used the Cauchy-Schwarz inequality, a standard trace inequality, Lemmas 2.4.5 and 2.4.6, and the definition of the full symmetric gradient norm (Definition 2.4.2). Next, upon combining all our results together, we have

$$a_h(\boldsymbol{v}, \boldsymbol{w}) \leq \left(2C_{\mathrm{tr}} + \eta + \frac{1}{2} + \frac{2(3-d)}{9} (C_1 C_2)^2 \right) \left\| \boldsymbol{v} \right\|_{\mathrm{sym},2} \left\| \boldsymbol{w} \right\|_{\mathrm{sym},2}. \tag{2.4.14}$$

Now, we may set $C_5 = 2C_{\mathrm{tr}} + \eta + \frac{1}{2} + \frac{2(3-d)}{9}(C_1 C_2)^2$ in order to obtain the desired result in Eq. (2.4.10). □

Lemma 2.4.10 (Semi-Coercivity of the Convective Trilinear Form for Velocity)**.** *Consider the functions* $\boldsymbol{\varrho}, \boldsymbol{w} \in \boldsymbol{W}^{1,2}(\mathcal{T}_h)$*. Then, the trilinear form* c_h *in Eq.* (2.3.8) *is semi-coercive on* $\boldsymbol{W}^{1,2}(\mathcal{T}_h)$*, such that*

$$c_h(\boldsymbol{\varrho}; \boldsymbol{w}, \boldsymbol{w}) = \zeta \left| \boldsymbol{w} \right|^2_{\boldsymbol{\varrho}}, \qquad \forall (\boldsymbol{\varrho}, \boldsymbol{w}) \in \boldsymbol{W}^{1,2}(\mathcal{T}_h) \times \boldsymbol{W}^{1,2}(\mathcal{T}_h), \tag{2.4.15}$$

where

$$|\boldsymbol{w}|_{\boldsymbol{\varrho}} = \left(\langle |\boldsymbol{\varrho} \cdot \boldsymbol{n}_F| \, [\![\boldsymbol{w}]\!] \, , [\![\boldsymbol{w}]\!] \rangle_{\mathcal{F}_h^i} \right)^{1/2}, \tag{2.4.16}$$

is a seminorm on Ω.

Proof. The proof appears in Lemma 6.4 of [41]. □

Lemma 2.4.11 (Boundedness of the Convective Trilinear Form for Velocity)**.** *Consider functions* $\boldsymbol{\varrho}, \boldsymbol{v}, \boldsymbol{w} \in \boldsymbol{W}^{1,2}(\mathcal{T}_h)$. *Then, the trilinear form* c_h *in Eq.* (2.3.8) *is bounded above as follows*

$$c_h(\boldsymbol{\varrho}; \boldsymbol{v}, \boldsymbol{w}) \leq C_6 \, \|\boldsymbol{\varrho}\|_{\text{grad},2} \, \|\boldsymbol{v}\|_{\text{grad},2} \, \|\boldsymbol{w}\|_{\text{grad},2} \, , \tag{2.4.17}$$

$$c_h(\boldsymbol{\varrho}; \boldsymbol{v}, \boldsymbol{w}) \leq C_7 \, \|\boldsymbol{\varrho}\|_{\text{grad},4} \, \|\boldsymbol{v}\|_{\text{grad},4} \, \|\boldsymbol{w}\|_{\boldsymbol{L}^2(\Omega)} \, , \tag{2.4.18}$$

$$\forall (\boldsymbol{\varrho}, \boldsymbol{v}, \boldsymbol{w}) \in \boldsymbol{W}^{1,2}(\mathcal{T}_h) \times \boldsymbol{W}^{1,2}(\mathcal{T}_h) \times \boldsymbol{W}^{1,2}(\mathcal{T}_h) \, .$$

Proof. A proof of the upper bound in Eq. (2.4.17) appears in [47], on p. 272. It remains for us to prove Eq. (2.4.18). In what follows, we construct the necessary bounds for each term on the RHS of Eq. (2.3.8).

Term 1

$$
\begin{aligned}
(\boldsymbol{\varrho} \cdot \nabla_h \boldsymbol{v}, \boldsymbol{w})_{\mathcal{T}_h} &= \sum_{K \in \mathcal{T}_h} \int_K \left(\sum_{i,j}^{d} \varrho_j \left(\partial_j v_i\right) w_i \right) dV \\
&\leq \sum_{K \in \mathcal{T}_h} \int_K \left(\sum_{i,j}^{d} \left(\varrho_j\right)^4 \right)^{1/4} \left(\sum_{i,j}^{d} \left(\partial_j v_i\right)^4 \right)^{1/4} \left(\sum_{i,j}^{d} \left(w_i\right)^2 \right)^{1/2} dV \\
&\leq d^{3/4} \left\|\boldsymbol{\varrho}\right\|_{\boldsymbol{L}^4(\Omega)} \left\|\nabla \boldsymbol{v}\right\|_{\boldsymbol{L}^4(\Omega) \times \boldsymbol{L}^4(\Omega)} \left\|\boldsymbol{w}\right\|_{\boldsymbol{L}^2(\Omega)}.
\end{aligned}
$$

Here, we used the discrete Cauchy-Schwarz inequality and Hölder's inequality. Next, we utilize the Sobolev embedding inequality (Eq. (B.1.6)) from Lemma B.1.3 as follows

$$
\begin{aligned}
(\boldsymbol{\varrho} \cdot \nabla_h \boldsymbol{v}, \boldsymbol{w})_{\mathcal{T}_h} &\leq d^{3/4} \left\|\boldsymbol{\varrho}\right\|_{\boldsymbol{L}^4(\Omega)} \left\|\nabla_h \boldsymbol{v}\right\|_{\boldsymbol{L}^4(\Omega) \times \boldsymbol{L}^4(\Omega)} \left\|\boldsymbol{w}\right\|_{\boldsymbol{L}^2(\Omega)} \\
&\leq d^{3/4} \sigma_{4,4} \left\|\boldsymbol{\varrho}\right\|_{\text{grad},4} \left\|\boldsymbol{v}\right\|_{\text{grad},4} \left\|\boldsymbol{w}\right\|_{\boldsymbol{L}^2(\Omega)}.
\end{aligned}
$$

Term 2

$$
\begin{aligned}
\frac{1}{2} \left(\left(\nabla \cdot \boldsymbol{\varrho}\right) \boldsymbol{v}, \boldsymbol{w}\right)_{\mathcal{T}_h} &= \frac{1}{2} \sum_{K \in \mathcal{T}_h} \int_K \left(\sum_{i}^{d} \left(\partial_i \varrho_i\right) \sum_{j}^{d} \left(v_j w_j\right) \right) dV \\
&\leq \frac{1}{2} \sum_{K \in \mathcal{T}_h} \int_K \left(\sum_{i}^{d} \left(\partial_i \varrho_i\right) \right) \left(\sum_{j}^{d} \left(v_j\right)^2 \right)^{1/2} \left(\sum_{j}^{d} \left(w_j\right)^2 \right)^{1/2} dV \\
&\leq \frac{d}{2} \left\|\nabla \cdot \boldsymbol{\varrho}\right\|_{L^4(\Omega)} \left\|\boldsymbol{v}\right\|_{\boldsymbol{L}^4(\Omega)} \left\|\boldsymbol{w}\right\|_{\boldsymbol{L}^2(\Omega)}.
\end{aligned}
$$

Here, we used the discrete Cauchy-Schwarz inequality, Hölder's inequality, and the root-mean square-arithmetic mean inequality. Next, we utilize the inequalities (Eqs. (B.1.2) and (B.1.6)) from Lemmas B.1.2 and B.1.3 as follows

$$\frac{1}{2}\left(\left(\nabla\cdot\boldsymbol{\varrho}\right)\boldsymbol{v},\boldsymbol{w}\right)_{\mathcal{T}_h}\leq\frac{d^{7/4}}{2}\sigma_{4,4}\left\|\boldsymbol{\varrho}\right\|_{\mathrm{grad},4}\left\|\boldsymbol{v}\right\|_{\mathrm{grad},4}\left\|\boldsymbol{w}\right\|_{\boldsymbol{L}^2(\Omega)}.$$

Term 3

$$\begin{aligned}
&\left\langle\left(\{\{\boldsymbol{\varrho}\}\}\cdot\boldsymbol{n}_F\right)[\![\boldsymbol{v}]\!],\{\{\boldsymbol{w}\}\}\right\rangle_{\mathcal{F}_h^i}\\
&=\sum_{F\in\mathcal{F}_h^i}\int_F\left(\sum_i^d\{\{\varrho_i\}\}\,n_{Fi}\sum_j^d[\![v_j]\!]\,\{\{w_j\}\}\right)dA\\
&\leq\sum_{F\in\mathcal{F}_h^i}\int_F\left(\sum_i^d\{\{\varrho_i\}\}^2\right)^{1/2}\left(\sum_j^d[\![v_j]\!]^2\right)^{1/2}\left(\sum_j^d\{\{w_j\}\}^2\right)^{1/2}dA\\
&\leq d^{1/2}\left(\sum_{F\in\mathcal{F}_h^i}h_F\int_F\sum_i^d\{\{\varrho_i\}\}^4\,dA\right)^{1/4}\left(\sum_{F\in\mathcal{F}_h^i}\frac{1}{h_F^3}\int_F\sum_j^d[\![v_j]\!]^4\,dA\right)^{1/4}\\
&\times\left(\sum_{F\in\mathcal{F}_h^i}h_F\int_F\sum_j^d\{\{w_j\}\}^2\,dA\right)^{1/2}.
\end{aligned}$$

Here, we used the discrete Cauchy-Schwarz inequality, Hölder's inequality, and the root-mean square-arithmetic mean inequality. Next, we use the discrete trace inequalities (Eqs. (B.1.8) and (B.1.9)) in Lemma B.1.4, and the embedding inequality

(Eq. (B.1.6)) in Lemma B.1.3

$$
\begin{aligned}
&\langle (\{\{\boldsymbol{\varrho}\}\} \cdot \boldsymbol{n}_F) \, [\![\boldsymbol{v}]\!] \, , \{\{\boldsymbol{w}\}\} \rangle_{\mathcal{F}_h^i} \\
&\leq d^{1/2} \left(\frac{1}{2} N_\partial C_{\mathrm{tr},4}^4 \, \|\boldsymbol{\varrho}\|_{\boldsymbol{L}^4(\Omega)}^4 \right)^{1/4} \|\boldsymbol{v}\|_{\mathrm{grad},4} \left(\frac{1}{2} N_\partial C_{\mathrm{tr},2}^2 \, \|\boldsymbol{w}\|_{\boldsymbol{L}^2(\Omega)}^2 \right)^{1/2} \\
&\leq d^{1/2} \left(\frac{N_\partial}{2} \right)^{3/4} C_{\mathrm{tr},4} C_{\mathrm{tr},2} \sigma_{4,4} \, \|\boldsymbol{\varrho}\|_{\mathrm{grad},4} \, \|\boldsymbol{v}\|_{\mathrm{grad},4} \, \|\boldsymbol{w}\|_{\boldsymbol{L}^2(\Omega)} .
\end{aligned}
$$

Term 4

$$
\begin{aligned}
&\zeta \, \langle |\{\{\boldsymbol{\varrho}\}\} \cdot \boldsymbol{n}_F| \, [\![\boldsymbol{v}]\!] \, , [\![\boldsymbol{w}]\!] \rangle_{\mathcal{F}_h^i} \\
&\leq \zeta d^{1/2} \left(\sum_{F \in \mathcal{F}_h^i} h_F \int_F \sum_i^d \{\{\varrho_i\}\}^4 \, dA \right)^{1/4} \left(\sum_{F \in \mathcal{F}_h^i} \frac{1}{h_F^3} \int_F \sum_j^d [\![v_j]\!]^4 \, dA \right)^{1/4} \\
&\times \left(\sum_{F \in \mathcal{F}_h^i} h_F \int_F \sum_j^d [\![w_j]\!]^2 \, dA \right)^{1/2} .
\end{aligned}
$$

Here, we followed the steps for bounding term 3. Next, we use the discrete trace inequalities (Eqs. (B.1.7) and (B.1.9)) in Lemma B.1.4, and the embedding inequality (Eq. (B.1.6)) in Lemma B.1.3

$$\begin{aligned}
&\zeta \left\langle \left| \{\{\boldsymbol{\varrho}\}\} \cdot \boldsymbol{n}_F \right| [\![\boldsymbol{v}]\!] , [\![\boldsymbol{w}]\!] \right\rangle_{\mathcal{F}_h^i} \\
&\leq \zeta d^{1/2} \left(\frac{1}{2} N_\partial C_{\mathrm{tr},4}^4 \left\| \boldsymbol{\varrho} \right\|_{\boldsymbol{L}^4(\Omega)}^4 \right)^{1/4} \left\| \boldsymbol{v} \right\|_{\mathrm{grad},4} \left(2 N_\partial C_{\mathrm{tr},2}^2 \left\| \boldsymbol{w} \right\|_{\boldsymbol{L}^2(\Omega)}^2 \right)^{1/2} \\
&\leq \zeta d^{1/2} 2^{1/4} N_\partial^{3/4} C_{\mathrm{tr},4} C_{\mathrm{tr},2} \sigma_{4,4} \left\| \boldsymbol{\varrho} \right\|_{\mathrm{grad},4} \left\| \boldsymbol{v} \right\|_{\mathrm{grad},4} \left\| \boldsymbol{w} \right\|_{\boldsymbol{L}^2(\Omega)} .
\end{aligned}$$

Finally, we obtain the desired result (Eq. (2.4.18)) by combining the bounds for terms 1–4, and setting

$$C_7 = \left(d^{3/4} + \frac{d^{7/4}}{2} + d^{1/2} \left(\frac{N_\partial}{2} \right)^{3/4} C_{\mathrm{tr},4} C_{\mathrm{tr},2} + \zeta d^{1/2} 2^{1/4} N_\partial^{3/4} C_{\mathrm{tr},4} C_{\mathrm{tr},2} \right) \sigma_{4,4}.$$

□

Lemma 2.4.12 (Coercivity of the Temperature Bilinear Form)**.** *The following inequality holds for piecewise-H1 scalar fields*

$$\underline{a}_h \left(r, r \right) \geq C_8 \left\| r \right\|_{\mathrm{grad},2}^2 , \qquad \forall r \in W^{1,2} \left(\mathcal{T}_h \right) . \tag{2.4.19}$$

Proof. The proof appears in Lemma 4.12 of [47], . □

Lemma 2.4.13 (Boundedness of the Temperature Bilinear Form)**.** *The following* *inequality holds for piecewise-H1 scalar fields*

$$\underline{a}_h(\theta, r) \leq C_9 \|\theta\|_{\text{grad},2} \|r\|_{\text{grad},2}, \qquad (2.4.20)$$

$$\forall (\theta, r) \in W^{1,2}(\mathcal{T}_h) \times W^{1,2}(\mathcal{T}_h).$$

Proof. The proof appears in Lemma 4.16 of [47]. □

Lemma 2.4.14 (Semi-Coercivity of the Convective Trilinear Form for Temperature)**.** *Consider the functions* $\boldsymbol{\varrho} \in \boldsymbol{W}^{1,2}(\mathcal{T}_h)$ *and* $r \in W^{1,2}(\mathcal{T}_h)$*. Then, the trilinear form* $\underline{c}_h$ *in Eq.* (2.3.10) *is semi-coercive on* $\boldsymbol{W}^{1,2}(\mathcal{T}_h) \times W^{1,2}(\mathcal{T}_h)$*, such that*

$$\underline{c}_h(\boldsymbol{\varrho}; r, r) = \delta |r|^2_{\boldsymbol{\varrho}}, \qquad \forall (\boldsymbol{\varrho}, r) \in \boldsymbol{W}^{1,2}(\mathcal{T}_h) \times W^{1,2}(\mathcal{T}_h), \qquad (2.4.21)$$

where

$$|r|_{\boldsymbol{\varrho}} = \left(\langle |\boldsymbol{\varrho} \cdot \boldsymbol{n}_F| \llbracket r \rrbracket, \llbracket r \rrbracket \rangle_{\mathcal{F}_h^i} \right)^{1/2}, \qquad (2.4.22)$$

is a seminorm on Ω*.*

Proof. One may begin by substituting $\boldsymbol{\varrho}_h = \boldsymbol{\varrho}$ and $\theta_h = r_h = r$ into Eq. (2.3.10) as follows

$$\underline{c}_h(\boldsymbol{\varrho}; r, r) = (\boldsymbol{\varrho} \cdot \nabla_h r, r)_{\mathcal{T}_h} + \frac{1}{2}((\nabla_h \cdot \boldsymbol{\varrho}) r, r)_{\mathcal{T}_h} \qquad (2.4.23)$$

$$- \langle (\boldsymbol{\varrho} \cdot \boldsymbol{n}_F) \llbracket r \rrbracket, \{\{r\}\} \rangle_{\mathcal{F}_h^i} + \delta \langle |\boldsymbol{\varrho} \cdot \boldsymbol{n}_F| \llbracket r \rrbracket, \llbracket r \rrbracket \rangle_{\mathcal{F}_h^i}.$$

Next, we note that the following identity holds

$$(\boldsymbol{\varrho} \cdot \nabla_h r, r)_{\mathcal{T}_h} + \frac{1}{2}\left((\nabla_h \cdot \boldsymbol{\varrho})\, r, r\right)_{\mathcal{T}_h} = \langle (\boldsymbol{\varrho} \cdot \boldsymbol{n}_F) \llbracket r \rrbracket , \{\{r\}\} \rangle_{\mathcal{F}_h^i} .$$

Upon substituting this identity into Eq. (2.4.23), one obtains

$$\underline{c}_h (\boldsymbol{\varrho}; r, r) = \delta \left\langle |\boldsymbol{\varrho} \cdot \boldsymbol{n}_F| \llbracket r \rrbracket , \llbracket r \rrbracket \right\rangle_{\mathcal{F}_h^i} . \tag{2.4.24}$$

Finally, on substituting the definition of the seminorm into Eq. (2.4.24), we obtain the desired result (Eq. (2.4.21)). □

Lemma 2.4.15 (Poincaré Inequality)**.** *The following Poincaré inequalities hold for H1 scalar and vector fields which vanish on the domain boundary* $\partial\Omega$

$$\begin{aligned} &\|r\|_{L^2(\Omega)} \leq C_{10} \|\nabla r\|_{L^2(\Omega)} , \\ &\|\boldsymbol{\varrho}\|_{L^2(\Omega)} \leq C_{11} \|\nabla \boldsymbol{\varrho}\|_{\boldsymbol{L}^2(\Omega) \times \boldsymbol{L}^2(\Omega)} , \\ &\forall\, (r, \boldsymbol{\varrho}) \subset H_0^1(\Omega) \times \boldsymbol{H}_0^1(\Omega). \end{aligned}$$

Proof. The proof appears in [48]. □

Assumption 2.4.16 (Weighted-Poincaré Inequality)**.** *The following weighted-Poincaré inequality holds for H1 scalar fields which vanish on the domain boundary* $\partial\Omega$

$$\begin{aligned} &\left(|\nabla \cdot \boldsymbol{\varrho}|\, r, r\right)_{\mathcal{T}_h} \leq C_{12} \left(|\nabla \cdot \boldsymbol{\varrho}|\, \nabla r, \nabla r\right)_{\mathcal{T}_h} , \\ &\forall\, (r, \boldsymbol{\varrho}) \in H_0^1(\Omega) \times \boldsymbol{H}_0(\mathrm{div}; \Omega) , \end{aligned}$$

where $|\nabla \cdot \boldsymbol{\varrho}|$ *is a non-negative weighting function. Note: a comprehensive review of weighted-Poincaré inequalities appears in [49].*

Assumption 2.4.17 (Generalized Inf-Sup Condition)**.** *Consider test functions* $q_h \in Q_h$ *and* $\boldsymbol{w}_h \in \boldsymbol{W}_h$*, where* Q_h *and* $\boldsymbol{W}_h$ *form an inf-sup stable pair. Then, we assume that the following inequality holds for the bilinear form* b_h *in Eq.* (2.3.7)

$$\frac{1}{C_{13}} \left\| q_h \right\|_{L^{p'}(\Omega)} \leq \sup_{\boldsymbol{w}_h \in \boldsymbol{W}_h \setminus \{\boldsymbol{0}\}} \frac{\left(q_h \, , \nabla \cdot \boldsymbol{w}_h\right)_{\mathcal{T}_h}}{\left\| \boldsymbol{w}_h \right\|_{\text{grad,p}}}, \tag{2.4.25}$$

where $1 < p < \infty$, $\frac{1}{p} + \frac{1}{p'} = 1$*, and* $C_{13} > 0$ *is a constant that is independent of* h*. Furthermore, we assume that the following classical inf-sup condition also holds*

$$\frac{1}{C_{13}} \leq \inf_{q_h \in Q_h \setminus \{0\}} \left[\sup_{\boldsymbol{w}_h \in \boldsymbol{W}_h \setminus \{\boldsymbol{0}\}} \frac{\left(q_h \, , \nabla \cdot \boldsymbol{w}_h\right)_{\mathcal{T}_h}}{\left\| q_h \right\|_{L^{p'}(\Omega)} \left\| \boldsymbol{w}_h \right\|_{\text{grad,p}}} \right]. \tag{2.4.26}$$

Finally, these inf-sup conditions ensure that the space of weakly divergence-free vector-valued functions is non-trivial

$$\boldsymbol{W}_h^{\text{div}} := \left\{ \boldsymbol{w}_h \in \boldsymbol{W}_h \,|\, b_h\left(\boldsymbol{w}_h, q_h\right) = 0, \forall q_h \in Q_h \right\} \neq \left\{ \boldsymbol{0} \right\}. \tag{2.4.27}$$

Lemma 2.4.18 (Generalized Inf-Sup Condition, Taylor-Hood)**.** *Consider test functions* $q_h \in Q_h^C$ *and* $\boldsymbol{w}_h \in \boldsymbol{W}_h^{TH}$*, where* Q_h^C *and* $\boldsymbol{W}_h^{TH}$ *form a Taylor-Hood inf-sup stable pair. Then, the following inequality holds for the bilinear form* b_h *in*

Eq. (2.3.7)

$$\frac{1}{C_{13}} \left\| q_h \right\|_{L^{p'}(\Omega)} \leq \sup_{\boldsymbol{w}_h \in \boldsymbol{W}_h \setminus \{\boldsymbol{0}\}} \frac{\left(q_h \,, \nabla \cdot \boldsymbol{w}_h \right)_{\mathcal{T}_h}}{\left\| \boldsymbol{w}_h \right\|_{\text{grad,p}}}, \tag{2.4.28}$$

where $1 < p < \infty$, $\frac{1}{p} + \frac{1}{p'} = 1$, *and* $C_{13} > 0$ *is a constant that is independent of* h. *Furthermore, the following classical inf-sup condition also holds*

$$\frac{1}{C_{13}} \leq \inf_{q_h \in Q_h \setminus \{0\}} \left[\sup_{\boldsymbol{w}_h \in \boldsymbol{W}_h \setminus \{\boldsymbol{0}\}} \frac{\left(q_h \,, \nabla \cdot \boldsymbol{w}_h \right)_{\mathcal{T}_h}}{\left\| q_h \right\|_{L^{p'}(\Omega)} \left\| \boldsymbol{w}_h \right\|_{\text{grad,p}}} \right]. \tag{2.4.29}$$

Finally, the inf-sup condition ensures that the space of weakly divergence-free vector-valued functions is non-trivial

$$\boldsymbol{W}_h^{\text{div}} := \left\{ \boldsymbol{w}_h \in \boldsymbol{W}_h \,|\, b_h \left(\boldsymbol{w}_h, q_h \right) = 0, \forall q_h \in Q_h \right\} \neq \left\{ \boldsymbol{0} \right\}. \tag{2.4.30}$$

Proof. We start with [50] Lemma 4.24 (p. 194) which contains the following inf-sup condition

$$\frac{1}{C_{13}} \leq \inf_{q_h \in Q_h \setminus \{0\}} \left[\sup_{\boldsymbol{w}_h \in \boldsymbol{W}_h \setminus \{\boldsymbol{0}\}} \frac{\left(q_h \,, \nabla \cdot \boldsymbol{w}_h \right)_{\mathcal{T}_h}}{\left\| q_h \right\|_{L^{p'}(\Omega)} \left\| \boldsymbol{w}_h \right\|_{\boldsymbol{W}^{1,p}(\Omega)}} \right].$$

This expression can be rewritten as follows

$$\frac{1}{C_{13}} \leq \inf_{q_h \in Q_h \setminus \{0\}} \left[\sup_{\boldsymbol{w}_h \in \boldsymbol{W}_h \setminus \{\boldsymbol{0}\}} \frac{\left(q_h \,, \nabla \cdot \boldsymbol{w}_h \right)_{\mathcal{T}_h}}{\left\| q_h \right\|_{L^{p'}(\Omega)} \left\| \boldsymbol{w}_h \right\|_{\text{grad},p}} \frac{\left\| \boldsymbol{w}_h \right\|_{\text{grad},p}}{\left\| \boldsymbol{w}_h \right\|_{\boldsymbol{W}^{1,p}(\Omega)}} \right]. \tag{2.4.31}$$

Finally, we note that

$$\|\boldsymbol{w}_h\|_{\mathrm{grad},p} \leq \|\boldsymbol{w}_h\|_{\boldsymbol{W}^{1,p}(\Omega)} ,$$

which follows by the definition of $\|\cdot\|_{\boldsymbol{W}^{1,p}(\Omega)}$, and by the fact that the jumps in $\boldsymbol{w}_h$ vanish for Taylor-Hood elements. Upon substituting this result into Eq. (2.4.31), we obtain the desired result (Eq. (2.4.29)). □

Assumption 2.4.19 (Interpolation Operators)**.** *Let us assume that for integers $k_u \geq 1$, $k_T \geq 1$, and $k_p \geq 1$ there are bounded linear operators $j_u : \boldsymbol{W} \to \boldsymbol{W_h}$ and $j_p : Q \to Q_h$ such that for all $K \in \mathcal{T}_h$, for all $\boldsymbol{w} \in \boldsymbol{W} \cap \boldsymbol{W}^{l_u,2}(\Omega)$ with $1 \leq l_u \leq k_u + 1$:*

$$\|\boldsymbol{w} - j_u\boldsymbol{w}\|_{L^2(K)} + h_K \|\nabla (\boldsymbol{w} - j_u\boldsymbol{w})\|_{\boldsymbol{L}^2(K)\times\boldsymbol{L}^2(K)} \leq Ch_K^{l_u} \|\boldsymbol{w}\|_{W^{l_u,2}(K)} ,$$

and for all $q \in Q \cap W^{l_p,2}(\Omega)$ with $1 \leq l_p \leq k_p + 1$:

$$\|q - j_p q\|_{L^2(K)} + h_K \|\nabla (q - j_p q)\|_{L^2(K)} \leq Ch_K^{l_p} \|q\|_{W^{l_p,2}(K)} .$$

We also assume that for $K \in \mathcal{T}_h$

$$\|\boldsymbol{w} - j_u\boldsymbol{w}\|_{L^\infty(K)} \leq Ch_K |\boldsymbol{w}|_{W^{1,\infty}(K)} , \quad \forall \boldsymbol{w} \in \boldsymbol{W}^{1,\infty}(\Omega).$$

In addition, there is a bounded linear interpolation operator $j_T : R \to R_h$ such that *for all $K \in \mathcal{T}_h$ and for all $r \in R \cap W^{l_T,2}(\Omega)$ with $1 \leq l_T \leq k_T + 1$:*

$$\|r - j_T r\|_{L^2(K)} + h_K \|\nabla (r - j_T r)\|_{L^2(K)} \leq C h_K^{l_T} \|r\|_{W^{l_T,2}(K)} .$$

We also assume that for $K \in \mathcal{T}_h$

$$\|r - j_T r\|_{L^\infty(K)} \leq C h_K |r|_{W^{1,\infty}(K)} , \quad \forall r \in W^{1,\infty}(\Omega),$$

$$\|\nabla (r - j_T r)\|_{L^\infty(K)} \leq C \|r\|_{W^{1,\infty}(K)} , \quad \forall r \in W^{1,\infty}(\Omega).$$

2.4.3 Discrete Stability

In this section, we establish the discrete stability of the temperature, velocity, and kinematic pressure fields for versatile mixed methods. It turns out that the discrete stability of the methods depends on our choice of finite elements: namely, H1-conforming, non-pointwise divergence-free elements versus H(div)-conforming, pointwise divergence-free elements. In particular, in order to guarantee the stability of the discrete temperature field for the H1-conforming methods, we must choose an appropriate value of the stabilization constant C_{mod}. In addition, there is an indirect effect of the C_{mod} stabilization on the momentum equation, as the temperature field influences the momentum equation through the Boussinesq bouyancy term. Conversely, the pointwise divergence-free, H(div)-conforming methods maintain stability of the discrete temperature, velocity, and kinematic pressure fields, independent of the particular choice of C_{mod}. These ideas are summarized by the following theorems.

Theorem 2.4.20 (Stability of the Discrete Temperature)**.** *Consider the mixed finite element methods in Eqs.* (2.3.1) – (2.3.3)*, equipped with a forcing function* f_T *where* $f_T(t) \in L^1(t_0, t_n; L^2(\Omega))$*, a discrete velocity field* $\boldsymbol{u}_h \in \boldsymbol{W}_h$ *where* $\boldsymbol{u}_h(t) \in L^2(t_0, t_n; \boldsymbol{H}_0(\mathrm{div}; \Omega))$*, and an initial condition* $T_h(t_0) \in R_h \subset H_0^1(\Omega)$*. In addition, let Assumption 2.4.16 hold. Subject to these assumptions, the discrete temperature* T_h *is governed by the following equation at time* $t_n \geq t_0$

$$\frac{1}{2}\|T_h(t_n)\|^2_{L^2(\Omega)} + \delta |T_h|^2_{L^2(t_0,t_n;\boldsymbol{u}_h)} + \alpha\gamma C_8 \|T_h\|^2_{L^2(t_0,t_n;\mathrm{grad},2)} + (\gamma - 1)\,\Psi(T_h)_{L^1(t_0,t_n;\boldsymbol{u}_h)}$$
$$\leq \|T_h(t_0)\|^2_{L^2(\Omega)} + \frac{3}{2}\|f_T\|^2_{L^1(t_0,t_n;L^2(\Omega))}, \tag{2.4.32}$$

where

$$|T_h|_{L^2(t_0,t_n;\boldsymbol{u}_h)} = \left(\int_{t_0}^{t_n} |T_h(s)|^2_{\boldsymbol{u}_h}\, ds\right)^{1/2}, \tag{2.4.33}$$

$$\|T_h\|_{L^2(t_0,t_n;\mathrm{grad},2)} = \left(\int_{t_0}^{t_n} \|T_h(s)\|^2_{\mathrm{grad},2}\, ds\right)^{1/2}, \tag{2.4.34}$$

$$\|f_T\|_{L^1(t_0,t_n;L^2(\Omega))} = \int_{t_0}^{t_n} \|f_T(s)\|_{L^2(\Omega)}\, ds, \tag{2.4.35}$$

$$\Psi(T_h)_{L^1(t_0,t_n;\boldsymbol{u}_h)} = \int_{t_0}^{t_n} \Psi(\boldsymbol{u}_h(s), T_h(s))\, ds, \tag{2.4.36}$$

are Bochner-type seminorms and norms on $(t_0, t_n) \times \Omega$*. In addition, we define the following function*

$$\Psi(\boldsymbol{u}_h, T_h) = ((\nabla \cdot \boldsymbol{u}_h) T_h, T_h)_{\mathcal{T}_h} + C_{\mathrm{mod}}\left(|\nabla \cdot \boldsymbol{u}_h| \nabla_h T_h, \nabla_h T_h\right)_{\mathcal{T}_h},$$

where we require $C_{\text{mod}} \geq C_{12}$ *such that* $\Psi\left(\boldsymbol{u}_h, T_h\right) \geq 0$.

Proof. We start by setting $r_h = T_h$ in Eq. (2.3.6) as follows

$$\begin{aligned}&\left(\partial_t T_h, T_h\right)_{\mathcal{T}_h} + \underline{c}_h\left(\boldsymbol{u}_h; T_h, T_h\right) + \alpha\gamma\, \underline{a}_h\left(T_h, T_h\right) \\ &= -\left(\gamma - 1\right)\Big[\left(\left(\nabla\cdot\boldsymbol{u}_h\right)T_h, T_h\right)_{\mathcal{T}_h} + C_{\text{mod}}\left(\left|\nabla\cdot\boldsymbol{u}_h\right|\nabla_h T_h, \nabla_h T_h\right)_{\mathcal{T}_h}\Big] + \left(f_T, T_h\right)_{\mathcal{T}_h},\end{aligned}$$

or equivalently

$$\begin{aligned}&\frac{1}{2}\frac{d}{dt}\left\|T_h\right\|^2_{L^2(\Omega)} + \underline{c}_h\left(\boldsymbol{u}_h; T_h, T_h\right) + \alpha\gamma\, \underline{a}_h\left(T_h, T_h\right) \\ &= -\left(\gamma - 1\right)\Big[\left(\left(\nabla\cdot\boldsymbol{u}_h\right)T_h, T_h\right)_{\mathcal{T}_h} + C_{\text{mod}}\left(\left|\nabla\cdot\boldsymbol{u}_h\right|\nabla_h T_h, \nabla_h T_h\right)_{\mathcal{T}_h}\Big] + \left(f_T, T_h\right)_{\mathcal{T}_h}.\end{aligned}$$

Next, we invoke the coercivity of $\underline{a}_h$ (Lemma 2.4.12) and the semi-coercivity of $\underline{c}_h$ (Lemma 2.4.14) as follows

$$\begin{aligned}&\frac{1}{2}\frac{d}{dt}\left\|T_h\right\|^2_{L^2(\Omega)} + \delta\left|T_h\right|^2_{\boldsymbol{u}_h} + \alpha\gamma C_8\left\|T_h\right\|^2_{\text{grad},2} \\ &\leq -\left(\gamma - 1\right)\Big[\left(\left(\nabla\cdot\boldsymbol{u}_h\right)T_h, T_h\right)_{\mathcal{T}_h} + C_{\text{mod}}\left(\left|\nabla\cdot\boldsymbol{u}_h\right|\nabla_h T_h, \nabla_h T_h\right)_{\mathcal{T}_h}\Big] + \left(f_T, T_h\right)_{\mathcal{T}_h},\end{aligned} \tag{2.4.37}$$

or equivalently,

$$\frac{1}{2}\frac{d}{dt}\left\|T_h\right\|^2_{L^2(\Omega)} + \delta\left|T_h\right|^2_{\boldsymbol{u}_h} + \alpha\gamma C_8\left\|T_h\right\|^2_{\text{grad},2} + \left(\gamma - 1\right)\Psi\left(\boldsymbol{u}_h, T_h\right) \leq \left(f_T, T_h\right)_{\mathcal{T}_h}. \tag{2.4.38}$$

In order for Eq. (2.4.38) to serve as a meaningful inequality, we require that $\Psi(\boldsymbol{u}_h, T_h) \geq 0$. This property is guaranteed to hold if we choose $C_{\text{mod}} \geq C_{12}$, in accordance with the weighted-Poincaré inequality in Assumption 2.4.16.

Based on equation (2.4.38), we observe that

$$\frac{1}{2}\frac{d}{dt}\left\|T_h\right\|_{L^2(\Omega)}^2 \leq \left(f_T, T_h\right)_{\mathcal{T}_h},$$

and equivalently, by the Cauchy-Schwarz inequality

$$\begin{aligned}\left\|T_h\right\|_{L^2(\Omega)}\frac{d}{dt}\left\|T_h\right\|_{L^2(\Omega)} &\leq \left\|f_T\right\|_{L^2(\Omega)}\left\|T_h\right\|_{L^2(\Omega)}\\ \frac{d}{dt}\left\|T_h\right\|_{L^2(\Omega)} &\leq \left\|f_T\right\|_{L^2(\Omega)}.\end{aligned} \tag{2.4.39}$$

Next, we integrate Eq. (2.4.39) from $t = t_0$ to $t = t_n$ as follows

$$\begin{aligned}\left\|T_h(t_n)\right\|_{L^2(\Omega)} &\leq \left\|T_h(t_0)\right\|_{L^2(\Omega)} + \int_{t_0}^{t_n}\left\|f_T(s)\right\|_{L^2(\Omega)} ds\\ &= \left\|T_h(t_0)\right\|_{L^2(\Omega)} + \left\|f_T\right\|_{L^1(t_0,t_n;L^2(\Omega))}.\end{aligned} \tag{2.4.40}$$

We will utilize this result shortly. For now, we turn our attention back to Eq. (2.4.38). On integrating this equation from $t = t_0$ to $t = t_n$, we find that

$$\begin{aligned}&\frac{1}{2}\left\|T_h(t_n)\right\|_{L^2(\Omega)}^2 + \int_{t_0}^{t_n}\Big(\delta\left|T_h(s)\right|_{\boldsymbol{u}_h}^2 + \alpha\gamma C_8\left\|T_h(s)\right\|_{\text{grad},2}^2 + (\gamma-1)\,\Psi\left(\boldsymbol{u}_h(s), T_h(s)\right)\Big)\, ds\\ &\leq \frac{1}{2}\left\|T_h(t_0)\right\|_{L^2(\Omega)}^2 + \int_{t_0}^{t_n}\left(f_T(s), T_h(s)\right)_{\mathcal{T}_h} ds.\end{aligned} \tag{2.4.41}$$

We can rewrite the last term on the RHS of Eq. (2.4.41) as follows

$$\int_{t_0}^{t_n} \left(f_T(s), T_h(s)\right)_{\mathcal{T}_h} ds \leq \int_{t_0}^{t_n} \|f_T(s)\|_{L^2(\Omega)} \|T_h(s)\|_{L^2(\Omega)} ds$$
$$\leq \int_{t_0}^{t_n} \left[\|f_T(s)\|_{L^2(\Omega)} \left(\|T_h(t_0)\|_{L^2(\Omega)} + \|f_T\|_{L^1(t_0,s;L^2(\Omega))} \right) \right] ds,$$
$$\leq \int_{t_0}^{t_n} \|f_T(s)\|_{L^2(\Omega)} ds \times \left(\|T_h(t_0)\|_{L^2(\Omega)} + \|f_T\|_{L^1(t_0,t_n;L^2(\Omega))} \right).$$

Here, we have used the Cauchy-Schwarz inequality and Eq. (2.4.40). Next, we bound the remaining term in the integral above, and obtain

$$\int_{t_0}^{t_n} \left(f_T(s), T_h(s)\right)_{\mathcal{T}_h} ds \leq \|f_T\|_{L^1(t_0,t_n;L^2(\Omega))} \left(\|T_h(t_0)\|_{L^2(\Omega)} + \|f_T\|_{L^1(t_0,t_n;L^2(\Omega))} \right)$$
$$\leq \frac{1}{2} \|T_h(t_0)\|^2_{L^2(\Omega)} + \frac{3}{2} \|f_T\|^2_{L^1(t_0,t_n;L^2(\Omega))}. \tag{2.4.42}$$

Finally, upon combining Eq. (2.4.42) with Eq. (2.4.41), and substituting in the space-time norm definitions from Eqs. (2.4.33)–(2.4.36), we obtain the desired result (see Eq. (2.4.32)). □

Corollary 2.4.21 (Pointwise Divergence-Free Case)**.** *Suppose that the mixed finite element methods in Eqs.* (2.3.1) – (2.3.3) *are pointwise divergence-free. In addition, suppose we impose a forcing function* f_T *where* $f_T(t) \in L^1(t_0, t_n; L^2(\Omega))$*, a discrete velocity field* $\boldsymbol{u}_h \in \boldsymbol{W}_h$ *where* $\boldsymbol{u}_h(t) \in L^2(t_0, t_n; \boldsymbol{H}_0(\mathrm{div}; \Omega))$*, and a temperature field* $T_h(t_0) \in R_h \subset H^1_0(\Omega)$*. Subject to these assumptions, the discrete temperature*

T_h is governed by the following equation at time $t_n \geq t_0$

$$
\begin{aligned}
&\frac{1}{2}\left\|T_h\left(t_n\right)\right\|_{L^2(\Omega)}^2+\delta\left|T_h\right|_{L^2\left(t_0, t_n ; \boldsymbol{u}_h\right)}^2+\alpha \gamma C_8\left\|T_h\right\|_{L^2\left(t_0, t_n ; \text{grad}, 2\right)}^2 \\
&\leq\left\|T_h\left(t_0\right)\right\|_{L^2(\Omega)}^2+\frac{3}{2}\left\|f_T\right\|_{L^1\left(t_0, t_n ; L^2(\Omega)\right)}^2 .
\end{aligned} \tag{2.4.43}
$$

Proof. The proof immediately follows from setting $\nabla \cdot \boldsymbol{u}_h = 0$ pointwise in Theorem 2.4.20. $\square$

Theorem 2.4.22 (Stability of the Discrete Velocity)**.** *Consider the mixed finite element methods in Eqs.* (2.3.1) – (2.3.3)*, in conjunction with a forcing function $\boldsymbol{f}_u \in L^1\left(t_0, t_n; \boldsymbol{L}^2\left(\Omega\right)\right)$, a discrete temperature field $T_h \in R_h$ where $T_h(t) \in L^1(t_0, t_n; L^2\left(\Omega\right))$, and an initial condition $\boldsymbol{u}_h\left(t_0\right) \in \boldsymbol{W}_h \subset \boldsymbol{H}_0(\text{div}; \Omega)$. Subject to these assumptions, the discrete velocity field $\boldsymbol{u}_h$ is governed by the following equation at time $t_n \geq t_0$*

$$
\begin{aligned}
&\frac{1}{2}\left\|\boldsymbol{u}_h\left(t_n\right)\right\|_{\boldsymbol{L}^2(\Omega)}^2+\zeta\left|\boldsymbol{u}_h\right|_{L^2\left(t_0, t_n ; \boldsymbol{u}_h\right)}^2+C_4 \nu\left\|\boldsymbol{u}_h\right\|_{L^2\left(t_0, t_n ; \text{sym}, 2\right)}^2 \\
&\leq \frac{1}{2}\left(3\left\|\boldsymbol{u}_h\left(t_0\right)\right\|_{\boldsymbol{L}^2(\Omega)}^2+5 \beta^2 g^2\left\|T_h\right\|_{L^1\left(t_0, t_n ; L^2(\Omega)\right)}^2+5\left\|\boldsymbol{f}_u\right\|_{L^1\left(t_0, t_n ; \boldsymbol{L}^2(\Omega)\right)}^2\right),
\end{aligned} \tag{2.4.44}
$$

where

$$
\left\|\boldsymbol{u}_h\right\|_{L^2\left(t_0, t_n ; \text{sym}, 2\right)}=\left(\int_{t_0}^{t_n}\left\|\boldsymbol{u}_h(s)\right\|_{\text{sym}, 2}^2 d s\right)^{1 / 2}, \tag{2.4.45}
$$

is a Bochner-type norm on $\left(t_0, t_n\right) \times \Omega$.

Proof. Let us begin by substituting $q_h = p_h$ and $\boldsymbol{w}_h = \boldsymbol{u}_h$ into Eqs. (2.3.4) and (2.3.5), in order to obtain

$$b_h\left(\boldsymbol{u}_h, p_h\right) = 0,$$

$$\left(\partial_t\, \boldsymbol{u}_h, \boldsymbol{u}_h\right)_{\mathcal{T}_h} + c_h\left(\boldsymbol{u}_h; \boldsymbol{u}_h, \boldsymbol{u}_h\right) + \nu a_h\left(\boldsymbol{u}_h, \boldsymbol{u}_h\right) - b_h\left(\boldsymbol{u}_h, p_h\right) = -\left(\beta T_h \boldsymbol{g}, \boldsymbol{u}_h\right)_{\mathcal{T}_h} + \left(\boldsymbol{f}_u, \boldsymbol{u}_h\right)_{\mathcal{T}_h}.$$

By adding these equations together, we obtain

$$\left(\partial_t\, \boldsymbol{u}_h, \boldsymbol{u}_h\right)_{\mathcal{T}_h} + c_h\left(\boldsymbol{u}_h; \boldsymbol{u}_h, \boldsymbol{u}_h\right) + \nu a_h\left(\boldsymbol{u}_h, \boldsymbol{u}_h\right) = -\left(\beta T_h \boldsymbol{g}, \boldsymbol{u}_h\right)_{\mathcal{T}_h} + \left(\boldsymbol{f}_u, \boldsymbol{u}_h\right)_{\mathcal{T}_h},$$

or equivalently, in accordance with the chain rule

$$\frac{1}{2}\frac{d}{dt}\left\|\boldsymbol{u}_h\right\|^2_{\boldsymbol{L}^2(\Omega)} + c_h\left(\boldsymbol{u}_h; \boldsymbol{u}_h, \boldsymbol{u}_h\right) + \nu a_h\left(\boldsymbol{u}_h, \boldsymbol{u}_h\right) = -\left(\beta T_h \boldsymbol{g}, \boldsymbol{u}_h\right)_{\mathcal{T}_h} + \left(\boldsymbol{f}_u, \boldsymbol{u}_h\right)_{\mathcal{T}_h}.$$

We can now leverage the coercivity of a_h (Lemma 2.4.8) and the semi-coercivity of c_h (Lemma 2.4.10) in order to obtain

$$\frac{1}{2}\frac{d}{dt}\left\|\boldsymbol{u}_h\right\|^2_{\boldsymbol{L}^2(\Omega)} + \zeta\left|\boldsymbol{u}_h\right|^2_{\boldsymbol{u}_h} + \nu\, C_4\left\|\boldsymbol{u}_h\right\|^2_{\mathrm{sym},2} \leq -\left(\beta T_h \boldsymbol{g}, \boldsymbol{u}_h\right)_{\mathcal{T}_h} + \left(\boldsymbol{f}_u, \boldsymbol{u}_h\right)_{\mathcal{T}_h}. \tag{2.4.46}$$

Following the approach of [51], we examine Eq. (2.4.46) and note that

$$\frac{1}{2}\frac{d}{dt}\left\|\boldsymbol{u}_h\right\|^2_{\boldsymbol{L}^2(\Omega)} \leq -\left(\beta T_h \boldsymbol{g}, \boldsymbol{u}_h\right)_{\mathcal{T}_h} + \left(\boldsymbol{f}_u, \boldsymbol{u}_h\right)_{\mathcal{T}_h},$$

and in accordance with the Cauchy-Schwarz inequality

$$\|\boldsymbol{u}_h\|_{\boldsymbol{L}^2(\Omega)} \frac{d}{dt} \|\boldsymbol{u}_h\|_{\boldsymbol{L}^2(\Omega)} \leq \beta g \|T_h\|_{L^2(\Omega)} \|\boldsymbol{u}_h\|_{\boldsymbol{L}^2(\Omega)} + \|\boldsymbol{f}_u\|_{\boldsymbol{L}^2(\Omega)} \|\boldsymbol{u}_h\|_{\boldsymbol{L}^2(\Omega)}$$
$$\frac{d}{dt} \|\boldsymbol{u}_h\|_{\boldsymbol{L}^2(\Omega)} \leq \beta g \|T_h\|_{L^2(\Omega)} + \|\boldsymbol{f}_u\|_{\boldsymbol{L}^2(\Omega)} . \tag{2.4.47}$$

Next, we integrate Eq. (2.4.47) from $t = t_0$ to $t = t_n$ in order to obtain

$$\|\boldsymbol{u}_h(t_n)\|_{\boldsymbol{L}^2(\Omega)} - \|\boldsymbol{u}_h(t_0)\|_{\boldsymbol{L}^2(\Omega)} \leq \beta g \int_{t_0}^{t_n} \|T_h(s)\|_{L^2(\Omega)}\, ds + \int_{t_0}^{t_n} \|\boldsymbol{f}_u(s)\|_{\boldsymbol{L}^2(\Omega)}\, ds,$$

and

$$\|\boldsymbol{u}_h(t_n)\|_{\boldsymbol{L}^2(\Omega)} \leq \|\boldsymbol{u}_h(t_0)\|_{\boldsymbol{L}^2(\Omega)} + \beta g \|T_h\|_{L^1(t_0,t_n,L^2(\Omega))} + \|\boldsymbol{f}_u\|_{L^1(t_0,t_n,\boldsymbol{L}^2(\Omega))} . \tag{2.4.48}$$

Putting aside Eq. (2.4.48) for the moment, we return our focus to Eq. (2.4.46). By integrating Eq. (2.4.46) from $t = t_0$ to $t = t_n$ we obtain

$$\frac{1}{2} \|\boldsymbol{u}_h(t_n)\|^2_{\boldsymbol{L}^2(\Omega)} + \int_{t_0}^{t_n} \left(\zeta \left|\boldsymbol{u}_h(s)\right|^2_{\boldsymbol{u}_h} + \nu\, C_4 \|\boldsymbol{u}_h(s)\|^2_{\text{sym},2} \right) ds \tag{2.4.49}$$
$$\leq \frac{1}{2} \|\boldsymbol{u}_h(t_0)\|^2_{\boldsymbol{L}^2(\Omega)} - \beta \int_{t_0}^{t_n} \left(T_h(s)\, \boldsymbol{g}, \boldsymbol{u}_h(s)\right)_{\mathcal{T}_h} ds + \int_{t_0}^{t_n} \left(\boldsymbol{f}_u(s), \boldsymbol{u}_h(s)\right)_{\mathcal{T}_h} ds.$$

We can rewrite the last two terms on the RHS of Eq. (2.4.49) by applying the

Cauchy-Schwarz inequality, Eq. (2.4.48), and Young's inequality as follows

$$
\begin{aligned}
& -\beta \int_{t_0}^{t_n} \left(T_h\left(s\right) \boldsymbol{g}, \boldsymbol{u}_h\left(s\right)\right)_{\mathcal{T}_h} ds \\
& \leq \beta g \int_{t_0}^{t_n} \left[\left\|T_h\left(s\right)\right\|_{L^2(\Omega)} \left\|\boldsymbol{u}_h\left(s\right)\right\|_{\boldsymbol{L}^2(\Omega)}\right] ds \\
& \leq \beta g \int_{t_0}^{t_n} \left[\left\|T_h\left(s\right)\right\|_{L^2(\Omega)} \left(\left\|\boldsymbol{u}_h\left(t_0\right)\right\|_{\boldsymbol{L}^2(\Omega)} + \beta g \left\|T_h\right\|_{L^1(t_0,s,L^2(\Omega))} + \left\|\boldsymbol{f}_u\right\|_{L^1(t_0,s,\boldsymbol{L}^2(\Omega))}\right)\right] ds \\
& \leq \beta g \int_{t_0}^{t_n} \left\|T_h\left(s\right)\right\|_{L^2(\Omega)} ds \left(\left\|\boldsymbol{u}_h\left(t_0\right)\right\|_{\boldsymbol{L}^2(\Omega)} + \beta g \left\|T_h\right\|_{L^1(t_0,t_n,L^2(\Omega))} + \left\|\boldsymbol{f}_u\right\|_{L^1(t_0,t_n,\boldsymbol{L}^2(\Omega))}\right) \\
& = \beta g \left\|T_h\right\|_{L^1(t_0,t_n,L^2(\Omega))} \left(\left\|\boldsymbol{u}_h\left(t_0\right)\right\|_{\boldsymbol{L}^2(\Omega)} + \beta g \left\|T_h\right\|_{L^1(t_0,t_n,L^2(\Omega))} + \left\|\boldsymbol{f}_u\right\|_{L^1(t_0,t_n,\boldsymbol{L}^2(\Omega))}\right) \\
& \leq \frac{1}{2} \left\|\boldsymbol{u}_h\left(t_0\right)\right\|^2_{\boldsymbol{L}^2(\Omega)} + 2\beta^2 g^2 \left\|T_h\right\|^2_{L^1(t_0,t_n,L^2(\Omega))} + \frac{1}{2} \left\|\boldsymbol{f}_u\right\|^2_{L^1(t_0,t_n,\boldsymbol{L}^2(\Omega))}. \qquad (2.4.50)
\end{aligned}
$$

and

$$
\begin{aligned}
& \int_{t_0}^{t_n} \left(\boldsymbol{f}_u\left(s\right), \boldsymbol{u}_h\left(s\right)\right)_{\mathcal{T}_h} ds \\
& \leq \int_{t_0}^{t_n} \left[\left\|\boldsymbol{f}_u\left(s\right)\right\|_{\boldsymbol{L}^2(\Omega)} \left\|\boldsymbol{u}_h\left(s\right)\right\|_{\boldsymbol{L}^2(\Omega)}\right] ds \\
& \leq \int_{t_0}^{t_n} \left[\left\|\boldsymbol{f}_u\left(s\right)\right\|_{\boldsymbol{L}^2(\Omega)} \left(\left\|\boldsymbol{u}_h\left(t_0\right)\right\|_{\boldsymbol{L}^2(\Omega)} + \beta g \left\|T_h\right\|_{L^1(t_0,s,L^2(\Omega))} + \left\|\boldsymbol{f}_u\right\|_{L^1(t_0,s,\boldsymbol{L}^2(\Omega))}\right)\right] ds \\
& \leq \int_{t_0}^{t_n} \left\|\boldsymbol{f}_u\left(s\right)\right\|_{\boldsymbol{L}^2(\Omega)} ds \left(\left\|\boldsymbol{u}_h\left(t_0\right)\right\|_{\boldsymbol{L}^2(\Omega)} + \beta g \left\|T_h\right\|_{L^1(t_0,t_n,L^2(\Omega))} + \left\|\boldsymbol{f}_u\right\|_{L^1(t_0,t_n,\boldsymbol{L}^2(\Omega))}\right) \\
& = \left\|\boldsymbol{f}_u\right\|_{L^1(t_0,t_n,\boldsymbol{L}^2(\Omega))} \left(\left\|\boldsymbol{u}_h\left(t_0\right)\right\|_{\boldsymbol{L}^2(\Omega)} + \beta g \left\|T_h\right\|_{L^1(t_0,t_n,L^2(\Omega))} + \left\|\boldsymbol{f}_u\right\|_{L^1(t_0,t_n,\boldsymbol{L}^2(\Omega))}\right) \\
& \leq \frac{1}{2} \left\|\boldsymbol{u}_h\left(t_0\right)\right\|^2_{\boldsymbol{L}^2(\Omega)} + \frac{1}{2}\beta^2 g^2 \left\|T_h\right\|^2_{L^1(t_0,t_n,L^2(\Omega))} + 2 \left\|\boldsymbol{f}_u\right\|^2_{L^1(t_0,t_n,\boldsymbol{L}^2(\Omega))}. \qquad (2.4.51)
\end{aligned}
$$

Upon combining Eqs. (2.4.49), (2.4.50), and (2.4.51), we obtain the desired bound on the discrete kinetic energy, (see Eq. (2.4.44)). $\square$

Theorem 2.4.23 (Stability of the Discrete Kinematic Pressure). *Consider the mixed finite element methods in Eqs.* (2.3.1) – (2.3.3), *in conjunction with a forcing function* $\boldsymbol{f}_u \in L^2(t_0, t_n; \boldsymbol{L}^2(\Omega))$, *a discrete temperature field* $T_h \in R_h$ *where* $T_h(t) \in L^2(t_0, t_n; L^2(\Omega))$, *and a discrete velocity field* $\boldsymbol{u}_h \in \boldsymbol{W}_h$ *where* $\boldsymbol{u}_h(t) \in L^4\left(t_0, t_n; \boldsymbol{H}_0(\mathrm{div}; \Omega) \cap \boldsymbol{W}_h^{1,4}(\mathcal{T}_h)\right)$. *Subject to these assumptions, the discrete kinematic pressure field* p_h *is governed by the following equation at time* $t_n \geq t_0$

$$\begin{aligned}
\|p_h\|_{L^1(t_0,t_n;L^2(\Omega))} \leq C_{13} &\left(C_6 \|\boldsymbol{u}_h\|^2_{L^2(t_0,t_n;\mathrm{grad},2)} + \nu C_3 C_5 \|\boldsymbol{u}_h\|_{L^1(t_0,t_n;\mathrm{sym},2)} \right) \\
&+ C_t C_{13} \sigma_{2,2} \left[\sqrt{\nu a_h\left(\boldsymbol{u}_h(t_0), \boldsymbol{u}_h(t_0)\right)} + \sqrt{3} C_7 \|\boldsymbol{u}_h\|^2_{L^4(t_0,t_n;\mathrm{grad},4)} \right. \\
&\left. + \beta g \left(1 + \sqrt{3}\right) \|T_h\|_{L^2(t_0,t_n;L^2(\Omega))} + \left(1 + \sqrt{3}\right) \|\boldsymbol{f}_u\|_{L^2(t_0,t_n;\boldsymbol{L}^2(\Omega))} \right],
\end{aligned} \tag{2.4.52}$$

where C_t *is a constant that depends on the length of the time interval* $[t_0, t_n]$.

Proof. We begin by rewriting Eq. (2.3.5) as follows

$$\begin{aligned}
b_h\left(\boldsymbol{w}_h, p_h\right) = \left(\nabla \cdot \boldsymbol{w}_h, p_h\right)_{\mathcal{T}_h} =& c_h\left(\boldsymbol{u}_h; \boldsymbol{u}_h, \boldsymbol{w}_h\right) + \nu a_h\left(\boldsymbol{u}_h, \boldsymbol{w}_h\right) \\
&+ \left(\partial_t \boldsymbol{u}_h, \boldsymbol{w}_h\right)_{\mathcal{T}_h} + \left(\beta T_h \boldsymbol{g}, \boldsymbol{w}_h\right)_{\mathcal{T}_h} - \left(\boldsymbol{f}_u, \boldsymbol{w}_h\right)_{\mathcal{T}_h}.
\end{aligned}$$

Next, we can apply the Cauchy–Schwarz inequality, the boundedness of the convective trilinear form c_h (Lemma 2.4.11), and the boundedness of the bilinear form a_h (Lemma 2.4.9) as follows

$$
\begin{aligned}
(\nabla \cdot \boldsymbol{w}_h, p_h)_{\mathcal{T}_h} \leq{} & C_6 \left\|\boldsymbol{u}_h\right\|_{\text{grad},2}^2 \left\|\boldsymbol{w}_h\right\|_{\text{grad},2} + \nu C_5 \left\|\boldsymbol{u}_h\right\|_{\text{sym},2} \left\|\boldsymbol{w}_h\right\|_{\text{sym},2} \\
& + \left\|\partial_t \boldsymbol{u}_h\right\|_{\boldsymbol{L}^2(\Omega)} \left\|\boldsymbol{w}_h\right\|_{\boldsymbol{L}^2(\Omega)} + \beta g \left\|T_h\right\|_{L^2(\Omega)} \left\|\boldsymbol{w}_h\right\|_{\boldsymbol{L}^2(\Omega)} + \left\|\boldsymbol{f}_u\right\|_{\boldsymbol{L}^2(\Omega)} \left\|\boldsymbol{w}_h\right\|_{\boldsymbol{L}^2(\Omega)}.
\end{aligned}
$$

Upon applying the inverse Korn's inequality in Lemma 2.4.7, and the embedding inequality in Lemma B.1.3, one obtains

$$
\begin{aligned}
(\nabla \cdot \boldsymbol{w}_h, p_h)_{\mathcal{T}_h} \leq{} & C_6 \left\|\boldsymbol{u}_h\right\|_{\text{grad},2}^2 \left\|\boldsymbol{w}_h\right\|_{\text{grad},2} + \nu C_3 C_5 \left\|\boldsymbol{u}_h\right\|_{\text{sym},2} \left\|\boldsymbol{w}_h\right\|_{\text{grad},2} \\
& + \sigma_{2,2} \left(\left\|\partial_t \boldsymbol{u}_h\right\|_{\boldsymbol{L}^2(\Omega)} + \beta g \left\|T_h\right\|_{L^2(\Omega)} + \left\|\boldsymbol{f}_u\right\|_{\boldsymbol{L}^2(\Omega)} \right) \left\|\boldsymbol{w}_h\right\|_{\text{grad},2}.
\end{aligned}
\tag{2.4.53}
$$

We can simplify Eq. (2.4.53) by dividing both sides by $\left\|\boldsymbol{w}_h\right\|_{\text{grad},2}$, taking the supremum, and using the inf-sup condition (Lemma 2.4.17 or 2.4.18) with $q_h = p_h$ and $p = p' = 2$ as follows

$$
\begin{aligned}
\frac{1}{C_{13}} \left\|p_h\right\|_{L^2(\Omega)} &\leq \sup_{\boldsymbol{w}_h \in \boldsymbol{W}_h \setminus \{\boldsymbol{0}\}} \frac{(\nabla \cdot \boldsymbol{w}_h, p_h)_{\mathcal{T}_h}}{\left\|\boldsymbol{w}_h\right\|_{\text{grad},2}} \\
&\leq C_6 \left\|\boldsymbol{u}_h\right\|_{\text{grad},2}^2 + \nu C_3 C_5 \left\|\boldsymbol{u}_h\right\|_{\text{sym},2} \\
&\quad + \sigma_{2,2} \left(\left\|\partial_t \boldsymbol{u}_h\right\|_{\boldsymbol{L}^2(\Omega)} + \beta g \left\|T_h\right\|_{L^2(\Omega)} + \left\|\boldsymbol{f}_u\right\|_{\boldsymbol{L}^2(\Omega)} \right),
\end{aligned}
$$

or equivalently

$$\|p_h\|_{L^2(\Omega)} \leq C_{13}\Big(C_6 \|\boldsymbol{u}_h\|^2_{\text{grad},2} + \nu C_3 C_5 \|\boldsymbol{u}_h\|_{\text{sym},2}$$
$$+ \sigma_{2,2}\left(\|\partial_t \boldsymbol{u}_h\|_{\boldsymbol{L}^2(\Omega)} + \beta g \|T_h\|_{L^2(\Omega)} + \|\boldsymbol{f}_u\|_{\boldsymbol{L}^2(\Omega)}\right)\Big). \tag{2.4.54}$$

Eq. (2.4.54) can be integrated from $t = t_0$ to $t = t_n$. Thereafter, Hölder's inequality can be applied in order to obtain

$$\int_{t_0}^{t_n} \|p_h(s)\|_{L^2(\Omega)}\, ds$$
$$\leq C_{13}\left(C_6 \int_{t_0}^{t_n} \|\boldsymbol{u}_h(s)\|^2_{\text{grad},2}\, ds + \nu C_3 C_5 \int_{t_0}^{t_n} \|\boldsymbol{u}_h(s)\|_{\text{sym},2}\, ds\right)$$
$$+ C_t\, C_{13}\, \sigma_{2,2}\left[\left(\int_{t_0}^{t_n} \|\partial_t \boldsymbol{u}_h(s)\|^2_{\boldsymbol{L}^2(\Omega)}\, ds\right)^{1/2} + \beta g \left(\int_{t_0}^{t_n} \|T_h(s)\|^2_{L^2(\Omega)}\, ds\right)^{1/2}\right.$$
$$\left. + \left(\int_{t_0}^{t_n} \|\boldsymbol{f}_u(s)\|^2_{\boldsymbol{L}^2(\Omega)}\, ds\right)^{1/2}\right], \tag{2.4.55}$$

where $C_t = \sqrt{t_n - t_0}$.

It remains for us to create an upper bound for the following term above

$$\left(\int_{t_0}^{t_n} \|\partial_t \boldsymbol{u}_h(s)\|^2_{\boldsymbol{L}^2(\Omega)}\, ds\right)^{1/2}.$$

Towards this end, we can substitute $\boldsymbol{w}_h = \partial_t \boldsymbol{u}_h$ into Eq. (2.3.5)

$$\begin{aligned}(\partial_t \boldsymbol{u}_h, \partial_t \boldsymbol{u}_h)_{\mathcal{T}_h} =& - c_h(\boldsymbol{u}_h; \boldsymbol{u}_h, \partial_t \boldsymbol{u}_h) - \nu a_h(\boldsymbol{u}_h, \partial_t \boldsymbol{u}_h) + b_h(\partial_t \boldsymbol{u}_h, p_h) \\ & - (\beta T_h \boldsymbol{g}, \partial_t \boldsymbol{u}_h)_{\mathcal{T}_h} + (\boldsymbol{f}_u, \partial_t \boldsymbol{u}_h)_{\mathcal{T}_h}. \end{aligned} \tag{2.4.56}$$

We can introduce the following simplifications on the RHS of Eq. (2.4.56)

$$b_h(\partial_t \boldsymbol{u}_h, p_h) = (\nabla \cdot (\partial_t \boldsymbol{u}_h), p_h)_{\mathcal{T}_h} = 0,$$

and

$$a_h(\boldsymbol{u}_h, \partial_t \boldsymbol{u}_h) = \frac{1}{2}\frac{d}{dt}(a_h(\boldsymbol{u}_h, \boldsymbol{u}_h)),$$

where these relations hold because $\partial_t \boldsymbol{u}_h \in \boldsymbol{W}_h^{\text{div}}$, and the operator a_h possesses bilinear and symmetrical properties. Thereafter, one obtains

$$\begin{aligned}(\partial_t \boldsymbol{u}_h, \partial_t \boldsymbol{u}_h)_{\mathcal{T}_h} + \frac{\nu}{2}\frac{d}{dt}(a_h(\boldsymbol{u}_h, \boldsymbol{u}_h)) =& - c_h(\boldsymbol{u}_h; \boldsymbol{u}_h, \partial_t \boldsymbol{u}_h) \\ & - (\beta T_h \boldsymbol{g}, \partial_t \boldsymbol{u}_h)_{\mathcal{T}_h} + (\boldsymbol{f}_u, \partial_t \boldsymbol{u}_h)_{\mathcal{T}_h}. \end{aligned} \tag{2.4.57}$$

We can leverage the boundedness of the convective trilinear form (Lemma 2.4.11) and the Cauchy-Schwarz inequality to rewrite the RHS of Eq. (2.4.57) as follows

$$
\begin{aligned}
&(\partial_t \boldsymbol{u}_h, \partial_t \boldsymbol{u}_h)_{\mathcal{T}_h} + \frac{\nu}{2}\frac{d}{dt}\left(a_h(\boldsymbol{u}_h, \boldsymbol{u}_h)\right) \\
&\leq \left(C_7 \left\|\boldsymbol{u}_h\right\|_{\mathrm{grad},4}^2 + \beta g \left\|T_h\right\|_{L^2(\Omega)} + \left\|\boldsymbol{f}_u\right\|_{\boldsymbol{L}^2(\Omega)}\right) \left\|\partial_t \boldsymbol{u}_h\right\|_{\boldsymbol{L}^2(\Omega)},
\end{aligned}
$$

or equivalently, upon applying Young's inequality and the root-mean-square-arithmetic-mean inequality

$$
\begin{aligned}
&\left\|\partial_t \boldsymbol{u}_h\right\|_{\boldsymbol{L}^2(\Omega)}^2 + \frac{\nu}{2}\frac{d}{dt}\left(a_h(\boldsymbol{u}_h, \boldsymbol{u}_h)\right) \\
&\leq \frac{3}{2}\left(C_7^2 \left\|\boldsymbol{u}_h\right\|_{\mathrm{grad},4}^4 + \beta^2 g^2 \left\|T_h\right\|_{L^2(\Omega)}^2 + \left\|\boldsymbol{f}_u\right\|_{\boldsymbol{L}^2(\Omega)}^2\right) + \frac{1}{2}\left\|\partial_t \boldsymbol{u}_h\right\|_{\boldsymbol{L}^2(\Omega)}^2. \qquad (2.4.58)
\end{aligned}
$$

Next, we can integrate Eq. (2.4.58) from $t = t_0$ to $t = t_n$ as follows

$$
\begin{aligned}
&\int_{t_0}^{t_n} \left\|\partial_t \boldsymbol{u}_h(s)\right\|_{\boldsymbol{L}^2(\Omega)}^2 \, ds + \nu a_h\left(\boldsymbol{u}_h(t_n), \boldsymbol{u}_h(t_n)\right) \\
&\leq \nu a_h\left(\boldsymbol{u}_h(t_0), \boldsymbol{u}_h(t_0)\right) + 3\Bigg[C_7^2 \int_{t_0}^{t_n} \left\|\boldsymbol{u}_h(s)\right\|_{\mathrm{grad},4}^4 \, ds \\
&+ \beta^2 g^2 \int_{t_0}^{t_n} \left\|T_h(s)\right\|_{L^2(\Omega)}^2 \, ds + \int_{t_0}^{t_n} \left\|\boldsymbol{f}_u(s)\right\|_{\boldsymbol{L}^2(\Omega)}^2 \, ds\Bigg]. \qquad (2.4.59)
\end{aligned}
$$

On taking the square root of both sides of Eq. (2.4.59), one obtains

$$\begin{aligned}
&\left(\int_{t_0}^{t_n} \|\partial_t \boldsymbol{u}_h(s)\|^2_{\boldsymbol{L}^2(\Omega)}\, ds\right)^{1/2} \\
&\leq \sqrt{\nu a_h\left(\boldsymbol{u}_h(t_0), \boldsymbol{u}_h(t_0)\right)} + \sqrt{3}\Bigg[C_7\left(\int_{t_0}^{t_n} \|\boldsymbol{u}_h(s)\|^4_{\text{grad},4}\, ds\right)^{1/2} \\
&+ \beta g\left(\int_{t_0}^{t_n} \|T_h(s)\|^2_{L^2(\Omega)}\, ds\right)^{1/2} + \left(\int_{t_0}^{t_n} \|\boldsymbol{f}_u(s)\|^2_{\boldsymbol{L}^2(\Omega)}\, ds\right)^{1/2}\Bigg].
\end{aligned} \tag{2.4.60}$$

Here, we have used the fact that $a_h\left(\boldsymbol{u}_h(t_n), \boldsymbol{u}_h(t_n)\right) \geq 0$. Now, upon substituting Eq. (2.4.60) into Eq. (2.4.55), we obtain the desired result

$$\begin{aligned}
&\int_{t_0}^{t_n} \|p_h(s)\|_{L^2(\Omega)}\, ds \\
&\leq C_{13}\left(C_6\int_{t_0}^{t_n} \|\boldsymbol{u}_h(s)\|^2_{\text{grad},2}\, ds + \nu C_3 C_5 \int_{t_0}^{t_n} \|\boldsymbol{u}_h(s)\|_{\text{sym},2}\, ds\right) \\
&+ C_t\, C_{13}\, \sigma_{2,2}\Bigg[\sqrt{\nu a_h\left(\boldsymbol{u}_h(t_0), \boldsymbol{u}_h(t_0)\right)} + \sqrt{3}C_7\left(\int_{t_0}^{t_n} \|\boldsymbol{u}_h(s)\|^4_{\text{grad},4}\, ds\right)^{1/2} \\
&+ \beta g(1+\sqrt{3})\left(\int_{t_0}^{t_n} \|T_h(s)\|^2_{L^2(\Omega)}\, ds\right)^{1/2} + (1+\sqrt{3})\left(\int_{t_0}^{t_n} \|\boldsymbol{f}_u(s)\|^2_{\boldsymbol{L}^2(\Omega)}\, ds\right)^{1/2}\Bigg],
\end{aligned} \tag{2.4.61}$$

□

Remark 2.4.1. Establishing the stability of the versatile mixed methods becomes more complicated if we incorporate additional physics into the temperature equation. This can be done by simply adding a viscous dissipation term to the RHS of

Eq. (2.2.3). In section 2.5, we briefly consider the formulation that arises when we incorporate this term. In addition, in the subsequent section (section 2.6), we will present the results of numerical experiments to establish the practical consequences of including the viscous dissipation term for both non-pointwise divergence-free, and pointwise divergence-free methods.

2.4.4 Error Estimates

In this section, we obtain error estimates for the discrete velocity, temperature, and kinematic pressure fields, for H1-conforming versatile mixed methods. We limit our analysis to the H1-conforming case, as the H(div)-conforming case has already been rigorously analyzed in the work of Schroeder et al. [43, 44], and it requires a different set of analysis techniques. The analysis in this section is a natural extension of Dallmann et al.'s work [1,7], which focused primarily on non-versatile, H1-conforming methods.

Theorem 2.4.24 (Error of the Discrete Velocity and Temperature)**.** *Consider the class of H1-conforming mixed methods that satisfy Eqs.* (2.3.1)–(2.3.3)*. Suppose that the exact solution* $(\boldsymbol{u}, T, p) : [t_0, t_n] \longrightarrow \boldsymbol{W} \times R \times Q$ *and approximate solution* $(\boldsymbol{u}_h, T_h, p_h) : [t_0, t_n] \longrightarrow \boldsymbol{W}_h \times R_h \times Q_h$ *reside in the following spaces*

$$\boldsymbol{u} \in L^\infty\left(t_0, t_n; \boldsymbol{W}^{1,\infty}(\Omega)\right), \qquad \partial_t \boldsymbol{u} \in L^2\left(t_0, t_n; \boldsymbol{L}^2(\Omega)\right), \qquad p \in L^2\left(t_0, t_n; Q \cap C^0(\Omega)\right),$$

$$T \in L^\infty\left(t_0, t_n; W^{1,\infty}(\Omega)\right), \qquad \partial_t T \in L^2\left(t_0, t_n; L^2(\Omega)\right), \qquad \boldsymbol{u}_h \in L^\infty\left(t_0, t_n; \boldsymbol{L}^\infty(\Omega)\right),$$

$$\nabla \cdot \boldsymbol{u}_h \in L^\infty\left(t_0, t_n; L^\infty(\Omega)\right).$$

In addition, suppose $\boldsymbol{u}_h(t_0) = j_u \boldsymbol{u}_0$ and $T_h(t_0) = j_T T_0$ and Assumption 2.4.19 holds. Under these circumstances, the discrete errors $\boldsymbol{e}_{u,h} = j_u \boldsymbol{u} - \boldsymbol{u}_h$ and $e_{T,h} = j_T T - T_h$ are bounded as follows

$$
\begin{aligned}
&\|e_{T,h}(t_n)\|^2_{L^2(\Omega)} + \|\boldsymbol{e}_{u,h}(t_n)\|^2_{L^2(\Omega)} + \int_{t_0}^{t_n} \Big(C_A \nu \|\boldsymbol{e}_{u,h}(s)\|^2_{\mathrm{sym},2} + C_B \alpha\gamma \|e_{T,h}(s)\|^2_{\mathrm{grad},2} \Big)\, ds \\
&\lesssim \int_{t_0}^{t_n} \left(\exp \int_s^{t_n} C_G(\vartheta)\, d\vartheta \right) \\
&\times \sum_{K\in\mathcal{T}_h} \Bigg[h_K^{2k_u} \Big[\big(2 + \nu Re_K^2 + 2\nu + 3\nu(\gamma + (\gamma-1)C_{\mathrm{mod}})\big) \|\boldsymbol{u}(s)\|^2_{W^{k_u+1,2}(K)} \\
&+ \|\partial_t \boldsymbol{u}(s)\|^2_{W^{k_u,2}(K)} \Big] + \frac{h_K^{2k_p+2}}{\nu} \|p(s)\|^2_{W^{k_p+1}(K)} \\
&+ h_K^{2k_T} \left[\left(\alpha\gamma + \frac{\alpha}{\gamma} Pe_K^2 + h_K^2 \beta \|\boldsymbol{g}\|_{L^\infty(K)} \right) \|T(s)\|^2_{W^{k_T+1,2}(K)} + \|\partial_t T(s)\|^2_{W^{k_T,2}(K)} \right] \Bigg]\, ds,
\end{aligned} \tag{2.4.62}
$$

where $k_u = k+1$, $k_T = k+1$, and $k_p = k$. Finally, C_A and C_B are generic *constants, and C_G is the Gronwall constant*

$$\begin{aligned}
C_G(s) &= 1 + \beta \left\|\boldsymbol{g}\right\|_{L^\infty(\Omega)} + \left|\boldsymbol{u}(s)\right|_{W^{1,\infty}(\Omega)} \\
&\quad + \left(1 + \frac{1}{\nu}\right) \max_{K \in \mathcal{T}_h} \{h_K^2 \left|\boldsymbol{u}(s)\right|^2_{W^{1,\infty}(K)}\} + \frac{1}{\nu} \left\|\boldsymbol{u}(s)\right\|^2_{L^\infty(\Omega)} \\
&\quad + \left|T(s)\right|_{W^{1,\infty}(\Omega)} + \left(1 + \frac{\gamma}{\nu}\right) \max_{K \in \mathcal{T}_h} \{h_K^2 \left|T(s)\right|^2_{W^{1,\infty}(K)}\} + \frac{\gamma}{\nu} \left\|T(s)\right\|^2_{L^\infty(\Omega)} \\
&\quad + (\gamma - 1) \left\|\nabla \cdot \boldsymbol{u}_h(s)\right\|_{L^\infty(\Omega)} + \frac{C_{\text{mod}} \, (\gamma - 1)}{\nu} \max_{K \in \mathcal{T}_h} \{h_K^{-2}\} \left\|T(s)\right\|^2_{W^{1,\infty}(\Omega)} \\
&\quad + C_{\text{mod}} \, (\gamma - 1) \max_{K \in \mathcal{T}_h} \{h_K^{-2}\} \left\|\nabla \cdot \boldsymbol{u}_h(s)\right\|_{L^\infty(\Omega)} . \qquad (2.4.63)
\end{aligned}$$

Proof. We begin our proof by rewriting the discrete governing equations in terms of the exact solution $\boldsymbol{u}$, T, and p

$$b_h \left(\boldsymbol{u}, q\right) = 0, \qquad (2.4.64)$$

$$\begin{aligned}
&\left(\partial_t \, \boldsymbol{u}, \boldsymbol{w}\right)_{\mathcal{T}_h} + c_h \left(\boldsymbol{u}; \boldsymbol{u}, \boldsymbol{w}\right) + \nu a_h \left(\boldsymbol{u}, \boldsymbol{w}\right) - b_h \left(\boldsymbol{w}, p\right) \\
&= - \left(\beta T \boldsymbol{g}, \boldsymbol{w}\right)_{\mathcal{T}_h} + \left(\boldsymbol{f}_u, \boldsymbol{w}\right)_{\mathcal{T}_h} , \qquad (2.4.65)
\end{aligned}$$

$$\begin{aligned}
&\left(\partial_t T, r\right)_{\mathcal{T}_h} + \underline{c}_h \left(\boldsymbol{u}; T, r\right) + \alpha\gamma \, \underline{a}_h \left(T, r\right) \\
&= - \left(\gamma - 1\right) \Big[\left(\left(\nabla \cdot \boldsymbol{u}\right) T, r\right)_{\mathcal{T}_h} + C_{\text{mod}} \left(\left|\nabla \cdot \boldsymbol{u}\right| \nabla T, \nabla r\right)_{\mathcal{T}_h} \Big] + \left(f_T, r\right)_{\mathcal{T}_h} . \qquad (2.4.66)
\end{aligned}$$

We can likewise write out the equations for our H1-conforming finite element methods

$$b_h\left(\boldsymbol{u}_h, q_h\right) = 0, \tag{2.4.67}$$

$$\left(\partial_t \, \boldsymbol{u}_h, \boldsymbol{w}_h\right)_{\mathcal{T}_h} + c_h\left(\boldsymbol{u}_h; \boldsymbol{u}_h, \boldsymbol{w}_h\right) + \nu a_h\left(\boldsymbol{u}_h, \boldsymbol{w}_h\right) - b_h\left(\boldsymbol{w}_h, p_h\right)$$

$$= -\left(\beta T_h \boldsymbol{g}, \boldsymbol{w}_h\right)_{\mathcal{T}_h} + \left(\boldsymbol{f}_u, \boldsymbol{w}_h\right)_{\mathcal{T}_h}, \tag{2.4.68}$$

$$\left(\partial_t T_h, r_h\right)_{\mathcal{T}_h} + \underline{c}_h\left(\boldsymbol{u}_h; T_h, r_h\right) + \alpha\gamma \, \underline{a}_h\left(T_h, r_h\right)$$

$$= -\left(\gamma - 1\right)\Big[\left(\left(\nabla \cdot \boldsymbol{u}_h\right) T_h, r_h\right)_{\mathcal{T}_h} + C_{\text{mod}}\left(\left|\nabla \cdot \boldsymbol{u}_h\right| \nabla T_h, \nabla r_h\right)_{\mathcal{T}_h}\Big] + \left(f_T, r_h\right)_{\mathcal{T}_h}. \tag{2.4.69}$$

We then set $\boldsymbol{w}_h = \boldsymbol{e}_{u,h}$ and $r_h = e_{T,h}$, and subtract Eq. (2.4.68) from (2.4.65), and Eq. (2.4.69) from (2.4.66) in order to obtain error equations for the linear momentum and temperature, respectively

$$\left(\partial_t \, \left(\boldsymbol{u} - \boldsymbol{u}_h\right), \boldsymbol{e}_{u,h}\right)_{\mathcal{T}_h} + c_h\left(\boldsymbol{u}; \boldsymbol{u}, \boldsymbol{e}_{u,h}\right) - c_h\left(\boldsymbol{u}_h; \boldsymbol{u}_h, \boldsymbol{e}_{u,h}\right) + \nu a_h\left(\boldsymbol{u} - \boldsymbol{u}_h, \boldsymbol{e}_{u,h}\right)$$

$$- b_h\left(\boldsymbol{e}_{u,h}, p - p_h\right) = -\left(\beta\left(T - T_h\right)\boldsymbol{g}, \boldsymbol{e}_{u,h}\right)_{\mathcal{T}_h}, \tag{2.4.70}$$

$$\left(\partial_t\left(T - T_h\right), e_{T,h}\right)_{\mathcal{T}_h} + \underline{c}_h\left(\boldsymbol{u}; T, e_{T,h}\right) - \underline{c}_h\left(\boldsymbol{u}_h; T_h, e_{T,h}\right) + \alpha\gamma \, \underline{a}_h\left(T - T_h, e_{T,h}\right)$$

$$= -\left(\gamma - 1\right)\Big[\left(\left(\nabla \cdot \boldsymbol{u}\right) T, e_{T,h}\right)_{\mathcal{T}_h} - \left(\left(\nabla \cdot \boldsymbol{u}_h\right) T_h, e_{T,h}\right)_{\mathcal{T}_h}$$

$$+ C_{\text{mod}}\left(\left|\nabla \cdot \boldsymbol{u}\right| \nabla T, \nabla e_{T,h}\right)_{\mathcal{T}_h} - C_{\text{mod}}\left(\left|\nabla \cdot \boldsymbol{u}_h\right| \nabla T_h, \nabla e_{T,h}\right)_{\mathcal{T}_h}\Big]. \tag{2.4.71}$$

Focusing on Eq. (2.4.70), we can rewrite $\boldsymbol{u} - \boldsymbol{u}_h$ as $\boldsymbol{\eta}_{u,h} + \boldsymbol{e}_{u,h}$ using Definition 2.4.3. Then, using the fact that $b_h\left(e_{p,h}, \boldsymbol{e}_{u,h}\right) = 0$ because $\boldsymbol{e}_{u,h} \in \boldsymbol{H}_0(\text{div}; \Omega)$, we obtain the following expression

$$
\begin{aligned}
&\left(\partial_t \boldsymbol{e}_{u,h}, \boldsymbol{e}_{u,h}\right)_{\mathcal{T}_h} + \nu a_h\left(\boldsymbol{e}_{u,h}, \boldsymbol{e}_{u,h}\right) \\
&= -\left(\partial_t \boldsymbol{\eta}_{u,h}, \boldsymbol{e}_{u,h}\right)_{\mathcal{T}_h} - c_h\left(\boldsymbol{u}; \boldsymbol{u}, \boldsymbol{e}_{u,h}\right) + c_h\left(\boldsymbol{u}_h; \boldsymbol{u}_h, \boldsymbol{e}_{u,h}\right) \\
&- \nu a_h\left(\boldsymbol{\eta}_{u,h}, \boldsymbol{e}_{u,h}\right) + b_h\left(\boldsymbol{e}_{u,h}, \eta_{p,h}\right) - \left(\beta \eta_{T,h} \boldsymbol{g}, \boldsymbol{e}_{u,h}\right)_{\mathcal{T}_h} - \left(\beta e_{T,h} \boldsymbol{g}, \boldsymbol{e}_{u,h}\right)_{\mathcal{T}_h}.
\end{aligned} \tag{2.4.72}
$$

We can bound the non-convective terms in Eq. (2.4.72) as follows

$$
\begin{aligned}
\left(\partial_t \boldsymbol{e}_{u,h}, \boldsymbol{e}_{u,h}\right)_{\mathcal{T}_h} &= \frac{1}{2}\partial_t \left\|\boldsymbol{e}_{u,h}\right\|_{L^2(\Omega)}^2, \\
\nu a_h\left(\boldsymbol{e}_{u,h}, \boldsymbol{e}_{u,h}\right) &\geq \nu C_4 \left\|\boldsymbol{e}_{u,h}\right\|_{\mathrm{sym},2}^2, \\
\left(\partial_t \boldsymbol{\eta}_{u,h}, \boldsymbol{e}_{u,h}\right)_{\mathcal{T}_h} &\leq \left\|\partial_t \boldsymbol{\eta}_{u,h}\right\|_{L^2(\Omega)} \left\|\boldsymbol{e}_{u,h}\right\|_{L^2(\Omega)} \leq \frac{1}{4}\left\|\partial_t \boldsymbol{\eta}_{u,h}\right\|_{L^2(\Omega)}^2 + \left\|\boldsymbol{e}_{u,h}\right\|_{L^2(\Omega)}^2, \\
\nu a_h\left(\boldsymbol{\eta}_{u,h}, \boldsymbol{e}_{u,h}\right) &\leq \nu C_5 \left\|\boldsymbol{\eta}_{u,h}\right\|_{\mathrm{sym},2} \left\|\boldsymbol{e}_{u,h}\right\|_{\mathrm{sym},2}, \\
b_h\left(\boldsymbol{e}_{u,h}, \eta_{p,h}\right) &\leq C_1 C_2 \left\|\eta_{p,h}\right\|_{L^2(\Omega)} \left\|\boldsymbol{e}_{u,h}\right\|_{\mathrm{sym},2},
\end{aligned}
$$

$$
\begin{aligned}
(\beta\eta_{T,h}\boldsymbol{g},\boldsymbol{e}_{u,h})_{\mathcal{T}_h} + (\beta e_{T,h}\boldsymbol{g},\boldsymbol{e}_{u,h})_{\mathcal{T}_h} &\le \beta\left\|\boldsymbol{g}\right\|_{L^\infty(\Omega)}\left(\left\|e_{T,h}\right\|_{L^2(\Omega)} + \left\|\eta_{T,h}\right\|_{L^2(\Omega)}\right)\left\|\boldsymbol{e}_{u,h}\right\|_{L^2(\Omega)} \\
&\le \beta\left\|\boldsymbol{g}\right\|_{L^\infty(\Omega)}\Bigg(\left\|e_{T,h}\right\|^2_{L^2(\Omega)} + \frac{1}{4}\left\|\boldsymbol{e}_{u,h}\right\|^2_{L^2(\Omega)} \\
&+ \frac{1}{3}\left\|\eta_{T,h}\right\|^2_{L^2(\Omega)} + \frac{3}{4}\left\|\boldsymbol{e}_{u,h}\right\|^2_{L^2(\Omega)}\Bigg) \\
&= \beta\left\|\boldsymbol{g}\right\|_{L^\infty(\Omega)}\left(\left\|e_{T,h}\right\|^2_{L^2(\Omega)} + \left\|\boldsymbol{e}_{u,h}\right\|^2_{L^2(\Omega)}\right) \\
&+ \frac{\beta\left\|\boldsymbol{g}\right\|_{L^\infty(\Omega)}}{3}\left\|\eta_{T,h}\right\|^2_{L^2(\Omega)}.
\end{aligned}
$$

Here, we have used Lemmas 2.4.6–2.4.8, along with Young's inequality. The previous equation (Eq. (2.4.72)) can now be rewritten as follows

$$
\begin{aligned}
&\frac{1}{2}\partial_t\left\|\boldsymbol{e}_{u,h}\right\|^2_{L^2(\Omega)} + \nu C_4\left\|\boldsymbol{e}_{u,h}\right\|^2_{\mathrm{sym},2} \\
&\le \frac{1}{4}\left\|\partial_t\boldsymbol{\eta}_{u,h}\right\|^2_{L^2(\Omega)} + \left\|\boldsymbol{e}_{u,h}\right\|^2_{L^2(\Omega)} \\
&- c_h\left(\boldsymbol{u};\boldsymbol{u},\boldsymbol{e}_{u,h}\right) + c_h\left(\boldsymbol{u}_h;\boldsymbol{u}_h,\boldsymbol{e}_{u,h}\right) + \left\|\boldsymbol{e}_{u,h}\right\|_{\mathrm{sym},2}\left(C_1C_2\left\|\eta_{p,h}\right\|_{L^2(\Omega)} + \nu C_5\left\|\boldsymbol{\eta}_{u,h}\right\|_{\mathrm{sym},2}\right) \\
&+ \beta\left\|\boldsymbol{g}\right\|_{L^\infty(\Omega)}\left(\left\|e_{T,h}\right\|^2_{L^2(\Omega)} + \left\|\boldsymbol{e}_{u,h}\right\|^2_{L^2(\Omega)}\right) + \frac{\beta\left\|\boldsymbol{g}\right\|_{L^\infty(\Omega)}}{3}\left\|\eta_{T,h}\right\|^2_{L^2(\Omega)}.
\end{aligned}
$$

Then, via Young's inequality

$$
\begin{aligned}
&\frac{1}{2}\partial_t \left\|\boldsymbol{e}_{u,h}\right\|^2_{L^2(\Omega)} + \nu\left(C_4 - 2\varepsilon\right)\left\|\boldsymbol{e}_{u,h}\right\|^2_{\mathrm{sym},2} \\
&\leq \frac{1}{4}\left\|\partial_t \boldsymbol{\eta}_{u,h}\right\|^2_{L^2(\Omega)} + \left\|\boldsymbol{e}_{u,h}\right\|^2_{L^2(\Omega)} \\
&- c_h\left(\boldsymbol{u};\boldsymbol{u},\boldsymbol{e}_{u,h}\right) + c_h\left(\boldsymbol{u}_h;\boldsymbol{u}_h,\boldsymbol{e}_{u,h}\right) + \frac{(C_1C_2)^2}{4\varepsilon\nu}\left\|\eta_{p,h}\right\|^2_{L^2(\Omega)} + \frac{C_5^2\nu}{4\varepsilon}\left\|\boldsymbol{\eta}_{u,h}\right\|^2_{\mathrm{sym},2} \\
&+ \beta\left\|\boldsymbol{g}\right\|_{L^\infty(\Omega)}\left(\left\|e_{T,h}\right\|^2_{L^2(\Omega)} + \left\|\boldsymbol{e}_{u,h}\right\|^2_{L^2(\Omega)}\right) + \frac{\beta\left\|\boldsymbol{g}\right\|_{L^\infty(\Omega)}}{3}\left\|\eta_{T,h}\right\|^2_{L^2(\Omega)}. \qquad (2.4.73)
\end{aligned}
$$

An upper bound for the convective terms in the equation above can be expressed as follows

$$
\begin{aligned}
&c_h\left(\boldsymbol{u};\boldsymbol{u},\boldsymbol{e}_{u,h}\right) - c_h\left(\boldsymbol{u}_h;\boldsymbol{u}_h,\boldsymbol{e}_{u,h}\right) \\
&\quad\leq \frac{1}{4\varepsilon}\sum_{K\in\mathcal{T}_h}\frac{1+\nu Re_K^2}{h_K^2}\left\|\boldsymbol{\eta}_{u,h}\right\|^2_{L^2(K)} + \left(3(C_1C_2)^2 + C_2^2\right)\varepsilon\nu\left\|\boldsymbol{e}_{u,h}\right\|^2_{\mathrm{sym},2} \\
&\quad+ 3(C_1C_2)^2\varepsilon\nu\left\|\boldsymbol{\eta}_{u,h}\right\|^2_{\mathrm{sym},2} + \left\|\boldsymbol{e}_{u,h}\right\|^2_{L^2(\Omega)}\Bigg(\left|\boldsymbol{u}\right|_{W^{1,\infty}(\Omega)} + \varepsilon\max_{K\in\mathcal{T}_h}\{h_K^2\left|\boldsymbol{u}\right|^2_{W^{1,\infty}(K)}\} \\
&\quad+ \frac{C}{\varepsilon\nu}\max_{K\in\mathcal{T}_h}\{h_K^2\left|\boldsymbol{u}\right|^2_{W^{1,\infty}(K)}\} + \frac{1}{8\varepsilon\nu}\left\|\boldsymbol{u}\right\|^2_{L^\infty(\Omega)}\Bigg). \qquad (2.4.74)
\end{aligned}
$$

Details of the derivation of this expression can be found in Appendix C.1. Having established the above result, we can now revisit Eq. (2.4.73). Upon substituting

Eq. (2.4.74) into Eq. (2.4.73), and using Lemma 2.4.7, we obtain the following

$$
\begin{aligned}
&\frac{1}{2}\partial_t \left\|\boldsymbol{e}_{u,h}\right\|^2_{L^2(\Omega)} + \nu\left(C_4 - \varepsilon\left(2 + 3(C_1C_2)^2 + C_2^2\right)\right)\left\|\boldsymbol{e}_{u,h}\right\|^2_{\mathrm{sym},2} \\
&\leq \frac{1}{4}\left\|\partial_t \boldsymbol{\eta}_{u,h}\right\|^2_{L^2(\Omega)} + \frac{1}{4\varepsilon}\sum_{K\in\mathcal{T}_h}\frac{1+\nu Re_K^2}{h_K^2}\left\|\boldsymbol{\eta}_{u,h}\right\|^2_{L^2(K)} + \frac{(C_1C_2)^2}{4\varepsilon\nu}\left\|\eta_{p,h}\right\|^2_{L^2(\Omega)} \\
&+ \left(\frac{C_5^2}{4\varepsilon} + 3(C_1C_2)^2\varepsilon\right)C_3^2\nu\left\|\boldsymbol{\eta}_{u,h}\right\|^2_{\mathrm{grad},2} + \left\|\boldsymbol{e}_{u,h}\right\|^2_{L^2(\Omega)}\Big(1 + \beta\left\|\boldsymbol{g}\right\|_{L^\infty(\Omega)} + \left|\boldsymbol{u}\right|_{W^{1,\infty}(\Omega)} \\
&+ \varepsilon\max_{K\in\mathcal{T}_h}\{h_K^2\left|\boldsymbol{u}\right|^2_{W^{1,\infty}(K)}\} + \frac{C}{\varepsilon\nu}\max_{K\in\mathcal{T}_h}\{h_K^2\left|\boldsymbol{u}\right|^2_{W^{1,\infty}(K)}\} + \frac{1}{8\varepsilon\nu}\left\|\boldsymbol{u}\right\|^2_{L^\infty(\Omega)}\Big) \\
&+ \beta\left\|\boldsymbol{g}\right\|_{L^\infty(\Omega)}\left(\left\|e_{T,h}\right\|^2_{L^2(\Omega)} + \frac{1}{3}\left\|\eta_{T,h}\right\|^2_{L^2(\Omega)}\right).
\end{aligned}
\tag{2.4.75}
$$

This completes our analysis of the linear momentum equation for the time being.

Turning our attention to Eq. (2.4.71), we can bound the individual terms as we did with Eq. (2.4.70). We begin by replacing $T - T_h$ with $\eta_{T,h} + e_{T,h}$ and using the fact that $\nabla \cdot \boldsymbol{u} = 0$ as follows

$$
\begin{aligned}
&\left(\partial_t e_{T,h}, e_{T,h}\right)_{\mathcal{T}_h} + \alpha\gamma\underline{a}_h\left(e_{T,h}, e_{T,h}\right) \\
&= -\left(\partial_t \eta_{T,h}, e_{T,h}\right)_{\mathcal{T}_h} - \alpha\gamma\underline{a}_h\left(\eta_{T,h}, e_{T,h}\right) - \underline{c}_h\left(\boldsymbol{u}; T, e_{T,h}\right) + \underline{c}_h\left(\boldsymbol{u}_h; T_h, e_{T,h}\right) \\
&+ (\gamma - 1)\Big[\left(\left(\nabla\cdot\boldsymbol{u}_h\right)T_h, e_{T,h}\right)_{\mathcal{T}_h} + C_{\mathrm{mod}}\left(\left|\nabla\cdot\boldsymbol{u}_h\right|\nabla T_h, \nabla e_{T,h}\right)_{\mathcal{T}_h}\Big].
\end{aligned}
\tag{2.4.76}
$$

Next, we can bound terms on the first and second lines of Eq. (2.4.76)

$$
\begin{aligned}
\left(\partial_t e_{T,h}, e_{T,h}\right)_{\mathcal{T}_h} &= \frac{1}{2}\partial_t \left\|e_{T,h}\right\|^2_{L^2(\Omega)}, \\
\alpha\gamma \underline{a}_h\left(e_{T,h}, e_{T,h}\right) &\geq \alpha\gamma C_8 \left\|e_{T,h}\right\|^2_{\text{grad},2}, \\
\left(\partial_t \eta_{T,h}, e_{T,h}\right)_{\mathcal{T}_h} &\leq \left\|\partial_t \eta_{T,h}\right\|_{L^2(\Omega)} \left\|e_{T,h}\right\|_{L^2(\Omega)} \leq \frac{1}{4}\left\|\partial_t \eta_{T,h}\right\|^2_{L^2(\Omega)} + \left\|e_{T,h}\right\|^2_{L^2(\Omega)}, \\
\alpha\gamma \underline{a}_h\left(\eta_{T,h}, e_{T,h}\right) &\leq C_9 \alpha\gamma \left\|\eta_{T,h}\right\|_{\text{grad},2} \left\|e_{T,h}\right\|_{\text{grad},2}.
\end{aligned}
\tag{2.4.77}
$$

Here, we have used Lemmas 2.4.12 and 2.4.13, along with Young's inequality. It remains for us to bound the leftover terms on the second and third lines of Eq. (2.4.76). We begin by analyzing the first term on the last line. This term can be partitioned into three parts as follows

$$
\begin{aligned}
&\left(\left(\nabla \cdot \boldsymbol{u}_h\right) T_h, e_{T,h}\right)_{\mathcal{T}_h} = \left(\left(\nabla \cdot \boldsymbol{u}_h\right)\left(j_T T - e_{T,h}\right), e_{T,h}\right)_{\mathcal{T}_h} \\
&= \left(\left(\nabla \cdot \boldsymbol{u}_h\right) j_T T, e_{T,h}\right)_{\mathcal{T}_h} - \left(\left(\nabla \cdot \boldsymbol{u}_h\right), e^2_{T,h}\right)_{\mathcal{T}_h} \\
&= \underbrace{\left(\left(\nabla \cdot \boldsymbol{u}_h\right) T, e_{T,h}\right)_{\mathcal{T}_h}}_{\Xi_1} - \underbrace{\left(\left(\nabla \cdot \boldsymbol{u}_h\right) \eta_{T,h}, e_{T,h}\right)_{\mathcal{T}_h}}_{\Xi_2} - \underbrace{\left(\left(\nabla \cdot \boldsymbol{u}_h\right), e^2_{T,h}\right)_{\mathcal{T}_h}}_{\Xi_3}.
\end{aligned}
$$

Here, Ξ_1 can be treated in a similar fashion to $\Lambda^u_{3,2}$ (from Appendix C.1) by using the identity $\boldsymbol{u}_h = -\boldsymbol{\eta}_{u,h} - \boldsymbol{e}_{u,h} + \boldsymbol{u}$ and utilizing the fact that $\nabla \cdot \boldsymbol{u} = 0$ as follows

$$\begin{aligned}
\Xi_1 &= \left(\left(\nabla \cdot \boldsymbol{u}_h\right) T, e_{T,h}\right)_{\mathcal{T}_h} \leq \left| \left(\left(\nabla \cdot \left(-\boldsymbol{\eta}_{u,h} - \boldsymbol{e}_{u,h} + \boldsymbol{u}\right)\right) T, e_{T,h}\right)_{\mathcal{T}_h} \right| \\
&\leq \left| \left(\left(\nabla \cdot \boldsymbol{\eta}_{u,h}\right) T, e_{T,h}\right)_{\mathcal{T}_h} \right| + \left| \left(\left(\nabla \cdot \boldsymbol{e}_{u,h}\right) T, e_{T,h}\right)_{\mathcal{T}_h} \right| \\
&\leq \sum_{K \in \mathcal{T}_h} \Big(\|T\|_{L^\infty(K)} \|\nabla \cdot \boldsymbol{\eta}_{u,h}\|_{L^2(K)} \|e_{T,h}\|_{L^2(K)} + \|T\|_{L^\infty(K)} \|\nabla \cdot \boldsymbol{e}_{u,h}\|_{L^2(K)} \|e_{T,h}\|_{L^2(K)} \Big) \\
&\leq 2(C_1C_2)^2 \varepsilon\nu \|\boldsymbol{\eta}_{u,h}\|_{\mathrm{sym},2}^2 + 2(C_1C_2)^2 \varepsilon\nu \|\boldsymbol{e}_{u,h}\|_{\mathrm{sym},2}^2 + \frac{1}{4\varepsilon\nu} \|e_{T,h}\|_{L^2(\Omega)}^2 \|T\|_{L^\infty(\Omega)}^2 .
\end{aligned} \tag{2.4.78}$$

Here, we have used Lemmas 2.4.5 and 2.4.6 on the last line. Next, Ξ_2 can be handled in much the same way as $\Lambda_{3,1}^u$ (from Appendix C.1)

$$\begin{aligned}
\Xi_2 &= -\left(\left(\nabla \cdot \boldsymbol{u}_h\right) \eta_{T,h}, e_{T,h}\right)_{\mathcal{T}_h} \leq \left| \left(\left(\nabla \cdot \left(-\boldsymbol{\eta}_{u,h} - \boldsymbol{e}_{u,h} + \boldsymbol{u}\right)\right) \eta_{T,h}, e_{T,h}\right)_{\mathcal{T}_h} \right| \\
&= \left| \left(\left(\nabla \cdot \boldsymbol{\eta}_{u,h}\right) \eta_{T,h}, e_{T,h}\right)_{\mathcal{T}_h} \right| + \left| \left(\left(\nabla \cdot \boldsymbol{e}_{u,h}\right) \eta_{T,h}, e_{T,h}\right)_{\mathcal{T}_h} \right| \\
&\leq \sum_{K \in \mathcal{T}_h} \|\eta_{T,h}\|_{L^\infty(K)} \|e_{T,h}\|_{L^2(K)} \Big(\|\nabla \cdot \boldsymbol{\eta}_{u,h}\|_{L^2(K)} + \|\nabla \cdot \boldsymbol{e}_{u,h}\|_{L^2(K)} \Big) \\
&\leq (C_1C_2)^2 \varepsilon\nu \|\boldsymbol{\eta}_{u,h}\|_{\mathrm{sym},2}^2 + (C_1C_2)^2 \varepsilon\nu \|\boldsymbol{e}_{u,h}\|_{\mathrm{sym},2}^2 + \frac{C}{\varepsilon\nu} \|e_{T,h}\|_{L^2(\Omega)}^2 \max_{K \in \mathcal{T}_h} \{h_K^2 |T|_{W^{1,\infty}(K)}^2\}.
\end{aligned} \tag{2.4.79}$$

Finally, Ξ_3 can be bounded as follows

$$\begin{aligned}\Xi_3 &= -\left(\left(\nabla \cdot \boldsymbol{u}_h\right), e_{T,h}^2\right)_{\mathcal{T}_h} \leq \left|\left(\left(\nabla \cdot \boldsymbol{u}_h\right), e_{T,h}^2\right)_{\mathcal{T}_h}\right| \\ &\leq \sum_{K \in \mathcal{T}_h} \left\|\nabla \cdot \boldsymbol{u}_h\right\|_{L^\infty(K)} \left\|e_{T,h}\right\|_{L^2(K)}^2 \leq \left\|\nabla \cdot \boldsymbol{u}_h\right\|_{L^\infty(\Omega)} \left\|e_{T,h}\right\|_{L^2(\Omega)}^2 . \end{aligned} \tag{2.4.80}$$

In a similar fashion, the second term on the last line of Eq. (2.4.76) can be handled by partitioning it into three new terms

$$\begin{aligned}&C_{\text{mod}}\left(\left|\nabla \cdot \boldsymbol{u}_h\right| \nabla T_h, \nabla e_{T,h}\right)_{\mathcal{T}_h} = C_{\text{mod}}\left(\left|\nabla \cdot \boldsymbol{u}_h\right| \nabla\left(j_T T - e_{T,h}\right), \nabla e_{T,h}\right)_{\mathcal{T}_h} \\ &= C_{\text{mod}}\Big[\left(\left|\nabla \cdot \boldsymbol{u}_h\right| \nabla j_T T, \nabla e_{T,h}\right)_{\mathcal{T}_h} - \left(\left|\nabla \cdot \boldsymbol{u}_h\right| \nabla e_{T,h}, \nabla e_{T,h}\right)_{\mathcal{T}_h}\Big] \\ &= C_{\text{mod}}\Big[\underbrace{\left(\left|\nabla \cdot \boldsymbol{u}_h\right| \nabla T, \nabla e_{T,h}\right)_{\mathcal{T}_h}}_{\Upsilon_1} - \underbrace{\left(\left|\nabla \cdot \boldsymbol{u}_h\right| \nabla \eta_{T,h}, \nabla e_{T,h}\right)_{\mathcal{T}_h}}_{\Upsilon_2} - \underbrace{\left(\left|\nabla \cdot \boldsymbol{u}_h\right| \nabla e_{T,h}, \nabla e_{T,h}\right)_{\mathcal{T}_h}}_{\Upsilon_3}\Big].\end{aligned}$$

Next, we can rewrite Υ_1 by substituting $\boldsymbol{u}_h = -\boldsymbol{\eta}_{u,h} - \boldsymbol{e}_{u,h} + \boldsymbol{u}$ into it, and applying

Young's inequality as follows

$$
\begin{aligned}
\Upsilon_1 &= \left(|\nabla\cdot\boldsymbol{u}_h|\,\nabla T, \nabla e_{T,h}\right)_{\mathcal{T}_h} \le \left|\left(|\nabla\cdot(-\boldsymbol{\eta}_{u,h} - \boldsymbol{e}_{u,h} + \boldsymbol{u})|\,\nabla T, \nabla e_{T,h}\right)_{\mathcal{T}_h}\right| \\
&\le \left|\left(|\nabla\cdot\boldsymbol{\eta}_{u,h}|\,\nabla T, \nabla e_{T,h}\right)_{\mathcal{T}_h}\right| + \left|\left(|\nabla\cdot\boldsymbol{e}_{u,h}|\,\nabla T, \nabla e_{T,h}\right)_{\mathcal{T}_h}\right| \\
&\le \sum_{K\in\mathcal{T}_h} \Big(\|\nabla T\|_{L^\infty(K)} \|\nabla\cdot\boldsymbol{\eta}_{u,h}\|_{L^2(K)} \|\nabla e_{T,h}\|_{L^2(K)} \\
&+ \|\nabla T\|_{L^\infty(K)} \|\nabla\cdot\boldsymbol{e}_{u,h}\|_{L^2(K)} \|\nabla e_{T,h}\|_{L^2(K)} \Big) \\
&\le 2(C_1C_2)^2\varepsilon\nu\,\|\boldsymbol{\eta}_{u,h}\|^2_{\mathrm{sym},2} + 2(C_1C_2)^2\varepsilon\nu\,\|\boldsymbol{e}_{u,h}\|^2_{\mathrm{sym},2} + \frac{1}{4\varepsilon\nu}\|\nabla e_{T,h}\|^2_{L^2(\Omega)} |T|^2_{W^{1,\infty}(\Omega)}\,.
\end{aligned}
\tag{2.4.81}
$$

Here, we have used Lemmas 2.4.5 and 2.4.6 on the last line. We can perform the same substitution on Υ_2, in addition to using Assumption 2.4.19 and Young's inequality as follows

$$
\begin{aligned}
\Upsilon_2 &= -\left(|\nabla\cdot\boldsymbol{u}_h|\,\nabla\eta_{T,h}, \nabla e_{T,h}\right)_{\mathcal{T}_h} \le \left|\left(|\nabla\cdot(-\boldsymbol{\eta}_{u,h} - \boldsymbol{e}_{u,h} + \boldsymbol{u})|\,\nabla\eta_{T,h}, \nabla e_{T,h}\right)_{\mathcal{T}_h}\right| \\
&\le \left|\left(|\nabla\cdot\boldsymbol{\eta}_{u,h}|\,\nabla\eta_{T,h}, \nabla e_{T,h}\right)_{\mathcal{T}_h}\right| + \left|\left(|\nabla\cdot\boldsymbol{e}_{u,h}|\,\nabla\eta_{T,h}, \nabla e_{T,h}\right)_{\mathcal{T}_h}\right| \\
&\le \sum_{K\in\mathcal{T}_h} \|\nabla\eta_{T,h}\|_{L^\infty(K)} \|\nabla e_{T,h}\|_{L^2(K)} \Big(\|\nabla\cdot\boldsymbol{\eta}_{u,h}\|_{L^2(K)} + \|\nabla\cdot\boldsymbol{e}_{u,h}\|_{L^2(K)} \Big) \\
&\le (C_1C_2)^2\varepsilon\nu\,\|\boldsymbol{\eta}_{u,h}\|^2_{\mathrm{sym},2} + (C_1C_2)^2\varepsilon\nu\,\|\boldsymbol{e}_{u,h}\|^2_{\mathrm{sym},2} + \frac{C}{\varepsilon\nu}\|\nabla e_{T,h}\|^2_{L^2(\Omega)} \|T\|^2_{W^{1,\infty}(\Omega)}\,.
\end{aligned}
\tag{2.4.82}
$$

Finally, Υ_3 can be bounded as follows

$$\begin{aligned}\Upsilon_3 &= -\left(\left|\nabla\cdot\boldsymbol{u}_h\right|\nabla e_{T,h},\nabla e_{T,h}\right)_{\mathcal{T}_h} \leq \left(\left|\nabla\cdot\boldsymbol{u}_h\right|\nabla e_{T,h},\nabla e_{T,h}\right)_{\mathcal{T}_h} \\ &\leq \sum_{K\in\mathcal{T}_h}\left\|\nabla\cdot\boldsymbol{u}_h\right\|_{L^\infty(K)}\left\|\nabla e_{T,h}\right\|^2_{L^2(K)} \leq \left\|\nabla\cdot\boldsymbol{u}_h\right\|_{L^\infty(\Omega)}\left\|\nabla e_{T,h}\right\|^2_{L^2(\Omega)}. \end{aligned} \tag{2.4.83}$$

We can now return our attention to Eq. (2.4.76). Upon substituting Eqs. (2.4.77)–(2.4.83) into (2.4.76), and using Young's inequality, we obtain

$$\begin{aligned}&\frac{1}{2}\partial_t\left\|e_{T,h}\right\|^2_{L^2(\Omega)} + (C_8-2\varepsilon)\alpha\gamma\left\|e_{T,h}\right\|^2_{\mathrm{grad},2} \\ &\leq \frac{1}{4}\left\|\partial_t\eta_{T,h}\right\|^2_{L^2(\Omega)} + \left\|e_{T,h}\right\|^2_{L^2(\Omega)} + \frac{\alpha\gamma C_9^2}{8\varepsilon}\left\|\eta_{T,h}\right\|^2_{\mathrm{grad},2} \\ &- \underline{c}_h\left(\boldsymbol{u};T,e_{T,h}\right) + \underline{c}_h\left(\boldsymbol{u}_h;T_h,e_{T,h}\right) \\ &+ (\gamma-1)\Bigg[3(C_1C_2)^2(1+C_{\mathrm{mod}})\varepsilon\nu\left\|\boldsymbol{\eta}_{u,h}\right\|^2_{\mathrm{sym},2} + 3(C_1C_2)^2(1+C_{\mathrm{mod}})\varepsilon\nu\left\|\boldsymbol{e}_{u,h}\right\|^2_{\mathrm{sym},2} \\ &+ \frac{1}{4\varepsilon\nu}\left\|e_{T,h}\right\|^2_{L^2(\Omega)}\left\|T\right\|^2_{L^\infty(\Omega)} + \frac{C}{\varepsilon\nu}\left\|e_{T,h}\right\|^2_{L^2(\Omega)}\max_{K\in\mathcal{T}_h}\{h_k^2\left|T\right|^2_{W^{1,\infty}(K)}\} \\ &+ \left\|\nabla\cdot\boldsymbol{u}_h\right\|_{L^\infty(\Omega)}\left\|e_{T,h}\right\|^2_{L^2(\Omega)} + \frac{C_{\mathrm{mod}}}{4\varepsilon\nu}\left\|\nabla e_{T,h}\right\|^2_{L^2(\Omega)}\left|T\right|^2_{W^{1,\infty}(\Omega)} \\ &+ \frac{CC_{\mathrm{mod}}}{\varepsilon\nu}\left\|\nabla e_{T,h}\right\|^2_{L^2(\Omega)}\left\|T\right\|^2_{W^{1,\infty}(\Omega)} + C_{\mathrm{mod}}\left\|\nabla\cdot\boldsymbol{u}_h\right\|_{L^\infty(\Omega)}\left\|\nabla e_{T,h}\right\|^2_{L^2(\Omega)}\Bigg]. \end{aligned} \tag{2.4.84}$$

An upper bound for the convective terms in the equation above can be expressed as follows

$$
\begin{aligned}
&\underline{c}_h\left(\boldsymbol{u};T,e_{T,h}\right)-\underline{c}_h\left(\boldsymbol{u}_h;T_h,e_{T,h}\right)\\
&\quad\le \frac{1}{4\varepsilon}\sum_{K\in\mathcal{T}_h}\frac{1}{h_K^2}\left\|\boldsymbol{\eta}_{u,h}\right\|_{L^2(K)}^2+\frac{1}{2}\left|T\right|_{W^{1,\infty}(\Omega)}\left\|\boldsymbol{e}_{u,h}\right\|_{L^2(\Omega)}^2+7\alpha\gamma\varepsilon\left\|e_{T,h}\right\|_{\mathrm{grad},2}^2\\
&\quad+\frac{1}{28\varepsilon}\sum_{K\in\mathcal{T}_h}\frac{\alpha}{h_K^2\gamma}Pe_K^2\left\|\eta_{T,h}\right\|_{L^2(K)}^2+3(C_1C_2)^2\varepsilon\nu\left\|\boldsymbol{e}_{u,h}\right\|_{\mathrm{sym},2}^2+3(C_1C_2)^2\varepsilon\nu\left\|\boldsymbol{\eta}_{u,h}\right\|_{\mathrm{sym},2}^2\\
&\quad+\left\|e_{T,h}\right\|_{L^2(\Omega)}^2\left[\frac{1}{2}\left|T\right|_{W^{1,\infty}(\Omega)}+\left(\varepsilon+\frac{C}{\varepsilon\nu}\right)\max_{K\in\mathcal{T}_h}\{h_K^2\left|T\right|_{W^{1,\infty}(K)}^2\}+\frac{1}{8\varepsilon\nu}\left\|T\right\|_{L^\infty(\Omega)}^2\right].
\end{aligned}
\tag{2.4.85}
$$

Details of the derivation can be found in Appendix C.3. Now, upon substituting

Eq. (2.4.85) into Eq. (2.4.84), and using Lemma 2.4.7, we obtain

$$
\begin{aligned}
&\frac{1}{2}\partial_t \left\|e_{T,h}\right\|^2_{L^2(\Omega)} + (C_8 - 9\varepsilon)\alpha\gamma \left\|e_{T,h}\right\|^2_{\mathrm{grad},2} \\
&\leq \frac{1}{4}\left\|\partial_t \eta_{T,h}\right\|^2_{L^2(\Omega)} + \frac{1}{4\varepsilon}\sum_{K\in\mathcal{T}_h}\frac{1}{h_K^2}\left\|\boldsymbol{\eta}_{u,h}\right\|^2_{L^2(K)} + \frac{\alpha\gamma C_9^2}{8\varepsilon}\left\|\eta_{T,h}\right\|^2_{\mathrm{grad},2} \\
&+ \frac{1}{2}\left|T\right|_{W^{1,\infty}(\Omega)}\left\|\boldsymbol{e}_{u,h}\right\|^2_{L^2(\Omega)} + \frac{1}{28\varepsilon}\sum_{K\in\mathcal{T}_h}\frac{\alpha}{h_K^2\gamma}Pe_K^2\left\|\eta_{T,h}\right\|^2_{L^2(K)} \\
&+ 3\left(\gamma + (\gamma-1)\,C_{\mathrm{mod}}\right)(C_1C_2)^2\varepsilon\nu\left\|\boldsymbol{e}_{u,h}\right\|^2_{\mathrm{sym},2} \\
&+ 3\left(\gamma + (\gamma-1)\,C_{\mathrm{mod}}\right)(C_1C_2C_3)^2\varepsilon\nu\left\|\boldsymbol{\eta}_{u,h}\right\|^2_{\mathrm{grad},2} \\
&+ \left\|e_{T,h}\right\|^2_{L^2(\Omega)}\Bigg[1 + \frac{1}{2}\left|T\right|_{W^{1,\infty}(\Omega)} + \left(\varepsilon + \frac{C\gamma}{\varepsilon\nu}\right)\max_{K\in\mathcal{T}_h}\{h_K^2\left|T\right|^2_{W^{1,\infty}(K)}\} + \frac{2\gamma-1}{8\varepsilon\nu}\left\|T\right\|^2_{L^\infty(\Omega)} \\
&+ (\gamma-1)\left\|\nabla\cdot\boldsymbol{u}_h\right\|_{L^\infty(\Omega)}\Bigg] + C_{\mathrm{mod}}\,(\gamma-1)\left\|\nabla e_{T,h}\right\|^2_{L^2(\Omega)}\Bigg[\frac{1}{4\varepsilon\nu}\left|T\right|^2_{W^{1,\infty}(\Omega)} \\
&+ \frac{C}{\varepsilon\nu}\left\|T\right\|^2_{W^{1,\infty}(\Omega)} + \left\|\nabla\cdot\boldsymbol{u}_h\right\|_{L^\infty(\Omega)}\Bigg].
\end{aligned}
\tag{2.4.86}
$$

Next, we combine Eqs. (2.4.75) and (2.4.86), and introduce the constants $C_A = C_4 - \varepsilon\left(2 + C_2^2 + 3(C_1C_2)^2(\gamma + 1 + (\gamma-1)C_{\mathrm{mod}})\right)$ and $C_B = C_8 - 9\varepsilon$. Here, we require that $C_A > 0$ and $C_B > 0$. As a result, we must choose

$$
\varepsilon < \min\left[\frac{C_4}{2 + C_2^2 + 3(C_1C_2)^2(\gamma + 1 + (\gamma-1)C_{\mathrm{mod}})}, \frac{C_8}{9}\right].
$$

Upon choosing an appropriate value for ε, we obtain the following expression

$$
\begin{aligned}
&\frac{1}{2}\partial_t \left\|e_{T,h}\right\|^2_{L^2(\Omega)} + C_A\nu \left\|\boldsymbol{e}_{u,h}\right\|^2_{\text{sym},2} + \frac{1}{2}\partial_t \left\|\boldsymbol{e}_{u,h}\right\|^2_{L^2(\Omega)} + C_B\alpha\gamma \left\|e_{T,h}\right\|^2_{\text{grad},2} \\
&\lesssim \left\|\partial_t \eta_{T,h}\right\|^2_{L^2(\Omega)} + \gamma\alpha \left\|\eta_{T,h}\right\|^2_{\text{grad},2} + \left(2 + 3(\gamma + (\gamma-1)C_{\text{mod}})\right)\nu \left\|\boldsymbol{\eta}_{u,h}\right\|^2_{\text{grad},2} \\
&+ \left\|\partial_t \boldsymbol{\eta}_{u,h}\right\|^2_{L^2(\Omega)} + \sum_{K\in\mathcal{T}_h} \frac{2+\nu Re_K^2}{h_K^2} \left\|\boldsymbol{\eta}_{u,h}\right\|^2_{L^2(K)} + \frac{1}{\nu}\left\|\eta_{p,h}\right\|^2_{L^2(\Omega)} \\
&+ \left\|\boldsymbol{e}_{u,h}\right\|^2_{L^2(\Omega)} \Bigg[1 + \beta\left\|\boldsymbol{g}\right\|_{L^\infty(\Omega)} + \left|\boldsymbol{u}\right|_{W^{1,\infty}(\Omega)} + \left|T\right|_{W^{1,\infty}(\Omega)} \\
&+ \left(1+\frac{1}{\nu}\right)\max_{K\in\mathcal{T}_h}\{h_K^2 \left|\boldsymbol{u}\right|^2_{W^{1,\infty}(K)}\} + \frac{1}{\nu}\left\|\boldsymbol{u}\right\|^2_{L^\infty(\Omega)}\Bigg] \\
&+ \left\|\eta_{T,h}\right\|^2_{L^2(\Omega)} \left[\sum_{K\in\mathcal{T}_h} \frac{\alpha}{h_K^2\gamma} Pe_K^2 + \beta\left\|\boldsymbol{g}\right\|_{L^\infty(\Omega)}\right] \\
&+ \left\|e_{T,h}\right\|^2_{L^2(\Omega)} \Bigg[1 + \beta\left\|\boldsymbol{g}\right\|_{L^\infty(\Omega)} + \left|T\right|_{W^{1,\infty}(\Omega)} + \left(1+\frac{\gamma}{\nu}\right)\max_{K\in\mathcal{T}_h}\{h_K^2\left|T\right|^2_{W^{1,\infty}(K)}\} + \frac{\gamma}{\nu}\left\|T\right\|^2_{L^\infty(\Omega)} \\
&+ (\gamma-1)\left\|\nabla\cdot\boldsymbol{u}_h\right\|_{L^\infty(\Omega)} + \frac{C_{\text{mod}}(\gamma-1)}{\nu}\max_{K\in\mathcal{T}_h}\{h_K^{-2}\}\left\|T\right\|^2_{W^{1,\infty}(\Omega)} \\
&+ C_{\text{mod}}(\gamma-1)\max_{K\in\mathcal{T}_h}\{h_K^{-2}\}\left\|\nabla\cdot\boldsymbol{u}_h\right\|_{L^\infty(\Omega)}\Bigg],
\end{aligned}
\tag{2.4.87}
$$

where we have introduced $\lesssim$ to denote that the RHS of Eq. (2.4.87) is multiplied by a generic constant. In addition, we have used the following inverse inequality to rewrite the $\left\|\nabla e_{T,h}\right\|_{L^2(\Omega)}$ terms on the last two lines of Eq. (2.4.87)

$$
\left\|\nabla e_{T,h}\right\|^2_{L^2(\Omega)} = \sum_{K\in\mathcal{T}_h}\left\|\nabla e_{T,h}\right\|^2_{L^2(K)} \leq C\sum_{K\in\mathcal{T}_h} h_K^{-2}\left\|e_{T,h}\right\|^2_{L^2(K)} \leq C\max_{K\in\mathcal{T}_h}\left\{h_K^{-2}\right\}\left\|e_{T,h}\right\|^2_{L^2(\Omega)}.
$$

We can now obtain an error estimate through application of Gronwall's Lemma. First, we integrate Eq. (2.4.87) from $t = t_0$ to $t = t_n$ in order to obtain

$$
\begin{aligned}
&\|e_{T,h}(t_n)\|^2_{L^2(\Omega)} + \|\boldsymbol{e}_{u,h}(t_n)\|^2_{L^2(\Omega)} + \int_{t_0}^{t_n} \left(C_A\nu \|\boldsymbol{e}_{u,h}(s)\|^2_{\text{sym},2} + C_B\alpha\gamma \|e_{T,h}(s)\|^2_{\text{grad},2}\right) ds \\
&\lesssim \int_{t_0}^{t_n} \Bigg[\|\partial_t \eta_{T,h}(s)\|^2_{L^2(\Omega)} + \|\partial_t \boldsymbol{\eta}_{u,h}(s)\|^2_{L^2(\Omega)} + \alpha\gamma \|\eta_{T,h}(s)\|^2_{\text{grad},2} + \frac{1}{\nu} \|\eta_{p,h}(s)\|^2_{L^2(\Omega)} \\
&+ \sum_{K\in\mathcal{T}_h} \frac{2+\nu Re_K^2}{h_K^2} \|\boldsymbol{\eta}_{u,h}(s)\|^2_{L^2(K)} + (2 + 3(\gamma + (\gamma-1)C_{\text{mod}}))\,\nu \|\boldsymbol{\eta}_{u,h}(s)\|^2_{\text{grad},2} \\
&+ \left(\sum_{K\in\mathcal{T}_h} \frac{\alpha}{h_K^2\gamma} Pe_K^2 + \beta \|\boldsymbol{g}\|_{L^\infty(\Omega)}\right) \|\eta_{T,h}(s)\|^2_{L^2(\Omega)} \Bigg] ds \\
&+ \int_{t_0}^{t_n} \left(\|e_{T,h}(s)\|^2_{L^2(\Omega)} + \|\boldsymbol{e}_{u,h}(s)\|^2_{L^2(\Omega)}\right) \Bigg[1 + \beta \|\boldsymbol{g}\|_{L^\infty(\Omega)} + |\boldsymbol{u}(s)|_{W^{1,\infty}(\Omega)} \\
&+ \left(1 + \frac{1}{\nu}\right) \max_{K\in\mathcal{T}_h} \{h_K^2 |\boldsymbol{u}(s)|^2_{W^{1,\infty}(K)}\} + \frac{1}{\nu} \|\boldsymbol{u}(s)\|^2_{L^\infty(\Omega)} \\
&+ |T(s)|_{W^{1,\infty}(\Omega)} + \left(1 + \frac{\gamma}{\nu}\right) \max_{K\in\mathcal{T}_h} \{h_K^2 |T(s)|^2_{W^{1,\infty}(K)}\} + \frac{\gamma}{\nu} \|T(s)\|^2_{L^\infty(\Omega)} \\
&+ (\gamma - 1) \|\nabla\cdot\boldsymbol{u}_h(s)\|_{L^\infty(\Omega)} + \frac{C_{\text{mod}}(\gamma-1)}{\nu} \max_{K\in\mathcal{T}_h} \{h_K^{-2}\} \|T(s)\|^2_{W^{1,\infty}(\Omega)} \\
&+ C_{\text{mod}}(\gamma-1) \max_{K\in\mathcal{T}_h} \{h_K^{-2}\} \|\nabla\cdot\boldsymbol{u}_h(s)\|_{L^\infty(\Omega)} \Bigg] ds.
\end{aligned}
$$

Next, via Gronwall's Lemma

$$
\begin{aligned}
&\|e_{T,h}(t_n)\|^2_{L^2(\Omega)} + \|\boldsymbol{e}_{u,h}(t_n)\|^2_{L^2(\Omega)} + \int_{t_0}^{t_n} \Big(C_A\nu \, \|\boldsymbol{e}_{u,h}(s)\|^2_{\text{sym},2} + C_B\alpha\gamma \, \|e_{T,h}(s)\|^2_{\text{grad},2} \Big) \, ds \\
&\lesssim \int_{t_0}^{t_n} \left(\exp \int_s^{t_n} C_G(\vartheta) \, d\vartheta \right) \Bigg[\|\partial_t \eta_{T,h}(s)\|^2_{L^2(\Omega)} + \|\partial_t \boldsymbol{\eta}_{u,h}(s)\|^2_{L^2(\Omega)} + \alpha\gamma \, \|\eta_{T,h}(s)\|^2_{\text{grad},2} \\
&+ \frac{1}{\nu} \|\eta_{p,h}(s)\|^2_{L^2(\Omega)} + \sum_{K\in\mathcal{T}_h} \frac{2+\nu Re_K^2}{h_K^2} \|\boldsymbol{\eta}_{u,h}(s)\|^2_{L^2(K)} \\
&+ (2 + 3(\gamma + (\gamma-1)C_{\text{mod}}))\, \nu \, \|\boldsymbol{\eta}_{u,h}(s)\|^2_{\text{grad},2} \\
&+ \left(\sum_{K\in\mathcal{T}_h} \frac{\alpha}{h_K^2\gamma} Pe_K^2 + \beta \, \|\boldsymbol{g}\|_{L^\infty(\Omega)} \right) \|\eta_{T,h}(s)\|^2_{L^2(\Omega)} \Bigg] \, ds.
\end{aligned} \tag{2.4.88}
$$

Here, C_G is the Gronwall constant, in accordance with the definition in Eq. (2.4.63). We can now precisely bound the RHS terms in Eq. (2.4.88). We introduce k as the polynomial order and denote $k_u = k+1, k_T = k+1$, and $k_p = k$ as the polynomial orders for the velocity, temperature, and kinematic pressure respectively.

Thereafter, using Assumption 2.4.19 we can show that

$$
\begin{aligned}
&(2+3(\gamma+(\gamma-1)C_{\mathrm{mod}}))\,\nu\,\|\boldsymbol{\eta}_{u,h}(s)\|_{\mathrm{grad},2}^2+\sum_{K\in\mathcal{T}_h}\frac{2+\nu Re_K^2}{h_K^2}\,\|\boldsymbol{\eta}_{u,h}(s)\|_{L^2(K)}^2\\
&+\frac{1}{\nu}\,\|\eta_{p,h}(s)\|_{L^2(\Omega)}^2+\alpha\gamma\,\|\eta_{T,h}(s)\|_{\mathrm{grad},2}^2\\
&+\left(\sum_{K\in\mathcal{T}_h}\frac{\alpha}{h_K^2\gamma}Pe_K^2+\beta\,\|\boldsymbol{g}\|_{L^\infty(\Omega)}\right)\|\eta_{T,h}(s)\|_{L^2(\Omega)}^2\\
&\leq C\sum_{K\in\mathcal{T}_h}h_K^{2k_u}\left(2+\nu Re_K^2+2\nu+3\nu(\gamma+(\gamma-1)C_{\mathrm{mod}})\right)\|\boldsymbol{u}(s)\|_{W^{k_u+1,2}(K)}^2\\
&+C\sum_{K\in\mathcal{T}_h}h_K^{2k_p+2}\frac{1}{\nu}\,\|p(s)\|_{W^{k_p+1}(K)}^2\\
&+C\sum_{K\in\mathcal{T}_h}h_K^{2k_T}\left(\alpha\gamma+\frac{\alpha}{\gamma}Pe_K^2+h_K^2\beta\,\|\boldsymbol{g}\|_{L^\infty(K)}\right)\|T(s)\|_{W^{k_T+1,2}(K)}^2\,,
\end{aligned}
$$

and

$$
\begin{aligned}
\|\partial_t\boldsymbol{\eta}_{u,h}(s)\|_{L^2(\Omega)}^2&\leq C\sum_{K\in\mathcal{T}_h}h_K^{2k_u}\,\|\partial_t\boldsymbol{u}(s)\|_{W^{k_u,2}(K)}^2\,,\\
\|\partial_t\eta_{T,h}(s)\|_{L^2(\Omega)}^2&\leq C\sum_{K\in\mathcal{T}_h}h_K^{2k_T}\,\|\partial_t T(s)\|_{W^{k_T,2}(K)}^2\,.
\end{aligned}
$$

Finally, we obtain a total error estimate

$$
\begin{aligned}
&\|e_{T,h}(t_n)\|^2_{L^2(\Omega)} + \|\boldsymbol{e}_{u,h}(t_n)\|^2_{L^2(\Omega)} + \int_{t_0}^{t_n} \left(C_A \nu \|\boldsymbol{e}_{u,h}(s)\|^2_{\text{sym},2} + C_B \alpha\gamma \|e_{T,h}(s)\|^2_{\text{grad},2} \right) ds \\
&\lesssim \int_{t_0}^{t_n} \left(\exp \int_s^{t_n} C_G(\vartheta)\, d\vartheta \right) \\
&\times \sum_{K \in \mathcal{T}_h} \Bigg[h_K^{2k_u} \Big[\left(2 + \nu Re_K^2 + 2\nu + 3\nu(\gamma + (\gamma - 1)C_{\text{mod}})\right) \|\boldsymbol{u}(s)\|^2_{W^{k_u+1,2}(K)} \\
&+ \|\partial_t \boldsymbol{u}(s)\|^2_{W^{k_u,2}(K)} \Big] + \frac{h_K^{2k_p+2}}{\nu} \|p(s)\|^2_{W^{k_p+1}(K)} \\
&+ h_K^{2k_T} \Big[\left(\alpha\gamma + \frac{\alpha}{\gamma} Pe_K^2 + h_K^2 \beta \|\boldsymbol{g}\|_{L^\infty(K)} \right) \|T(s)\|^2_{W^{k_T+1,2}(K)} + \|\partial_t T(s)\|^2_{W^{k_T,2}(K)} \Big] \Bigg] ds.
\end{aligned}
\tag{2.4.89}
$$

This is identical to the desired result (2.4.62). □

Theorem 2.4.25 (Error of the Discrete Kinematic Pressure)**.** *Consider the class of H1-conforming mixed methods that satisfy Eqs.* (2.3.1)–(2.3.3)*. Suppose that the exact solution* $(\boldsymbol{u}, T, p) : [t_0, t_n] \longrightarrow \boldsymbol{W} \times R \times Q$ *and approximate solution* $(\boldsymbol{u}_h, T_h, p_h) : [t_0, t_n] \longrightarrow \boldsymbol{W}_h \times R_h \times Q_h$ *reside in the following spaces*

$$
\boldsymbol{u} \in L^\infty\left(t_0, t_n; \boldsymbol{W}^{1,\infty}(\Omega)\right), \qquad \boldsymbol{u}_h \in L^\infty\left(t_0, t_n; \boldsymbol{L}^\infty(\Omega)\right).
$$

In addition, suppose $p_h(t_0) = j_p p_0$ *and Assumption 2.4.19 holds. Under these* *circumstances, the discrete error* $e_{p,h} = j_p p - p_h$ *is bounded as follows*

$$\begin{aligned}
\|e_{p,h}\|^2_{L^2(t_0,t_n;L^2(\Omega))} \lesssim\; & \|\partial_t \boldsymbol{e}_{u,h}\|^2_{L^2(t_0,t_n;L^2(\Omega))} + \nu^2 \|\boldsymbol{e}_{u,h}\|^2_{L^2(t_0,t_n;\,\mathrm{grad},2)} \\
& + \left(\|\boldsymbol{u}\|^2_{L^2(t_0,t_n;L^\infty(\Omega))} + \|\boldsymbol{u}_h\|^2_{L^2(t_0,t_n;L^\infty(\Omega))}\right) \|\boldsymbol{e}_{u,h}\|^2_{L^\infty(t_0,t_n;L^2(\Omega))} \\
& + \|\boldsymbol{u}_h\|^2_{L^2(t_0,t_n;L^\infty(\Omega))} \|\boldsymbol{e}_{u,h}\|^2_{L^\infty(t_0,t_n;\,\mathrm{grad},2)} + \beta^2 g^2 \|e_{T,h}\|^2_{L^2(t_0,t_n;L^2(\Omega))} \\
& + \int_{t_0}^{t_n} \sum_{K\in\mathcal{T}_h} \Bigg[h_K^{2(k_p+1)} \|p(s)\|^2_{W^{k_p+1,2}(K)} + h_K^{2k_u} \|\partial_t \boldsymbol{u}(s)\|^2_{W^{k_u,2}(K)} \\
& + \left(\|\boldsymbol{u}(s)\|^2_{L^\infty(\Omega)} + \|\boldsymbol{u}_h(s)\|^2_{L^\infty(\Omega)}\right) h_K^{2(k_u+1)} \|\boldsymbol{u}(s)\|^2_{W^{k_u+1,2}(K)} \\
& + \nu^2 h_K^{2k_u} \|\boldsymbol{u}(s)\|^2_{W^{k_u+1,2}(K)} + \|\boldsymbol{u}_h(s)\|^2_{L^\infty(\Omega)} h_K^{2k_u} \|\boldsymbol{u}(s)\|^2_{W^{k_u+1,2}(K)} \\
& + \beta^2 g^2 h_K^{2(k_T+1)} \|T(s)\|^2_{W^{k_T+1,2}(K)} \Bigg] ds. \qquad (2.4.90)
\end{aligned}$$

Proof. We begin by rewriting Eq. (2.3.5) in terms of the exact solution fields $p, \boldsymbol{u}$, and T as follows

$$\begin{aligned}
& (\partial_t\, \boldsymbol{u}, \boldsymbol{w}_h)_{\mathcal{T}_h} + c_h(\boldsymbol{u}; \boldsymbol{u}, \boldsymbol{w}_h) + \nu a_h(\boldsymbol{u}, \boldsymbol{w}_h) - b_h(\boldsymbol{w}_h, p) \\
& = -(\beta T \boldsymbol{g}, \boldsymbol{w}_h)_{\mathcal{T}_h} + (\boldsymbol{f}_u, \boldsymbol{w}_h)_{\mathcal{T}_h}. \qquad (2.4.91)
\end{aligned}$$

Next, upon subtracting Eq. (2.3.5) from Eq. (2.4.91) and rearranging the result, one obtains

$$b_h\left(\boldsymbol{w}_h, p-p_h\right)=\left(\partial_t(\boldsymbol{u}-\boldsymbol{u}_h), \boldsymbol{w}_h\right)_{\mathcal{T}_h}+c_h\left(\boldsymbol{u}; \boldsymbol{u}, \boldsymbol{w}_h\right)-c_h\left(\boldsymbol{u}_h; \boldsymbol{u}_h, \boldsymbol{w}_h\right)$$
$$+\nu a_h\left(\boldsymbol{u}-\boldsymbol{u}_h, \boldsymbol{w}_h\right)+\left(\beta(T-T_h)\boldsymbol{g}, \boldsymbol{w}_h\right)_{\mathcal{T}_h}.$$

We can now substitute $p-p_h=\eta_{p,h}+e_{p,h}$, $\boldsymbol{u}-\boldsymbol{u}_h=\boldsymbol{\eta}_{u,h}+\boldsymbol{e}_{u,h}$, and $T-T_h=\eta_{T,h}+e_{T,h}$ into the equation above

$$b_h\left(\boldsymbol{w}_h, e_{p,h}\right)=-b_h\left(\boldsymbol{w}_h, \eta_{p,h}\right)+\left(\partial_t\boldsymbol{\eta}_{u,h}, \boldsymbol{w}_h\right)_{\mathcal{T}_h}+\left(\partial_t\boldsymbol{e}_{u,h}, \boldsymbol{w}_h\right)_{\mathcal{T}_h}$$
$$+c_h\left(\boldsymbol{u}; \boldsymbol{u}, \boldsymbol{w}_h\right)-c_h\left(\boldsymbol{u}_h; \boldsymbol{u}_h, \boldsymbol{w}_h\right)$$
$$+\nu a_h\left(\boldsymbol{\eta}_{u,h}, \boldsymbol{w}_h\right)+\nu a_h\left(\boldsymbol{e}_{u,h}, \boldsymbol{w}_h\right)+\left(\beta\eta_{T,h}\,\boldsymbol{g}, \boldsymbol{w}_h\right)_{\mathcal{T}_h}+\left(\beta e_{T,h}\,\boldsymbol{g}, \boldsymbol{w}_h\right)_{\mathcal{T}_h}.$$

By using the Cauchy-Schwarz inequality, Lemma 2.4.7, the boundedness of the viscous bilinear form (Lemma 2.4.9), the inequality of broken Sobolev norms (Lemma B.1.2), and the embedding inequality (Lemma B.1.3), one obtains

$$\begin{aligned} b_h\left(\boldsymbol{w}_h, e_{p,h}\right) \leq \Bigg[& d^{1/2}\left\|\eta_{p,h}\right\|_{L^2(\Omega)}+\sigma_{2,2}\left(\left\|\partial_t\boldsymbol{\eta}_{u,h}\right\|_{L^2(\Omega)}+\left\|\partial_t\boldsymbol{e}_{u,h}\right\|_{L^2(\Omega)}\right) \\ & +\nu C_5 C_3^2\left(\left\|\boldsymbol{\eta}_{u,h}\right\|_{\mathrm{grad},2}+\left\|\boldsymbol{e}_{u,h}\right\|_{\mathrm{grad},2}\right) \\ & +\beta g\sigma_{2,2}\left(\left\|\eta_{T,h}\right\|_{L^2(\Omega)}+\left\|e_{T,h}\right\|_{L^2(\Omega)}\right)\Bigg]\left\|\boldsymbol{w}_h\right\|_{\mathrm{grad},2} \\ & +c_h\left(\boldsymbol{u}; \boldsymbol{u}, \boldsymbol{w}_h\right)-c_h\left(\boldsymbol{u}_h; \boldsymbol{u}_h, \boldsymbol{w}_h\right). \end{aligned} \tag{2.4.92}$$

It remains for us to bound the convective terms on the RHS of Eq. (2.4.92). After some careful consideration (see Appendix C.2), we obtain the following result

$$
\begin{aligned}
& c_h\left(\boldsymbol{u};\boldsymbol{u},\boldsymbol{w}_h\right) - c_h\left(\boldsymbol{u}_h;\boldsymbol{u}_h,\boldsymbol{w}_h\right) \\
& \leq \Bigg[\Big(\|\boldsymbol{u}\|_{L^\infty(\Omega)} + \|\boldsymbol{u}_h\|_{L^\infty(\Omega)} \Big) \Big(\|\boldsymbol{\eta}_{u,h}\|_{L^2(\Omega)} + \|\boldsymbol{e}_{u,h}\|_{L^2(\Omega)} \Big) \\
& + d^{1/2}\sigma_{2,2} \|\boldsymbol{u}_h\|_{L^\infty(\Omega)} \Big(\|\boldsymbol{\eta}_{u,h}\|_{\text{grad},2} + \|\boldsymbol{e}_{u,h}\|_{\text{grad},2} \Big) \Bigg] \|\boldsymbol{w}_h\|_{\text{grad},2} . \qquad (2.4.93)
\end{aligned}
$$

Upon substituting Eq. (2.4.93) into Eq. (2.4.92), one obtains

$$
\begin{aligned}
\frac{b_h\left(\boldsymbol{w}_h, e_{p,h}\right)}{\|\boldsymbol{w}_h\|_{\text{grad},2}} \leq {} & d^{1/2} \|\eta_{p,h}\|_{L^2(\Omega)} + \sigma_{2,2} \Big(\|\partial_t \boldsymbol{\eta}_{u,h}\|_{L^2(\Omega)} + \|\partial_t \boldsymbol{e}_{u,h}\|_{L^2(\Omega)} \Big) \\
& + \nu C_5 C_3^2 \Big(\|\boldsymbol{\eta}_{u,h}\|_{\text{grad},2} + \|\boldsymbol{e}_{u,h}\|_{\text{grad},2} \Big) + \beta g \sigma_{2,2} \Big(\|\eta_{T,h}\|_{L^2(\Omega)} + \|e_{T,h}\|_{L^2(\Omega)} \Big) \\
& + \Big(\|\boldsymbol{u}\|_{L^\infty(\Omega)} + \|\boldsymbol{u}_h\|_{L^\infty(\Omega)} \Big) \Big(\|\boldsymbol{\eta}_{u,h}\|_{L^2(\Omega)} + \|\boldsymbol{e}_{u,h}\|_{L^2(\Omega)} \Big) \\
& + d^{1/2}\sigma_{2,2} \|\boldsymbol{u}_h\|_{L^\infty(\Omega)} \Big(\|\boldsymbol{\eta}_{u,h}\|_{\text{grad},2} + \|\boldsymbol{e}_{u,h}\|_{\text{grad},2} \Big) . \qquad (2.4.94)
\end{aligned}
$$

Equivalently, upon using the inf-sup condition (Lemma 2.4.18) with $q_h = e_{p,h}$

and $p = 2$ on the LHS of Eq. (2.4.94), one obtains

$$\begin{aligned}\|e_{p,h}\|_{L^2(\Omega)} \le C_{13} \Bigg[& d^{1/2} \|\eta_{p,h}\|_{L^2(\Omega)} + \sigma_{2,2} \left(\|\partial_t \boldsymbol{\eta}_{u,h}\|_{L^2(\Omega)} + \|\partial_t \boldsymbol{e}_{u,h}\|_{L^2(\Omega)} \right) \\ & + \nu C_5 C_3^2 \left(\|\boldsymbol{\eta}_{u,h}\|_{\text{grad},2} + \|\boldsymbol{e}_{u,h}\|_{\text{grad},2} \right) + \beta g \sigma_{2,2} \left(\|\eta_{T,h}\|_{L^2(\Omega)} + \|e_{T,h}\|_{L^2(\Omega)} \right) \\ & + \left(\|\boldsymbol{u}\|_{L^\infty(\Omega)} + \|\boldsymbol{u}_h\|_{L^\infty(\Omega)} \right) \left(\|\boldsymbol{\eta}_{u,h}\|_{L^2(\Omega)} + \|\boldsymbol{e}_{u,h}\|_{L^2(\Omega)} \right) \\ & + d^{1/2} \sigma_{2,2} \|\boldsymbol{u}_h\|_{L^\infty(\Omega)} \left(\|\boldsymbol{\eta}_{u,h}\|_{\text{grad},2} + \|\boldsymbol{e}_{u,h}\|_{\text{grad},2} \right) \Bigg].\end{aligned}$$

Next, we square both sides and apply the root-mean-square-arithmetic-mean inequality

$$\begin{aligned}\|e_{p,h}\|^2_{L^2(\Omega)} \le 13\, C_{13}^2 \Bigg[& d \|\eta_{p,h}\|^2_{L^2(\Omega)} + \sigma_{2,2}^2 \left(\|\partial_t \boldsymbol{\eta}_{u,h}\|^2_{L^2(\Omega)} + \|\partial_t \boldsymbol{e}_{u,h}\|^2_{L^2(\Omega)} \right) \\ & + \nu^2 C_5^2 C_3^4 \left(\|\boldsymbol{\eta}_{u,h}\|^2_{\text{grad},2} + \|\boldsymbol{e}_{u,h}\|^2_{\text{grad},2} \right) + \beta^2 g^2 \sigma_{2,2}^2 \left(\|\eta_{T,h}\|^2_{L^2(\Omega)} + \|e_{T,h}\|^2_{L^2(\Omega)} \right) \\ & + \left(\|\boldsymbol{u}\|^2_{L^\infty(\Omega)} + \|\boldsymbol{u}_h\|^2_{L^\infty(\Omega)} \right) \left(\|\boldsymbol{\eta}_{u,h}\|^2_{L^2(\Omega)} + \|\boldsymbol{e}_{u,h}\|^2_{L^2(\Omega)} \right) \\ & + d \sigma_{2,2}^2 \|\boldsymbol{u}_h\|^2_{L^\infty(\Omega)} \left(\|\boldsymbol{\eta}_{u,h}\|^2_{\text{grad},2} + \|\boldsymbol{e}_{u,h}\|^2_{\text{grad},2} \right) \Bigg],\end{aligned}$$

or equivalently,

$$
\begin{aligned}
\|e_{p,h}\|^2_{L^2(\Omega)} \lesssim\ & \|\eta_{p,h}\|^2_{L^2(\Omega)} + \|\partial_t \boldsymbol{\eta}_{u,h}\|^2_{L^2(\Omega)} + \|\partial_t \boldsymbol{e}_{u,h}\|^2_{L^2(\Omega)} \\
& + \nu^2 \left(\|\boldsymbol{\eta}_{u,h}\|^2_{\mathrm{grad},2} + \|\boldsymbol{e}_{u,h}\|^2_{\mathrm{grad},2} \right) + \beta^2 g^2 \left(\|\eta_{T,h}\|^2_{L^2(\Omega)} + \|e_{T,h}\|^2_{L^2(\Omega)} \right) \\
& + \left(\|\boldsymbol{u}\|^2_{L^\infty(\Omega)} + \|\boldsymbol{u}_h\|^2_{L^\infty(\Omega)} \right) \left(\|\boldsymbol{\eta}_{u,h}\|^2_{L^2(\Omega)} + \|\boldsymbol{e}_{u,h}\|^2_{L^2(\Omega)} \right) \\
& + \|\boldsymbol{u}_h\|^2_{L^\infty(\Omega)} \left(\|\boldsymbol{\eta}_{u,h}\|^2_{\mathrm{grad},2} + \|\boldsymbol{e}_{u,h}\|^2_{\mathrm{grad},2} \right). \qquad (2.4.95)
\end{aligned}
$$

Recall that the following interpolation estimates hold in accordance with Assumption 2.4.19

$$
\|\eta_{p,h}\|^2_{L^2(\Omega)} \le C \sum_{K \in \mathcal{T}_h} h_K^{2(k_p+1)} \|p\|^2_{W^{k_p+1,2}(K)}, \qquad (2.4.96)
$$

$$
\|\eta_{T,h}\|^2_{L^2(\Omega)} \le C \sum_{K \in \mathcal{T}_h} h_K^{2(k_T+1)} \|T\|^2_{W^{k_T+1,2}(K)}, \qquad (2.4.97)
$$

$$
\|\boldsymbol{\eta}_{u,h}\|^2_{L^2(\Omega)} \le C \sum_{K \in \mathcal{T}_h} h_K^{2(k_u+1)} \|\boldsymbol{u}\|^2_{W^{k_u+1,2}(K)}, \qquad (2.4.98)
$$

$$
\|\boldsymbol{\eta}_{u,h}\|^2_{\mathrm{grad},2} \le C \sum_{K \in \mathcal{T}_h} h_K^{2k_u} \|\boldsymbol{u}\|^2_{W^{k_u+1,2}(K)}, \qquad (2.4.99)
$$

$$
\|\partial_t \boldsymbol{\eta}_{u,h}\|^2_{L^2(\Omega)} \le C \sum_{K \in \mathcal{T}_h} h_K^{2k_u} \|\partial_t \boldsymbol{u}\|^2_{W^{k_u,2}(K)}. \qquad (2.4.100)
$$

We can substitute Eqs. (2.4.96) – (2.4.100) into Eq. (2.4.95) in order to obtain

$$\begin{aligned}
\|e_{p,h}\|^2_{L^2(\Omega)} \lesssim \; & \|\partial_t \boldsymbol{e}_{u,h}\|^2_{L^2(\Omega)} + \nu^2 \|\boldsymbol{e}_{u,h}\|^2_{\text{grad},2} + \beta^2 g^2 \|e_{T,h}\|^2_{L^2(\Omega)} \\
& + \left(\|\boldsymbol{u}\|^2_{L^\infty(\Omega)} + \|\boldsymbol{u}_h\|^2_{L^\infty(\Omega)} \right) \|\boldsymbol{e}_{u,h}\|^2_{L^2(\Omega)} + \|\boldsymbol{u}_h\|^2_{L^\infty(\Omega)} \|\boldsymbol{e}_{u,h}\|^2_{\text{grad},2} \\
& + \sum_{K \in \mathcal{T}_h} \Bigg[h_K^{2(k_p+1)} \|p\|^2_{W^{k_p+1,2}(K)} + h_K^{2k_u} \|\partial_t \boldsymbol{u}\|^2_{W^{k_u,2}(K)} + \nu^2 h_K^{2k_u} \|\boldsymbol{u}\|^2_{W^{k_u+1,2}(K)} \\
& + \beta^2 g^2 h_K^{2(k_T+1)} \|T\|^2_{W^{k_T+1,2}(K)} + \left(\|\boldsymbol{u}\|^2_{L^\infty(\Omega)} + \|\boldsymbol{u}_h\|^2_{L^\infty(\Omega)} \right) h_K^{2(k_u+1)} \|\boldsymbol{u}\|^2_{W^{k_u+1,2}(K)} \\
& + \|\boldsymbol{u}_h\|^2_{L^\infty(\Omega)} h_K^{2k_u} \|\boldsymbol{u}\|^2_{W^{k_u+1,2}(K)} \Bigg]. \qquad (2.4.101)
\end{aligned}$$

Lastly, upon integrating both sides of Eq. (2.4.101) from $t = t_0$ to $t = t_n$, we obtain the final result (Eq. (2.4.90)). □

2.5. Expanded Formulation with Viscous Dissipation Term

In this section, we introduce an expanded formulation of the temperature equation which contains a viscous dissipation term. We have waited until now to introduce this term, as it would have significantly complicated the analysis of the schemes in section 2.4, and a complete analytical treatment of this term is outside the scope of the current work. However, it is included here, as we intend to examine its bulk effects on the numerical experiments of the next section.

We begin by noting that the viscous dissipation term contains the Frobenius inner product of the viscous stress tensor with the velocity gradient tensor as follows

$$\frac{1}{C_v}\boldsymbol{\tau} : \nabla \boldsymbol{u}. \tag{2.5.1}$$

This term is usually considered negligible in incompressible flows (as its magnitude usually scales with Ma^2), but can become important if velocity gradients are sufficiently large, or if the fluid is compressible, and the dilatational term becomes large. In accordance with standard physical arguments (see [52]), we can add the viscous dissipation term to the RHS of Eq. (2.2.3) as follows

$$\partial_t T + \nabla \cdot (T\boldsymbol{u}) - \nabla \cdot (\alpha\gamma\nabla T) = \frac{1}{C_v}\boldsymbol{\tau} : \nabla \boldsymbol{u} - (\gamma - 1)\, T\, (\nabla \cdot \boldsymbol{u}) + f_T, \tag{2.5.2}$$

in order to obtain an expanded version of the temperature equation. Upon discretizing this equation using well-known finite element techniques, one may obtain the following semi-discrete equation

$$\begin{aligned}
&(\partial_t T_h, r_h)_{\mathcal{T}_h} - (T_h \boldsymbol{u}_h, \nabla_h r_h)_{\mathcal{T}_h} + \left\langle \widehat{\boldsymbol{\phi}}_{\text{inv}} \cdot \boldsymbol{n}, r_h \right\rangle_{\partial\mathcal{T}_h} - \frac{1}{2}\left((\nabla \cdot \boldsymbol{u}_h)\, T_h, r_h \right)_{\mathcal{T}_h} \\
&+ \alpha\gamma \left[(\nabla_h T_h, \nabla_h r_h)_{\mathcal{T}_h} - \left\langle \widehat{\boldsymbol{\phi}}_{\text{vis}} \cdot \boldsymbol{n}, r_h \right\rangle_{\partial\mathcal{T}_h} + \left\langle \widehat{\lambda}_{\text{vis}} - T_h, \nabla_h r_h \cdot \boldsymbol{n} \right\rangle_{\partial\mathcal{T}_h} \right] \\
&= \left(\frac{\nu}{C_v} \left(\nabla_h \boldsymbol{u}_h + \nabla_h \boldsymbol{u}_h^T - \frac{2}{3} (\nabla \cdot \boldsymbol{u}_h)\, \mathbb{I} \right) : \nabla_h \boldsymbol{u}_h, r_h \right)_{\mathcal{T}_h} \\
&- (\gamma - 1) \left[\left((\nabla \cdot \boldsymbol{u}_h)\, T_h, r_h \right)_{\mathcal{T}_h} + C_{\text{mod}} \left(|\nabla \cdot \boldsymbol{u}_h|\, \nabla_h T_h, \nabla_h r_h \right)_{\mathcal{T}_h} \right] + (f_T, r_h)_{\mathcal{T}_h}.
\end{aligned} \tag{2.5.3}$$

In a natural fashion, one may modify the versatile methods in section 2.3 by replacing Eq. (2.3.3) with (2.5.3).

2.6. Numerical Experiments

In this section, the results of several numerical simulations are presented to demonstrate the performance of the proposed methods. The following simulations were performed using both Taylor-Hood and Brezzi-Douglas-Marini elements with polynomials of degree k, $k+1$, and $k+1$ for the kinematic pressure, temperature, and velocity spaces respectively; i.e. for cases with $k = 1$ the polynomials for each space were degree 1, 2, and 2 respectively. In addition, we imposed a zero integral mean condition for the kinematic pressure via a Lagrange multiplier. The convective numerical fluxes were computed using upwind biased fluxes with $\zeta = \delta = 0.5$, and the viscous numerical fluxes were computed using $\eta = \varepsilon = 3(k+1)(k+2)$. The stability constant was $C_{\text{mod}} = 0$ unless otherwise stated. In each case, either a high-order BDF3 or BDF5 scheme was used for the time discretization. The meshes were developed using rectangular grids where the quadrilateral elements were split along the diagonals to create triangles. Throughout this section, mesh dimensions are reported as $N \times M$, where N and M refer to the number of quadrilaterals in the x and y directions, respectively. The total number of elements for each case was $2N \times 2M$ due to the splitting mentioned previously. Finally, each simulation was performed in the open-source finite element software package FEniCS [53].

The remainder of this section consists of several canonical test cases involving natural and mixed convection. More specifically, in section 2.6.1 we evaluate the order of accuracy of the formulation presented in section 2.3. In sections 2.6.2 and 2.6.3 we perform a comparison between the two formulations presented in sections 2.3 and 2.5. In addition, in subsection 2.6.3 we evaluate the effects of the stability term (the C_{mod} term). In the final section, 2.6.4, we demonstrate the methods' ability to simulate 3-dimensional natural convection-driven flows.

2.6.1 Non-Isothermal Taylor-Green Test

For the first test case, we compared solutions from our methods to an exact solution of a non-isothermal Taylor-Green vortex array in order to check the convergence rates of the discrete velocity, temperature, and kinematic pressure fields. Here, we prescribed the initial condition at $t = 0$ as follows

$$\begin{aligned}
\boldsymbol{u} &= \left(\sin x \cos y \exp\left(-2\nu t\right), -\cos x \sin y \exp\left(-2\nu t\right)\right), \\
p &= \frac{1}{4}\left(\cos 2x + \cos 2y\right) \exp\left(-4\nu t\right), \\
T &= \frac{1}{2}\left(\sin x \sin y\right) \exp\left(-2\gamma\alpha t\right),
\end{aligned}$$

on the domain $\Omega = [-1,1]^2$. The vortex array was simulated for $t \in [0, 0.5]$. During this time, we defined the gravitational and forcing functions as follows

$$\boldsymbol{g} = (0, -1), \qquad f_T = 0,$$
$$\boldsymbol{f}_u = \left(0, \frac{1}{2}\beta \sin x \sin y \exp\left(-2\gamma\alpha t\right)\right).$$

We considered a dimensionless formulation with $\alpha = \beta = \nu = \rho = 1$ and $\gamma = 1.4$. Note: in subsequent test cases, a dimensional formulation was considered.

The Taylor-Green test cases were run on a uniform periodic domain tessellated with $N \times N$ elements, where N ranged from 4 to 32. The time marching scheme used was BDF5 with a time step $\Delta t = 0.01$ for all k. For this case, we considered polynomial degrees of $k = 1$, 2, and 3. We expected a convergence rate of $k+2$ for the discrete velocity and temperature fields since the associated polynomial spaces were degree $k+1$, and a rate of $k+1$ for the kinematic pressure field since the associated polynomial space was degree k. One can see from tables 2.1 and 2.2 that we recover the predicted convergence rates for the Taylor-Hood and Brezzi-Douglas-Marini elements, respectively.

2.6.2 Heated Cavity Test

The second test case was a heated cavity as described by [1]. This case consisted of a square cavity $\Omega = [0,1]^2$ with stationary walls. The flow was driven by a temperature difference between the left and right walls, and thus consisted of purely

k	h	dofs	Velocity		Pressure		Temperature	
			L^2 error	order	L^2 error	order	L^2 error	order
1	2.221441	209	0.07310	-	0.008789	-	0.01342	-
	1.11072	833	0.007436	3.2972	0.003517	1.3214	0.001320	3.3460
	0.5536	3329	7.508e-4	3.3080	7,121e-4	2.3042	1.258e-4	3.3910
	0.27768	13313	8.5806e-5	3.1294	1,684e-4	2.0801	1.386e-5	3.1817
2	2.221441	197	0.007439	-	0.004243	-	0.001213	-
	1.11072	785	4.009e-4	4.2136	5.552e-4	2.9341	6.287e-5	4.2704
	0.5536	3137	2.351e-5	4.0920	7.584e-5	2.8722	3.702e-6	4.0858
	0.27768	12545	1.443e-6	4.0262	9.860e-6	2.9432	2.278e-7	4.0226
3	1.11072	913	8.750e-4	-	6.380e-4	-	1.369e-4	-
	0.5536	3649	2.953e-5	4.8887	4.374e-5	3.8664	4.573e-6	4.9044
	0.35543	14593	9.586e-7	4.9455	2.268e-6	4.26946	1.476e-7	4.9532
	0.27768	58369	3.029e-8	4.9838	1.336e-7	4.0857	4.721e-9	4.9668

Table 2.1: Velocity, kinematic pressure, and temperature L^2 errors for various polynomial degrees k and maximum element diameters h with Taylor-Hood elements.

k	h	dofs	Velocity		Pressure		Temperature	
			L^2 error	order	L^2 error	order	L^2 error	order
1	2.221441	401	0.09432	-	0.1373	-	0.01348	-
	1.11072	1601	0.009503	3.3111	0.05571	1.3022	0.001318	3.3544
	0.5536	6401	8.153e-4	3.5429	0.01544	1.8507	1.260e-4	3.3874
	0.27768	25601	8.0678e-5	3.3372	0.003971	1.9597	1.387e-5	3.1827
2	2.221441	785	0.008689	-	0.04225	-	0.001214	-
	1.11072	12545	4.384e-4	4.3088	0.006343	2.7360	6.285e-5	4.2722
	0.5536	3137	2.566e-5	4.0944	8.597e-4	2.8833	3.702e-6	4.0855
	0.27768	50177	1.574e-6	4.0274	1.108e-5	2.9547	2.278e-7	4.0225
3	1.11072	1297	0.001170	-	0.008204	-	1.369e-4	-
	0.5536	5185	3.571e-5	5.0348	5245e-4	3.9672	4.573e-6	4.9041
	0.35543	20737	1.116e-6	4.9992	3.209e-5	4.0309	1.476e-7	4.9532
	0.27768	82945	3.498e-8	4.9965	1.992e-6	4.0094	4.721e-9	4.9668

Table 2.2: Velocity, kinematic pressure, and temperature L^2 errors for various polynomial degrees k and maximum element diameters h with Brezzi-Douglas-Marini elements.

natural convection. Gravity $\mathbf{g} = (0, -1)^T \ \frac{m}{s^2}$ in conjunction with buoyancy effects influenced the fluid motion. For all heated cavity simulations, a fixed Prandtl number $Pr = 0.71$ defined as

$$Pr = \frac{\nu}{\alpha},$$

was used. Fluid properties for all cases were $\alpha = 2.208 \times 10^{-5} \ \frac{m^2}{s}$, $C_v = 717.8$ $\frac{J}{kg-K}$, $\rho = 1 \ \frac{kg}{m^3}$, and $\nu = 1.568 \times 10^{-5} \ \frac{m^2}{s}$ which denote an air-like fluid. In order to facilitate comparison to [1], our first set of simulations were generated using $\gamma = 1$. All walls were equipped with no-slip boundary conditions, where the left and right walls had fixed Dirichlet temperature boundary conditions $T_{left} = 0.5$ K and $T_{right} = -0.5$ K, and where the top and bottom walls were adiabatic. For this set of simulations, the Rayleigh number Ra was varied throughout. Specifically, we decided to vary the Rayleigh number by varying the parameter β, using the following formulas

$$Ra = \frac{\mathbf{g}\beta \Delta T L^3}{\nu^2}, \qquad \Delta T = (T_{left} - T_{right}),$$

where L is the width of the cavity. We were interested in computing the average steady state Nusselt number $\overline{Nu}$ based on the horizontal heat flux as follows

$$\overline{Nu} = \int_0^1 \frac{HL}{\alpha} dx, \qquad H = \frac{\langle q_x \rangle_y}{A \Delta T},$$
$$\langle q_x \rangle_y = \int_0^1 q_x dy, \qquad q_x = u_x T - \alpha \frac{\partial T}{\partial x},$$

where A is the domain area, and u_x is the velocity in the x-direction. The Nusselt number was calculated at Rayleigh numbers of $Ra = 10^4, 10^5, 10^6$, and 10^7 which enabled the flow to remain laminar. At each Rayleigh number, four different grids of size $N \times N$ were considered with $N = 8$, 16, 32, and 64. The only exception was for Rayleigh number $Ra = 10^7$, as the 8×8 grid could not be converged for this condition. The mesh used for each simulation was biased towards the walls using the mapping proposed by [54]

$$x_{refined} = \left(x - \frac{1}{2\pi}(1-a)\sin(2\pi x)\right),$$
$$y_{refined} = \left(y - \frac{1}{2\pi}(1-b)\sin(2\pi y)\right),$$
$$a = \left(\overline{Nu}\right)^{-1}, \qquad b = \left(\overline{Nu}\right)^{-1/3}.$$

Note: in order to generate our meshes, we used the average Nusselt numbers reported in [1]. On each mesh, a BDF3 scheme was used for the time discretization. We also note that, both Taylor-Hood and Brezzi-Douglas-Marini elements of degree $k = 2$ and 3 were used. In addition to using different function spaces (TH and BDM), we tested two different formulations. The first formulation employed the versatile methods outlined in section 2.3. This formulation is referred to as the non-dissipative formulation since we are neglecting the viscous dissipation term from the temperature equation. The other formulation of versatile mixed methods appears in section 2.5, which includes the viscous dissipation term. This version of the methods will henceforth be referred to as the dissipative formulation.

At the lowest Rayleigh number, the flow was dominated by a large central vortex seen in figure 2.1. As the Rayleigh number was increased, this vortex disappeared and thin boundary layers developed on the left and right walls as seen in figures 2.2 and 2.3. This is the same behavior observed by [1] during their simulations performed without a viscous dissipation term. We note that each of our figures was generated using Taylor Hood elements; however, all function spaces and formulations produced nearly identical figures. Here, we have simply elected to omit the remaining figures for the sake of brevity.

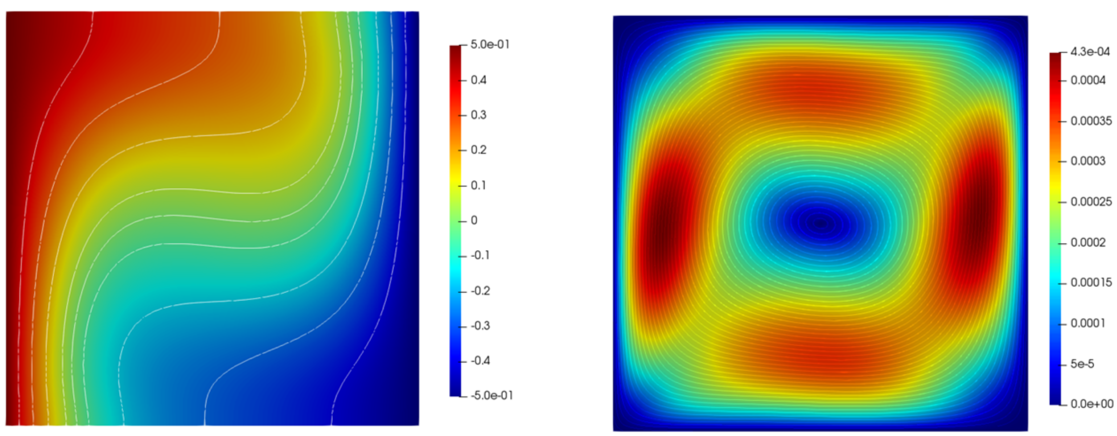

Figure 2.1: Temperature (left) and velocity magnitude (right) for Rayleigh number $Ra = 10^4$. The non-dissipative formulation with a 64×64 mesh and $k = 2$ Taylor Hood elements was used to generate these results.

We also saw very similar values of the average Nusselt numbers for all mesh resolutions, method formulations, function spaces, and polynomial degrees as seen in tables 2.3 and 2.4.

Finally, we ran a separate set of tests using $\gamma = 1.4$, $Ra = 10^4$, and $k = 2$ Taylor-Hood elements. The purpose of these tests was to assess the performance

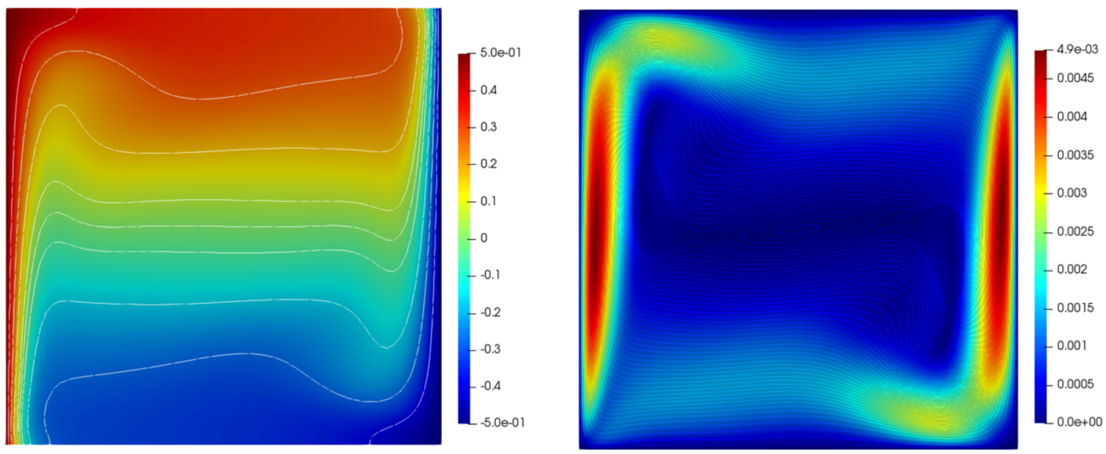

Figure 2.2: Temperature (left) and velocity magnitude (right) for Rayleigh number $Ra = 10^6$. The non-dissipative formulation with a 64×64 mesh and $k = 2$ Taylor Hood elements was used to generate these results.

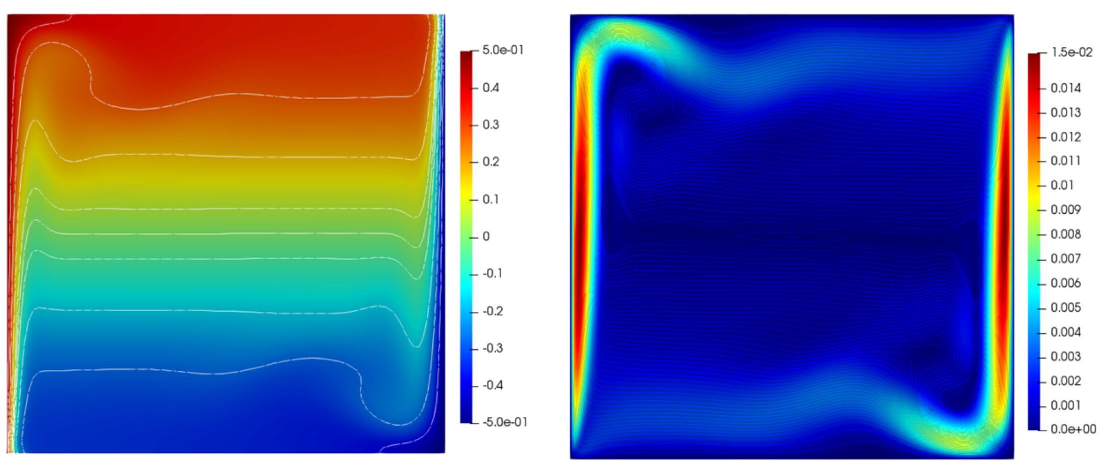

Figure 2.3: Temperature (left) and velocity magnitude (right) for Rayleigh number $Ra = 10^7$. The non-dissipative formulation with a 64×64 mesh and $k = 2$ Taylor Hood elements was used to generate these results.

of our mixed methods with and without the temperature-scaled divergence term, $-(\gamma - 1)\, T(\nabla \cdot \boldsymbol{u})$. In order to isolate the effects of this term, the viscous dissipation

Ra	N	$\overline{Nu}$ ref.	$\overline{Nu_{TH}}$		$\overline{Nu_{BDM}}$	
			$k=2$	$k=3$	$k=2$	$k=3$
10^4	8	-	2.24480	2.24481	2.24478	2.24481
	16	2.24478	2.24481	2.24481	2.24481	2.24481
	32	2.24481	2.24481	2.24481	2.24481	2.24481
	64	2.24482	2.24481	2.24481	2.24481	2.24481
10^5	8	-	4.52206	4.52162	4.52198	4.52161
	16	4.52124	4.52163	4.52163	4.52163	4.52163
	32	4.52162	4.52163	4.52163	4.52163	4.52163
	64	4.52163	4.52163	4.52163	4.52163	4.52163
10^6	8	-	8.81679	8.82497	8.64593	8.75790
	16	8.81573	8.82514	8.82519	8.82519	8.82519
	32	8.82502	8.82520	8.82520	8.82520	8.82520
	64	8.82519	8.82520	8.82520	8.82520	8.82520
10^7	16	15.3718	16.5190	16.5227	16.5224	16.5230
	32	16.5156	16.5229	16.5230	16.5230	16.5230
	64	16.5230	16.5230	16.5230	16.5230	16.5230

Table 2.3: Average Nusselt numbers for various Rayleigh numbers, mesh resolutions, function spaces, and polynomial degrees. All results were generated using the formulation of the versatile mixed methods *with* the viscous dissipation term. Reference values are taken from [1].

term was omitted. Table 2.5 summarizes the results of our tests. Here, it is clear that the simulations with and without the temperature-scaled divergence term yielded similar results, indicating that the inclusion of the term has minimal effects.

Ra	N	$\overline{Nu}$ ref.	$\overline{Nu_{TH}}$		$\overline{Nu_{BDM}}$	
			$k=2$	$k=3$	$k=2$	$k=3$
10^4	8	-	2.24480	2.24481	2.24482	2.24481
	16	2.24478	2.24481	2.24481	2.24481	2.24482
	32	2.24481	2.24481	2.24481	2.24481	2.24481
	64	2.24482	2.24481	2.24481	2.24481	2.24481
10^5	8	-	4.52201	4.52160	4.52164	4.52162
	16	4.52124	4.52163	4.52163	4.52163	4.52163
	32	4.52162	4.52163	4.52163	4.52163	4.52163
	64	4.52163	4.52163	4.52163	4.52163	4.52163
10^6	8	-	8.81900	8.82493	8.99810	8.70510
	16	8.81573	8.82514	8.82519	8.82519	8.82520
	32	8.82502	8.82520	8.82520	8.82520	8.82520
	64	8.82519	8.82520	8.82520	8.82520	8.82520
10^7	16	15.3718	16.5190	16.5227	16.5224	16.5230
	32	16.5156	16.5229	16.5230	16.5230	16.5230
	64	16.5230	16.5230	16.5230	16.5230	16.5230

Table 2.4: Average Nusselt numbers for various Rayleigh numbers, mesh resolutions, function spaces, and polynomial degrees. All results were generated using the formulation of the versatile mixed methods *without* the viscous dissipation term. Reference values are taken from [1].

Ra	N	$\overline{Nu}$ Without divergence term	$\overline{Nu}$ With divergence term
10^4	8	2.40656	2.40661
	16	2.40656	2.40656
	32	2.40656	2.40656
	64	2.40656	2.40656

Table 2.5: Average Nusselt numbers for the mixed methods with and without the temperature-scaled divergence term, for $\gamma = 1.4$ and $k = 2$ Taylor-Hood elements. All results were generated using the versatile mixed methods *without* the viscous dissipation term.

2.6.2.1 Heated Cavity Stability Test

Having confirmed that the versatile mixed methods can capture the behavior of buoyancy-driven flows, we sought to test the effects of the auxiliary stability term

$$-(\gamma-1)\, C_{\text{mod}} \left(\left|\nabla \cdot \boldsymbol{u}_h\right| \nabla_h T_h, \nabla_h r_h\right)_{\mathcal{T}_h}.$$

To this end, we chose to run the same heated cavity case presented in section 2.6.2 using $Ra = 5 \times 10^7$ and $k = 1$ Taylor-Hood elements. We again used an $N \times N$ mesh with $N = 64$. The same fluid properties prescribed in section 2.6.2 with $\gamma = 1.4$ are used again here. For this experiment, we used the non-dissipative formulation only. We ran two cases to affirm that the proposed stability term would work to diffuse (and help stabilize) the velocity and temperature fields. For this purpose, we ran a baseline case without the stability term, and a case with a relatively large value of the stability constant: $C_{\text{mod}} = 2.0 \times h^2$. Here h refers to the maximum diameter of an element in the mesh.

We can see from figures 2.4 and 2.5 the effects of the stability term. Figure 2.4 shows the case without the stability term, and here we can see the formation of a large diagonal vortex in the velocity field. In the temperature field, we can see relatively horizontal temperature contours. Figure 2.5 shows the case *with* the stability term, and here we can see that the vortex is diffused and is in the process of splitting into two smaller vortices. In the temperature field, we can see much more blending and less uniform contour lines. Based on these results, we can conclude that the stability term is working to smooth out and stabilize our solution.

2.6.3 Heated Cavity with Moving Wall Test

The next test case was a heated cavity with one moving wall, i.e. a mixed convection case. Here, the top wall moved at constant velocity V_{lid} and was heated, while the

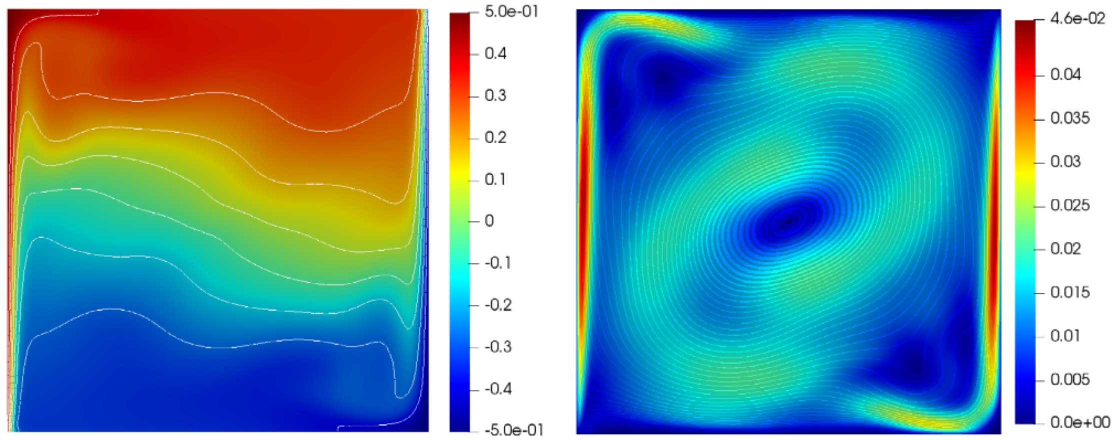

Figure 2.4: Temperature contours (left) and velocity magnitude contours with streamlines (right) for $Ra = 5 \times 10^7$ and $\gamma = 1.4$. The formulation *without* the stability term was used to obtain these results.

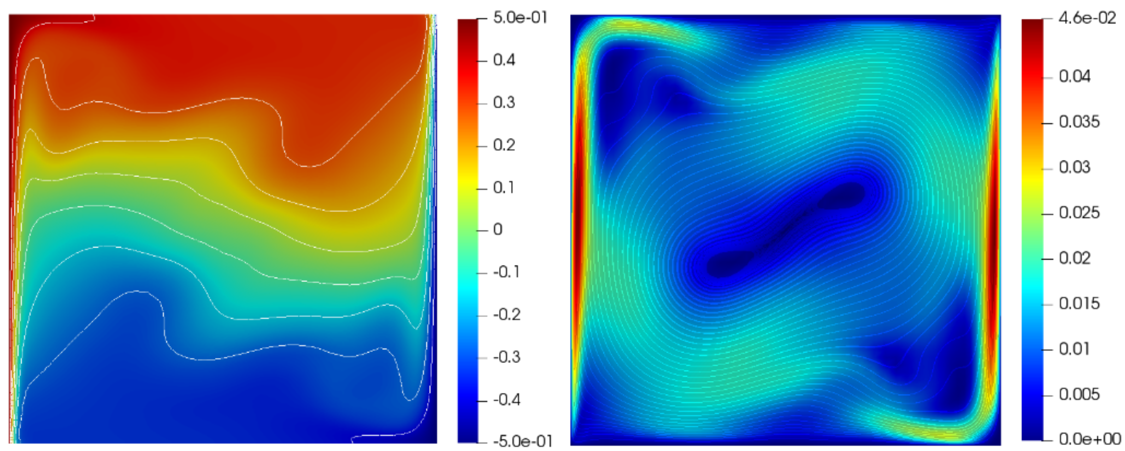

Figure 2.5: Temperature contours (left) and velocity magnitude contours with streamlines (right) for $Ra = 5 \times 10^7$ and $\gamma = 1.4$. The formulation *with* the stability term and $C_{\text{mod}} = 2.0 \times h^2$ was used to obtain these results.

bottom stationary wall was cooled as proposed by [2]. This case was run at a fixed

Grashof number $Gr = 10^4$ along with varied Richardson numbers Ri, where

$$Gr = \frac{\mathbf{g}\beta L \Delta T}{\nu^2}, \qquad \Delta T = (T_{top} - T_{bottom}), \qquad Ri = \frac{Gr}{Re^2}, \qquad Re = \frac{V_{lid} L}{\nu}.$$

We used the same fluid properties prescribed in the previous heated cavity case. In this case, we considered Richardson numbers $Ri = 0.01, 0.06$ and 1.0. The domain was a box $\Omega = [0,1]^2$ with a uniform mesh that consisted of 64×64, $k = 2$ elements. As with the previous experiments, two different types of function spaces were used (TH and BDM) in conjunction with two different formulations of the methods (dissipative and non-dissipative) along with $\gamma = 1$. A BDF3 scheme was used for the time discretization. The heated top wall was held at a constant temperature $T_{top} = 1$ K, while the bottom cold wall was held at $T_{bottom} = 0$ K, with the remaining walls having adiabatic boundary conditions. Gravity was again present in this case with $\mathbf{g} = (0, -1)^T \ \frac{m}{s^2}$. The quantity of interest for this case was again the average steady state Nusselt number $\overline{Nu}$; however for this case we were only interested in the Nusselt number along the top heated wall, referred to henceforth as $\overline{Nu}_{wall}$. We define the vertical heat flux q_y and $\overline{Nu}_{wall}$ as

$$\overline{Nu}_{wall} = \frac{HL}{\alpha}, \qquad H = \frac{\langle q_y \rangle_x}{A \Delta T},$$
$$q_y = -\frac{\partial T}{\partial y}, \qquad \langle q_y \rangle_x = \int_0^1 [q_y]_{y=1} dx.$$

The results for both formulations are similar and are shown in tables 2.6 and 2.7, alongside reference data from [2]. We note that the reference data was generated using a formulation without the viscous dissipation term. In each case, the best agreement with the reference data occurs for the largest Richardson number $Ri = 1$. The other two cases with Richardson numbers $Ri = 0.06$ and 0.01 show more deviation from the reference. We believe that the discrepancy comes from the

Ri	$\overline{Nu}_{wall}$ ref	$\overline{Nu}_{wall}$ TH	$\overline{Nu}_{wall}$ BDM
1.0	1.34	1.39	1.39
0.06	3.62	3.87	3.90
0.01	6.29	6.52	6.59

Table 2.6: $\overline{Nu}_{wall}$ at various Richardson numbers, for our versatile mixed methods with $k = 2$ and two different function spaces, alongside reference data. The data here was generated using the formulation *with* the viscous dissipation term. We use [2] for the reference values.

Ri	$\overline{Nu}_{wall}$ ref	$\overline{Nu}_{wall}$ TH	$\overline{Nu}_{wall}$ BDM
1.0	1.34	1.46	1.40
0.06	3.62	3.91	3.91
0.01	6.29	6.62	6.62

Table 2.7: $\overline{Nu}_{wall}$ at various Richardson numbers, for our versatile mixed methods with $k = 2$ and two different function spaces, alongside reference data. The data here was generated using the formulation *without* the viscous dissipation term. We use [2] for the reference values.

mesh resolution used. In the reference, a grid of $N = 128$ was used as opposed to the present study where $N = 64$. As seen in figures 2.6, 2.7, and 2.8, as the Richardson number increases, so too does the velocity at the wall. This explains why as Richardson number increases, we deviate from the reference as with the present mesh we are not completely resolving the velocity gradient at the wall which is needed to calculate the Nusselt number. Regardless, the trends observed in the

Ri	$\overline{Nu}_{wall}$ Without divergence term	$\overline{Nu}_{wall}$ With divergence term
1.0	1.30	1.30
0.06	3.48	3.48
0.01	5.92	5.86

Table 2.8: $\overline{Nu}_{wall}$ at various Richardson numbers for mixed methods with and without the temperature-scaled divergence term, for $\gamma = 1.4$ and $k = 2$ Taylor-Hood elements. The data here was generated using the formulation *without* the viscous dissipation term.

tables show that the predicted Nusselt numbers are still reasonable (relative to the reference), and that the two formulations do not produce dramatically different results on the same grid.

Finally, we re-ran the cases with $\gamma = 1.4$. We considered a formulation with the temperature-scaled divergence term, and a formulation without this term. For both methods, the viscous dissipation term was omitted. In table 2.8, we can see that the methods produced similar values of $\overline{Nu}_{wall}$ for the various Ri numbers tested.

2.6.4 Rayleigh-Bénard Convection Test

The final test case was Rayleigh-Bénard convection inside a cylindrical domain with dimensions

$$\Omega = \left\{ (x, y, z) \in \left(-\frac{1}{2}, \frac{1}{2} \right)^3 \Big| \sqrt{x^2 + y^2} \leq \frac{1}{2}, |z| \leq \frac{1}{2} \right\}. \qquad (2.6.1)$$

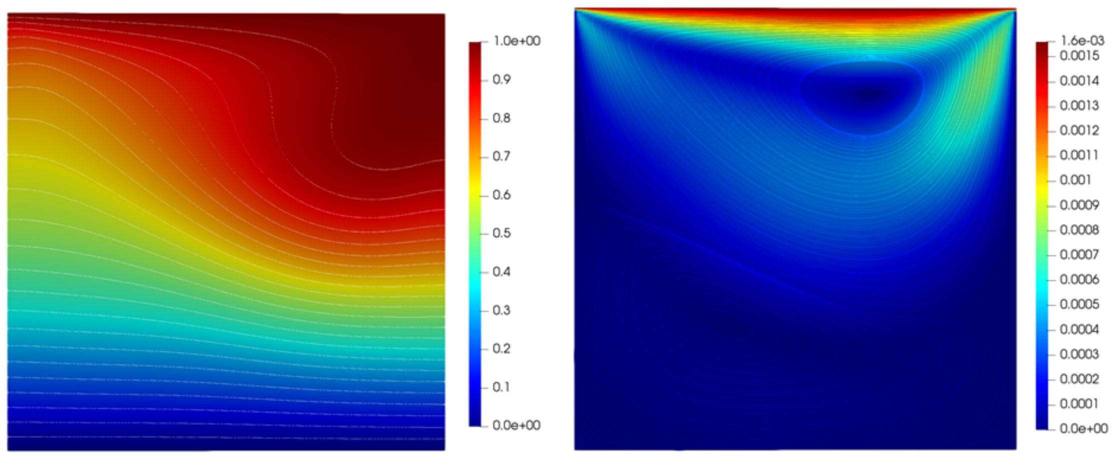

Figure 2.6: Temperature contours (left) and velocity magnitude contours with streamlines (right) for Richardson number $Ri = 1$. The non-dissipative formulation with a 64×64 mesh and $k = 2$ Taylor Hood elements was used to generate these results.

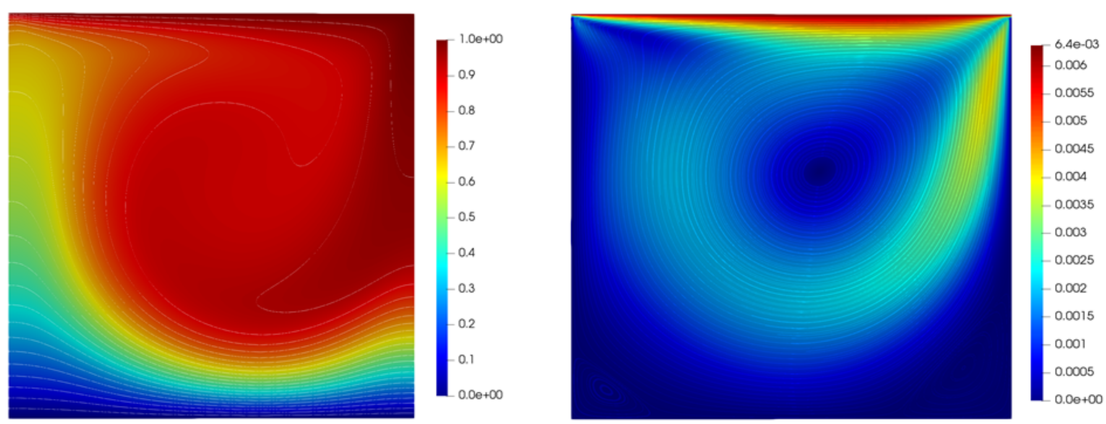

Figure 2.7: Temperature contours (left) and velocity magnitude contours with streamlines (right) for Richardson number $Ri = 0.06$. The non-dissipative formulation with a 64×64 mesh and $k = 2$ Taylor Hood elements was used to generate these results.

The computational domain was an unstructured tetrahedral mesh comprised of $50,000$ elements. Here, the lower wall was heated while the top was cooled in

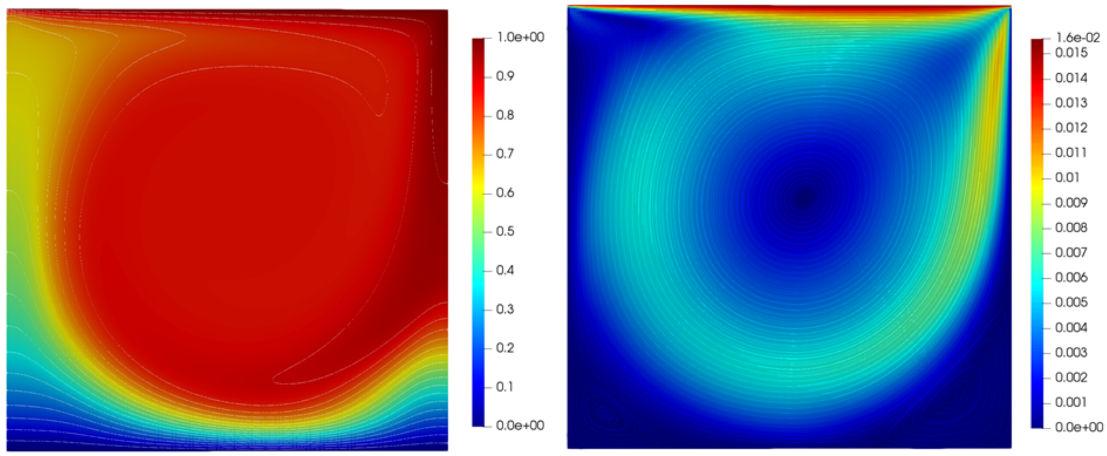

Figure 2.8: Temperature contours (left) and velocity magnitude contours with streamlines (right) for Richardson number $Ri = 0.01$. The non-dissipative formulation with a 64×64 mesh and $k = 2$ Taylor Hood elements was used to generate these results..

order to force mixing in the domain. Rayleigh numbers of $Ra = 10^5$ and $Ra = 10^6$ were used for this case. Fluid properties were defined as follows: $\alpha = 2.208 \times 10^{-5}$ $\frac{m^2}{s}$, $C_v = 717.8 \ \frac{J}{kg-K}$, $\rho = 1 \ \frac{kg}{m^3}$, and $\nu = 1.7354 \times 10^{-5} \ \frac{m^2}{s}$. The temperatures of the top and bottom walls were $T_{top} = -0.5$ K and $T_{bottom} = 0.5$ K, respectively. This case was run using $k = 1$, Taylor-Hood elements and the non-dissipative formulation. For this case, BDF5 was used with a time-step size of $\Delta t = 0.25$ seconds. The $Ra = 10^5$ case was run to a steady state whereas the $Ra = 10^6$ case was unsteady, and was run to a final time of $t = 1000$ seconds. The quantity of interest for this case is the Nu_{avg} over the whole domain which is defined as

$$Nu_{avg} = \frac{1}{\alpha \, |\Omega| \, (t_n - t_0) \, \Delta T} \int_{t_0}^{t_n} \int_{\Omega} q_z(x, y, z, t) \, dx \, dy \, dz \, dt.$$

We compare our Nu_{avg} values with [1] in table 2.9. For the case of $Ra = 10^5$, we have reported a Nu_{avg} value at the final steady state. For the case of $Ra = 10^6$, we have reported a Nu_{avg} value which was averaged over the interval $t = [150, 1000]$ seconds. The calculated Nu_{avg} values are in good agreement with the reference.

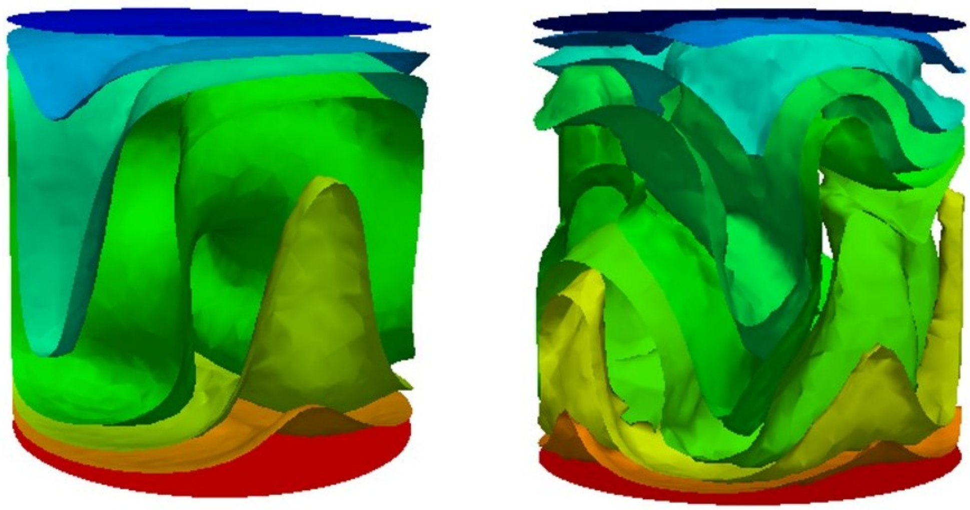

Figure 2.9: Temperature isocontours for the Rayleigh-Bénard convection cell for $Ra = 10^5$ (left) and $Ra = 10^6$ (right). The $Ra = 10^5$ case was run to steady state while the $Ra = 10^6$ case was run to $t = 1000$ seconds. The results were obtained with the non-dissipative formulation on a grid with 50,000 tetrahedra, and $k = 1$ Taylor-Hood elements.

Ra	Nu_{avg}	Nu_{avg} ref.
10^5	3.81	3.83
10^6	8.57	8.64

Table 2.9: Nu_{avg} at Ra=10^5 and Ra=10^6 as compared to the reference [1]. The results were obtained with the non-dissipative formulation on a grid with 50,000 tetrahedra, and $k = 1$ Taylor-Hood elements.

In addition, we can see from figure 2.9, the primary characteristics of the Rayleigh-

Bénard convection cell. The hot fluid at the bottom of the cavity rises to the top and this drives a mixing action in the cavity. The observed behavior matches the behavior seen by other authors (for example [1]) at these Rayleigh numbers.

2.7. Conclusion

In the present study, the mixed methods first put forward by Chen and Williams [41] are extended to non-isothermal incompressible flows. The primary advantages that these new methods possess are their generality and flexibility, as they utilize the full compressible formulation of the stress tensor and the expanded formulation of the temperature equation (which retains the dilatational term). In this chapter, the new versatile methods are constructed for weakly divergence-free Taylor-Hood elements, and pointwise divergence-free BDM and RT elements. Next, we establish the L2-stability of the discrete temperature, velocity, and kinematic pressure fields for these methods. In addition, we prove rigorous error estimates for the temperature, velocity, and kinematic pressure fields. Thereafter, we introduce an augmented formulation of the methods which includes an additional viscous dissipation term. Finally, the accuracy of the resulting Taylor-Hood and BDM methods is tested using four cases; these tests are used to confirm the formal order of accuracy of the methods, and demonstrate their performance on problems with natural and mixed convection. The two formulations of the methods (with and without the viscous dissipation term) are shown to produce similar results, and to provide good agreement with established reference data. It is our hope that the analysis and numerical experiments in this work will serve as a useful stepping stone towards the application of these methods to weakly-compressible and fully-compressible flows.

3 Versatile Mixed Methods for Compressible Flows

3.1. Motivation

In this chapter, we discuss the discretization of the compressible Navier-Stokes equations using 'versatile mixed finite element methods'. This paper introduces an important extension to previous mixed methods for solving the isothermal incompressible Navier-Stokes equations [41], and the *non-isothermal* incompressible Navier-Stokes equations [55]. While mixed finite element methods have seen significant interest for applications to incompressible flows, there has been very limited interest in applying them to compressible flows. This is primarily due to the greater complexity and non-linearity of compressible flows relative to incompressible flows. There are many numerical methods which have the potential to address this challenge. However, in this work we will focus on finite element methods due to their compact stencil, ability to operate on unstructured grids, high-order accuracy, and strong mathematical foundations.

Broadly speaking, we can classify finite element methods for simulating fluids into different categories based on their stabilization strategies. There are at least five stabilization strategies of immediate interest to us: i) residual-based stabilization, ii) numerical-flux-based stabilization, iii) entropy-based stabilization, iv) kinetic-energy-based stabilization, and v) inf-sup stabilization. Often, combinations of these stabilization strategies are used within the same finite element method. In what follows, we will describe each stabilization strategy, its strengths and weaknesses, and then provide some examples of finite element methods which use the strategy. Based on this broad discussion, we will identify the particular stabilization strategies which we deem most effective. Then, we will explain how versatile mixed methods achieve stability using these particular strategies, and how our methods fit into the general landscape of finite element methods for weakly- and fully-compressible flows.

Note: for those readers who are familiar with finite element stabilization strategies, they may skip section 3.1.1, and proceed directly to section 3.1.2.

3.1.1 Background

Let us begin by considering a residual-based stabilization strategy. For example, the standard continuous Galerkin (CG) finite element formulation is frequently augmented with a stabilization term which contains the product of the residual operator applied to the solution, a symmetric positive definite matrix, and a residual operator applied to the test functions. Streamline Upwind Petrov-Galerkin (SUPG) methods [32, 56, 57] use this strategy for stabilization, as they leverage a convection-based residual operator for the test functions. The SUPG methods are known for their excellent performance in convection-dominated flows, although they are not guaranteed to remain stable in the diffusive limit. Galerkin-Least-Squares (GLS) methods [57] are closely related to SUPG methods, with the caveat that they apply the full residual operator (both its advective and diffusive parts) to the test functions. See [15, 58, 59] for a general discussion of least-squares finite element methods. These methods often perform well in both convection- and diffusion-dominated flows, as they are mathematically guaranteed to maintain stability in both settings. Lastly, the Variational Multiscale (VMS) methods [60–63] are closely related to GLS methods, with the caveat that they apply the adjoint of the full residual operator to the test functions. In contrast to SUPG and GLS methods, these methods achieve adjoint consistency, although they are not guaranteed to maintain stability. A clear downside of residual-based stabilization is the substantial difficulty in constructing a well-behaved, positive-definite stabilization matrix. This user-specified matrix must be universal, as it must maintain stability and recover the correct order of accuracy in smooth parts of the flow, for all applications of interest.

Next, we consider a numerical-flux-based stabilization strategy. For example, the standard discontinuous Galerkin (DG) finite element formulation is frequently equipped with numerical fluxes which add artificial dissipation to the solution that is proportional to jumps in the solution and/or its gradient. The local DG (LDG) [64–68], Bassi-Rebay DG [69–71], and compact DG (CDG) [72–74] methods use this stabilization strategy. These DG methods have been effectively applied to many convection-dominated flows. Although they are not mathematically guaranteed to maintain stability, the numerical dissipation can be increased as necessary to achieve stabilization. More precisely, the numerical flux contains user-specified constants which can be increased in order to amplify the amount of dissipation. Of course, this strategy is not without risk, as it can result in significant convergence issues within Newton's method due to excessive numerical stiffness. In order to address this issue and to reduce cost, many variants of the classical DG methods have emerged, including hybridized discontinuous Galerkin (HDG) [75–77], embedded discontinuous Galerkin (EDG) [78, 79], discontinuous Petrov Galerkin (DPG) [80–83], and variational multiscale discontinuous (VMSD) [84–86] methods.

In addition, we can consider an entropy-based stabilization strategy. For this approach, the compressible Navier-Stokes equations are rewritten in terms of 'entropy variables' using a specialized entropy functional [87]. The development of this functional is based on symmetrizing techniques for conservation laws [88, 89]. Many researchers have applied CG and DG discretization methods to the entropy-symmetrized version of the governing equations, (see the reviews in [90–93] for details). The resulting schemes are provably stable for compressible flows. Furthermore, they discretely satisfying the Second Law of Thermodynamics, and can retain stability in the presence of shockwaves at low supersonic speeds without shock-capturing operators. Despite these advantages, there are two significant shortcomings of the entropy-based stabilization approach: a) the entropy variables are highly non-linear functions of the conservative variables, and as a result, they can impede the convergence of Newton's method; b) the entropy is not a useful quantity for controlling the solution as flow conditions approach the incompressible limit. Regarding the last point: the entropy is implicitly related to the compressibility of the flow. For an isothermal, incompressible flow, the entropy remains constant.

Next, we consider a kinetic-energy-based stabilization strategy. The key idea behind this approach is that kinetic energy is conserved within an unsteady, inviscid, incompressible flow. It turns out that, with the appropriate choice of numerical fluxes and function spaces, this kinetic energy conservation property can be reproduced at the discrete level. An elegant proof of this property for H(div)-conforming mixed methods and specialized DG methods appears in [94]. It is important to note that these methods are similar (but not identical) in nature to the kinetic energy preserving (KEP) DG methods [95–99]. These latter methods use a skew-symmetric formulation of the momentum equation in order to create a discrete formulation of the compressible kinetic energy equation which mimics the continuous equation. The KEP finite element methods are very similar to KEP finite volume methods which were developed earlier in [100, 101], and the DG method of [102]. There are potential advantages for using kinetic-energy-based stabilization instead of entropy-based stabilization, as some KEP schemes possess superior robustness, (see [101] for details). Furthermore, kinetic energy is a quantity that remains important in both compressible and incompressible flows, unlike entropy. Lastly, kinetic-energy-based methods avoid the use of highly-non-linear entropy variables. In particular, it is still possible to construct such a method while using conservative or primitive variables.

Finally, we consider an inf-sup stabilization strategy. For this strategy, the pressure and velocity spaces are required to satisfy an inf-sup compatibility condition. As a result of this condition, the pressure field remains unique and bounded for incompressible flows, (see [42, 45] for details). There are many mixed methods which satisfy the inf-sup condition. For example, H(div)- and H1-conforming mixed methods have been developed for isothermal incompressible flows [41, 43, 103, 104], and H1-conforming mixed methods have been developed for non-isothermal incompressible flows [51,55]. A more complete review of inf-sup-stable mixed methods appears in [41,55]. There has been very limited application of these mixed methods to *compressible* flows. An interesting step in this direction appears in [105,106]. Here, a hybrid mixed finite element method is developed for compressible flows which uses a DG method to discretize the convective terms, and an H(div)-conforming method to discretize the diffusive terms. While this approach is quite innovative, it does not utilize the correct pressure and velocity spaces, and thus inf-sup stability is not obtained. In addition, [107] developed an inf-sup stable mixed method for the stationary, barotropic, linearized, compressible Navier-Stokes equations. Unfortunately, these equations fail to maintain the non-linearity or complexity of the full compressible (or even incompressible) Navier-Stokes equations. A similar argument holds for the mixed methods of [108–110].

3.1.2 Current Work

Our primary goal is to create a mixed finite element method for compressible flows which uses the most effective and flexible stabilization strategies discussed in the previous section. Towards this end, we have developed versatile mixed methods. These methods utilize three of the five stabilization strategies mentioned above: numerical-flux-based stabilization, kinetic-energy-based stabilization, and inf-sup-based stabilization. We have chosen numerical-flux-based stabilization for our methods instead of residual-based stabilization, due to the inherent simplicity of constructing the numerical fluxes. Next, we have chosen kinetic-energy-based stabilization instead of entropy-based stabilization, due to the overall physical relevance of kinetic energy in both incompressible and compressible environments. Finally, we have chosen inf-sup stabilization due to our interest in developing methods which perform well in nearly-incompressible flows. A direct consequence of the stabilization choices (above), is that versatile mixed methods have very favorable properties. In particular, these methods are provably stable for non-isothermal incompressible flows, as we can rigorously prove L2-stability of the discrete temperature, velocity, and kinematic pressure fields. In addition, these methods are accurate, as we can obtain error estimates for all of the discrete fields. The mathematical properties of these methods have been rigorously established in [41, 55]. Furthermore, these properties are maintained in the presence of non-zero divergence of the velocity field. In particular, versatile mixed methods contain divergence terms in the mass, momentum, and temperature equations. The divergence terms in the latter two equations are usually neglected in the construction of conventional mixed methods for incompressible flows. However, these terms are retained in versatile mixed methods. This makes versatile mixed methods particularly suitable for extension to more complex flows which violate the incompressibility constraint.

It is still necessary for us to actually extend the versatile methods to simulate compressible flows. This task is the main focus of the present chapter.

The most straightforward application of our new methods is in the area of weakly-compressible flows. With this in mind, it is important for us to briefly discuss other methods which have been developed for weakly-compressible flows. In these flows, numerical methods often encounter problems that stem from discrepancies between wave speeds. This leads to poor conditioning of the matrix system and incorrect predictions of the flow. A way to remedy this issue is the so-called low-Mach-number preconditioners that introduce a preconditioner to the matrix system to bring the wave speeds closer together [111–115]. This approach has seen much success for steady state problems, but by design these methods have a very negative impact on temporal accuracy. A more sophisticated approach has been taken by flux preconditioners, where only the terms in the equation that are naturally dissipative are modified [116–119]. This allows the preservation of the temporal accuracy. In addition, we note that similar preconditioning methods have been developed specifically for finite element methods, (see the work in [120–123]). A recent article (c.f. [124]) offers an excellent review of research on this topic. While our approach is designed to work for low-Mach-number flows, we do not employ any of the preconditioner approaches outlined above. Instead, our method relies on the usage of function spaces which are normally leveraged to solve the incompressible Navier-Stokes equations.

3.1.3 Overview of the Rest of the Chapter

In section 3.2, we introduce the governing equations for compressible flow, and the associated mathematical machinery. In section 3.3, we outline the versatile mixed methods for compressible flows. In section 3.4, we demonstrate that our versatile methods for compressible flows retain their stability under incompressible conditions. In section 3.5, we present a series of numerical experiments to demonstrate the methods' ability to handle the flows of interest. Lastly, in section 3.6, we provide a brief summary of our work.

3.2. Preliminaries

Consider the flow of a compressible fluid in a d-dimensional domain Ω, where $d = 2$ or 3. Suppose that the fluid has a density field $\rho = \rho\,(t, \boldsymbol{x})$, a momentum field $\rho\boldsymbol{u} = \rho\boldsymbol{u}\,(t, \boldsymbol{x})$, and an internal energy field $\rho e = \rho e\,(t, \boldsymbol{x})$, where $\boldsymbol{u}$ is the velocity and e is the specific internal energy. We assume that $e = C_v T$ where T is the temperature, and C_v is the coefficient of specific heat at constant volume.

We seek a solution to the motion of the fluid on the time interval (t_0, t_n) that satisfies the compressible Navier-Stokes equations

$$\partial_t\, \rho + \nabla \cdot (\rho\boldsymbol{u}) = S_\rho, \tag{3.2.1}$$

$$\partial_t\, (\rho\boldsymbol{u}) + \nabla \cdot (\rho\boldsymbol{u} \otimes \boldsymbol{u} + P\mathbb{I}) - \nabla \cdot (\rho\boldsymbol{\tau}) = \boldsymbol{S}_u, \tag{3.2.2}$$

$$\partial_t\, (\rho T) + \nabla \cdot (\rho T\boldsymbol{u}) - \nabla \cdot \left(\frac{\kappa}{C_v}\nabla T\right) = -\,(\gamma - 1)\,\rho T\,(\nabla \cdot \boldsymbol{u}) + \frac{1}{C_v}\,(\rho\boldsymbol{\tau} : \nabla\boldsymbol{u}) + S_T, \tag{3.2.3}$$

subject to boundary and initial conditions

$$\mathcal{B}\left(\rho, T, \boldsymbol{u}\right) = \mathbf{0}, \qquad \text{on} \quad \left[t_0, t_n\right] \times \partial\Omega, \tag{3.2.4}$$

$$\rho\left(0, \boldsymbol{x}\right) = \rho_0\left(\boldsymbol{x}\right), \qquad \text{in} \qquad \Omega, \tag{3.2.5}$$

$$T\left(0, \boldsymbol{x}\right) = T_0\left(\boldsymbol{x}\right), \qquad \text{in} \qquad \Omega, \tag{3.2.6}$$

$$\boldsymbol{u}\left(0, \boldsymbol{x}\right) = \boldsymbol{u}_0\left(\boldsymbol{x}\right), \qquad \text{in} \qquad \Omega, \tag{3.2.7}$$

where $\partial_t\left(\cdot\right)$ is the temporal derivative operator, $\nabla\left(\cdot\right)$ is the spatial gradient operator, S_ρ is a source term for the mass, $\boldsymbol{S}_u$ is a source term for the linear momentum, S_T is a source term for the internal energy, P is the pressure, κ is the coefficient of heat conductivity, γ is the ratio of specific heats, and $\mathcal{B}\left(\cdot,\cdot,\cdot\right)$ is a Robin-type boundary condition operator. In addition, $\boldsymbol{\tau}$ is the viscous stress tensor

$$\boldsymbol{\tau} = \nu\left(\nabla\boldsymbol{u} + \nabla\boldsymbol{u}^T - \frac{2}{3}\left(\nabla\cdot\boldsymbol{u}\right)\mathbb{I}\right). \tag{3.2.8}$$

Here, $\nu = \mu/\rho$ is the kinematic viscosity coefficient, and μ is the dynamic viscosity coefficient. An explicit formula for $\mu = \mu\left(T\right)$ is given by Sutherland's law

$$\mu = \frac{C_{\text{ref}}T^{3/2}}{T + S_{\text{ref}}}, \tag{3.2.9}$$

where C_{ref} and S_{ref} are empirically determined constants. The heat conductivity coefficient κ is related to μ via the following formula

$$\kappa = \frac{C_p \, \mu}{\mathrm{Pr}}, \tag{3.2.10}$$

where C_p is the coefficient of specific heat at constant pressure and Pr is the Prandtl number.

In what follows, we will assume that the pressure, temperature, and density are related through an equation of state

$$P = \rho R T, \tag{3.2.11}$$

where R is the specific gas constant. With this assumption in mind, we can view Eqs. (3.2.1) – (3.2.7) as a system of equations for unknowns ρ, T, and $\boldsymbol{u}$, which is supplemented by the relations in Eqs. (3.2.8) – (3.2.11).

We now seek a discrete solution to the continuous equations (3.2.1) – (3.2.7). Therefore, we introduce a mesh $\mathcal{T}_h$ of straight-sided, simplex elements, each of which is denoted by K. We assume that the domain Ω is polygonal, and furthermore, that the straight-sided edges of the mesh conform to the geometry of the domain. We choose a mesh in which the individual elements are non-overlapping, and we denote the boundary of each element by ∂K. The total collection of faces in the mesh is denoted by $\mathcal{F}_h$, and each face is denoted by F. The faces associated with a particular element are denoted by $\mathcal{F}_K = \{F \in \mathcal{F}_h : F \subset \partial K\}$. The set of all interior faces is denoted by $\mathcal{F}_h^i = \{F \in \mathcal{F}_h : F \cap \partial\Omega = \emptyset\}$, and the set of all boundary faces by $\mathcal{F}_h^\partial = \{F \in \mathcal{F}_h : F \cap \partial\Omega \neq \emptyset\}$. We associate each face F

with a normal vector $\boldsymbol{n}_F$ which points from the negative (-) side of the face to the positive (+) side. In a similar fashion, the locally defined, outward pointing normal vector for each face of an element is denoted by $\boldsymbol{n}_{F_K}$ or, when the context is clear, simply $\boldsymbol{n}$.

Next, it is necessary to introduce notation for computing integrals over the elements and faces of the mesh. Suppose that ϕ is a scalar function, $\boldsymbol{v}$ and $\boldsymbol{w}$ are vector functions, and $\boldsymbol{T}$ and $\boldsymbol{U}$ are tensor functions which are defined on the mesh, and are assumed to be sufficiently smooth. Then, the integrated products of these functions on the mesh are defined as follows

$$
\begin{aligned}
(\phi\, \boldsymbol{v}, \boldsymbol{w})_{\mathcal{T}_h} &:= \sum_{K \in \mathcal{T}_h} \int_K \phi\, \boldsymbol{v} \cdot \boldsymbol{w}\, dV, & (\phi\, \boldsymbol{T}, \boldsymbol{U})_{\mathcal{T}_h} &:= \sum_{K \in \mathcal{T}_h} \int_K \phi\, \boldsymbol{T} : \boldsymbol{U}\, dV, \\
\langle \phi\, \boldsymbol{v}, \boldsymbol{w} \rangle_{\partial \mathcal{T}_h} &:= \sum_{K \in \mathcal{T}_h} \int_{\partial K} \phi\, \boldsymbol{v} \cdot \boldsymbol{w}\, dA, & \langle \phi\, \boldsymbol{T}, \boldsymbol{U} \rangle_{\partial \mathcal{T}_h} &:= \sum_{K \in \mathcal{T}_h} \int_{\partial K} \phi\, \boldsymbol{T} : \boldsymbol{U}\, dA, \\
\langle \phi\, \boldsymbol{v}, \boldsymbol{w} \rangle_{\mathcal{F}_h} &:= \sum_{F \in \mathcal{F}_h} \int_F \phi\, \boldsymbol{v} \cdot \boldsymbol{w}\, dA, & \langle \phi\, \boldsymbol{T}, \boldsymbol{U} \rangle_{\mathcal{F}_h} &:= \sum_{F \in \mathcal{F}_h} \int_F \phi\, \boldsymbol{T} : \boldsymbol{U}\, dA.
\end{aligned}
$$

On a related note, we would like to remind the reader of the following integration by parts formulas

$$
\begin{aligned}
\langle \phi \boldsymbol{v}, \boldsymbol{n} \rangle_{\partial K} &= (\phi, \nabla \cdot \boldsymbol{v})_K + (\boldsymbol{v}, \nabla \phi)_K\,, \\
\langle \boldsymbol{v}, \boldsymbol{T} \boldsymbol{n} \rangle_{\partial K} &= (\boldsymbol{v}, \nabla \cdot \boldsymbol{T})_K + (\boldsymbol{T}, \nabla \boldsymbol{v})_K\,.
\end{aligned}
$$

Generally speaking, the generic vector function $\boldsymbol{v}$, and the scalar function ϕ are not required to be continuous across element boundaries. As a result, it is useful to introduce jump $[\![\cdot]\!]$ and average $\{\{\cdot\}\}$ operators for the interior faces $F \in \mathcal{F}_h^i$

$$[\![\phi]\!] = \phi_+ - \phi_-, \qquad [\![\phi \boldsymbol{n}]\!] = \phi_+ \boldsymbol{n}_+ + \phi_- \boldsymbol{n}_-, \qquad \{\{\phi\}\} = \frac{1}{2}\left(\phi_+ + \phi_-\right),$$

$$[\![\boldsymbol{v}]\!] = \boldsymbol{v}_+ - \boldsymbol{v}_-, \qquad [\![\boldsymbol{v} \otimes \boldsymbol{n}]\!] = \boldsymbol{v}_+ \otimes \boldsymbol{n}_+ + \boldsymbol{v}_- \otimes \boldsymbol{n}_-, \qquad \{\{\boldsymbol{v}\}\} = \frac{1}{2}\left(\boldsymbol{v}_+ + \boldsymbol{v}_-\right).$$

In a similar fashion, for the boundary faces $F \in \mathcal{F}_h^\partial$, we define

$$[\![\phi]\!] = \phi, \qquad [\![\phi \boldsymbol{n}]\!] = \phi \boldsymbol{n}, \qquad \{\{\phi\}\} = \phi,$$

$$[\![\boldsymbol{v}]\!] = \boldsymbol{v}, \qquad [\![\boldsymbol{v} \otimes \boldsymbol{n}]\!] = \boldsymbol{v} \otimes \boldsymbol{n}, \qquad \{\{\boldsymbol{v}\}\} = \boldsymbol{v}.$$

Next, we introduce convenient function spaces for approximating the density

$$Q_h^C := \left\{q_h : q_h \in C^0\left(\Omega\right), q_h|_K \in \mathcal{P}_k\left(K\right), \forall K \in \mathcal{T}_h\right\},$$

$$Q_h^{DC} := \left\{q_h : q_h \in L^2\left(\Omega\right), q_h|_K \in \mathcal{P}_k\left(K\right), \forall K \in \mathcal{T}_h\right\},$$

where $\mathcal{P}_k\left(K\right)$ is the space of polynomials of degree $\leq k$. One may also approximate the temperature using the function space

$$R_h^C = Q_h^C := \left\{q_h : q_h \in C^0\left(\Omega\right), q_h|_K \in \mathcal{P}_k\left(K\right), \forall K \in \mathcal{T}_h\right\}.$$

Finally, one may approximate the velocity field using the Taylor-Hood, Raviart-

Thomas, or Brezzi-Douglas-Marini spaces

$$\boldsymbol{W}_h^{TH} := \left\{ \boldsymbol{w}_h : \boldsymbol{w}_h \in \boldsymbol{C}^0 (\Omega), \boldsymbol{w}_h|_K \in (\mathcal{P}_{k+1}(K))^d, \forall K \in \mathcal{T}_h \right\},$$

$$\boldsymbol{W}_h^{RT} := \{ \boldsymbol{w}_h : \boldsymbol{w}_h \in \boldsymbol{H}(\text{div}; \Omega), \boldsymbol{w}_h|_K \in \boldsymbol{RT}_k(K), \forall K \in \mathcal{T}_h \},$$

$$\boldsymbol{W}_h^{BDM} := \{ \boldsymbol{w}_h : \boldsymbol{w}_h \in \boldsymbol{H}(\text{div}; \Omega), \boldsymbol{w}_h|_K \in \boldsymbol{BDM}_{k+1}(K), \forall K \in \mathcal{T}_h \},$$

where $\boldsymbol{C}^0(\Omega) := (C^0(\Omega))^d$ is the vector-valued space of continuous functions, $\boldsymbol{RT}_k(K)$ is the Raviart-Thomas space of degree k

$$\boldsymbol{RT}_k(K) := (\mathcal{P}_k(K))^d \oplus \mathcal{P}_k(K)\,\boldsymbol{x},$$

and $\boldsymbol{BDM}_{k+1}(K)$ is the Brezzi-Douglas-Marini space of degree $k+1$, whose definition appears in [42].

3.3. Extension of Versatile Mixed Methods

In this section, we define a new class of mixed methods for discretizing Eqs. (3.2.1) – (3.2.3). The full derivation of these methods appears in Appendix D. The formal statement of the methods is as follows: 1) consider function spaces $Q_h \subset L^2(\Omega)$, $R_h \subset H^1(\Omega)$, and $\boldsymbol{W}_h \subset \boldsymbol{H}(\text{div}; \Omega)$; 2) choose a set of test functions $(q_h, r_h, \boldsymbol{w}_h)$ that span $Q_h \times R_h \times \boldsymbol{W}_h$; and 3) find $(\rho_h, T_h, \boldsymbol{u}_h)$ in $Q_h \times R_h \times \boldsymbol{W}_h$ that satisfy:

Discrete Mass Equation

$$\left(\partial_t \, \rho_h, q_h\right)_{\mathcal{T}_h} + \left(\nabla_h \cdot \left(\rho_h \boldsymbol{u}_h\right), q_h\right)_{\mathcal{T}_h} = \left(S_\rho, q_h\right)_{\mathcal{T}_h}, \tag{3.3.1}$$

Discrete Momentum Equation

$$\begin{aligned}
&\left(\partial_t \left(\rho_h \boldsymbol{u}_h\right), \boldsymbol{w}_h\right)_{\mathcal{T}_h} - \left(\left(\rho_h \boldsymbol{u}_h\right) \otimes \boldsymbol{u}_h, \nabla_h \boldsymbol{w}_h\right)_{\mathcal{T}_h} - R\left(\rho_h T_h, \nabla \cdot \boldsymbol{w}_h\right)_{\mathcal{T}_h} + \left\langle \widehat{\boldsymbol{\sigma}}_{\text{inv}} \, \boldsymbol{n}, \boldsymbol{w}_h \right\rangle_{\partial\mathcal{T}_h} \\
&+ \left(\rho_h \boldsymbol{\tau}_h, \nabla_h \boldsymbol{w}_h\right)_{\mathcal{T}_h} - \left\langle \widehat{\boldsymbol{\sigma}}_{\text{vis}} \, \boldsymbol{n}, \boldsymbol{w}_h \right\rangle_{\partial\mathcal{T}_h} \\
&+ \left\langle \widehat{\boldsymbol{\varphi}}_{\text{vis}} - \mu_h \boldsymbol{u}_h, \left(\nabla_h \boldsymbol{w}_h + \nabla_h \boldsymbol{w}_h^T - \frac{2}{3}\left(\nabla \cdot \boldsymbol{w}_h\right) \mathbb{I}\right) \boldsymbol{n} \right\rangle_{\partial\mathcal{T}_h} \\
&- \frac{1}{2}\left(\left(\partial_t \, \rho_h + \nabla_h \cdot \left(\rho_h \boldsymbol{u}_h\right) - S_\rho\right) \boldsymbol{u}_h, \boldsymbol{w}_h\right)_{\mathcal{T}_h} = \left(\boldsymbol{S}_u, \boldsymbol{w}_h\right)_{\mathcal{T}_h},
\end{aligned} \tag{3.3.2}$$

Discrete Temperature Equation

$$
\begin{aligned}
&\left(\partial_t\left(\rho_h T_h\right), r_h\right)_{\mathcal{T}_h}-\left(\rho_h T_h \boldsymbol{u}_h, \nabla_h r_h\right)_{\mathcal{T}_h}+\left\langle\widehat{\boldsymbol{\phi}}_{\text{inv}} \cdot \boldsymbol{n}, r_h\right\rangle_{\partial \mathcal{T}_h} \\
&+\left(\frac{\kappa_h}{C_v} \nabla_h T_h, \nabla_h r_h\right)_{\mathcal{T}_h}-\left\langle\widehat{\boldsymbol{\phi}}_{\text{vis}} \cdot \boldsymbol{n}, r_h\right\rangle_{\partial \mathcal{T}_h}+\left\langle\widehat{\lambda}_{\text{vis}}-\frac{\kappa_h}{C_v} T_h, \nabla_h r_h \cdot \boldsymbol{n}\right\rangle_{\partial \mathcal{T}_h} \\
&-\frac{1}{2}\left(\Big(\partial_t \rho_h+\nabla_h \cdot\left(\rho_h \boldsymbol{u}_h\right)-S_\rho\Big) T_h, r_h\right)_{\mathcal{T}_h} \\
&=-(\gamma-1)\left[\left(\rho_h T_h\left(\nabla \cdot \boldsymbol{u}_h\right), r_h\right)_{\mathcal{T}_h}+C_{\text{mod}}\left(\left|\rho_h(\nabla \cdot \boldsymbol{u}_h)\right| \nabla_h T_h, \nabla_h r_h\right)_{\mathcal{T}_h}\right] \\
&+\frac{1}{C_v}\left(\rho_h \boldsymbol{\tau}_{\boldsymbol{h}}: \nabla_h \boldsymbol{u}_h, r_h\right)_{\mathcal{T}_h}+\left(S_T, r_h\right)_{\mathcal{T}_h}, \qquad (3.3.3)
\end{aligned}
$$

where the quantities with hats (e.g. $\widehat{\boldsymbol{\sigma}}_{\text{inv}}$) denote user-defined numerical fluxes. In addition, we note that $\mu_h = \mu(T_h)$, $\boldsymbol{\tau}_h = \boldsymbol{\tau}(\rho_h, \mu_h, \boldsymbol{u}_h)$, and $\kappa_h = \kappa(T_h)$. For compressible flows, we recommend that the numerical fluxes are defined as follows

$$\widehat{\boldsymbol{\sigma}}_{\text{inv}} := \{\{\rho_h \boldsymbol{u}_h\}\} \otimes \{\{\boldsymbol{u}_h\}\} + R\,\{\{\rho_h T_h\}\}\,\mathbb{I} + \zeta\,\{\{\rho_h\}\}\,|\boldsymbol{u}_h \cdot \boldsymbol{n}_F|\,[\![\boldsymbol{u}_h \otimes \boldsymbol{n}]\!], \qquad (3.3.4)$$

$$\widehat{\boldsymbol{\sigma}}_{\text{vis}} := \{\{\rho_h \boldsymbol{\tau}_h\}\} - \frac{\eta}{h_F}\,\{\{\mu_h\}\}\,[\![\boldsymbol{u}_h \otimes \boldsymbol{n}]\!], \qquad (3.3.5)$$

$$\widehat{\boldsymbol{\phi}}_{\text{inv}} := \{\{\rho_h T_h\}\}\,\boldsymbol{u}_h + \delta\,\{\{\rho_h\}\}\,|\boldsymbol{u}_h \cdot \boldsymbol{n}_F|\,[\![T_h\,\boldsymbol{n}]\!], \qquad (3.3.6)$$

$$\widehat{\boldsymbol{\phi}}_{\text{vis}} := \frac{1}{C_v}\left(\{\{\kappa_h \nabla_h T_h\}\} - \frac{\varepsilon}{h_F}\,\{\{\kappa_h\}\}\,[\![T_h\,\boldsymbol{n}]\!]\right), \qquad (3.3.7)$$

$$\widehat{\boldsymbol{\varphi}}_{\text{vis}} := \{\{\mu_h \boldsymbol{u}_h\}\}, \qquad \widehat{\lambda}_{\text{vis}} := \frac{1}{C_v}\,\{\{\kappa_h T_h\}\}, \qquad (3.3.8)$$

where ζ, η, δ, and ε are adjustable parameters that control the amount of dissipation that is added to the scheme.

Returning our attention to the momentum and temperature equations above, one may observe that we have augmented the schemes by adding 'strong residual' terms to the left hand sides of Eqs. (3.3.2) and (3.3.3)

$$-\frac{1}{2}\Big(\Big(\partial_t\,\rho_h + \nabla_h\cdot(\rho_h\boldsymbol{u}_h) - S_\rho\Big)\boldsymbol{u}_h, \boldsymbol{w}_h\Big)_{\mathcal{T}_h},$$

$$-\frac{1}{2}\Big(\Big(\partial_t\,\rho_h + \nabla_h\cdot(\rho_h\boldsymbol{u}_h) - S_\rho\Big)T_h, r_h\Big)_{\mathcal{T}_h}.$$

These are skew-symmetrizing terms which maintain consistency, while helping to stabilize the schemes. In particular, they ensure that the convective operators in the momentum and temperature equations become semi-coercive in the incompressible limit.

Lastly, we have added the following term to the right hand side of Eq. (3.3.3)

$$-C_{\mathrm{mod}}\,(\gamma-1)\,(|\rho_h(\nabla\cdot\boldsymbol{u}_h)|\,\nabla_h T_h, \nabla_h r_h)_{\mathcal{T}_h}\,,$$

where C_{mod} is a stabilization constant. This term allows us to control the temperature field in flows which are dominated by temperature-dependent buoyancy effects. It is set to zero in most cases.

3.4. Incompressible Stability

In this section, we introduce a new type of non-linear stability for finite element methods. A finite element method for solving the compressible Navier-Stokes equations is said to possess *incompressible stability* or equivalently is said to be *incompressibly stable* if, upon setting $\rho_h = \text{const}$, $\mu_h = \text{const}$, $\kappa_h = \text{const}$, and $S_\rho = 0$, we recover an inf-sup stable method for the non-isothermal, *incompressible* Navier-Stokes equations. Broadly speaking, enforcing incompressible stability is a way of enforcing compatibility between the finite element discretizations for compressible and incompressible flows. We contend that, a method for compressible flows which possesses incompressible stability is more likely to maintain robust behavior in the incompressible limit.

In what follows, we will establish that the finite element methods in Eqs. (3.3.1)–(3.3.3) are incompressibly stable. Towards this end, we initially set $\rho_h = \rho_0 = \text{const}$ in Eq. (3.2.11)

$$P_h = \rho_0 R T_h,$$

or equivalently

$$p_h := R T_h, \tag{3.4.1}$$

where we have defined $p_h = P_h/\rho_0$ as the kinematic pressure. We can immediately observe that p_h and T_h now reside in the same function space, i.e. $(p_h, T_h) \in$

$R_h \times R_h$. Furthermore, if we choose $Q_h = R_h = Q_h^C$, then $p_h \in Q_h$.

Next, we observe that the viscous dissipation term

$$\frac{\rho_0}{C_v}\boldsymbol{\tau_h} : \nabla_h \boldsymbol{u}_h,$$

in the temperature equation (Eq. (3.2.3)) can be neglected in the incompressible limit. This property follows immediately from the arguments in Appendix A.1 of [55], and in Appendix A of this work.

We can use the observations above to rewrite Eqs. (3.3.1)–(3.3.3). Upon performing this operation, and setting $\rho_h = \rho_0 = \text{const}$, $\mu_h = \mu_0 = \text{const}$, $\kappa_h = \kappa_0 = \text{const}$, and $S_\rho = 0$ in Eqs. (3.3.1)–(3.3.3), we obtain the following simplified equations:

Discrete Mass Equation

$$(\nabla_h \cdot \boldsymbol{u}_h, q_h)_{\mathcal{T}_h} = 0, \tag{3.4.2}$$

Discrete Momentum Equation

$$
\begin{aligned}
&(\partial_t \boldsymbol{u}_h, \boldsymbol{w}_h)_{\mathcal{T}_h} - (\boldsymbol{u}_h \otimes \boldsymbol{u}_h, \nabla_h \boldsymbol{w}_h)_{\mathcal{T}_h} - (p_h, \nabla \cdot \boldsymbol{w}_h)_{\mathcal{T}_h} + \left\langle \frac{\widehat{\boldsymbol{\sigma}}_{\text{inv}}}{\rho_0}\, \boldsymbol{n}, \boldsymbol{w}_h \right\rangle_{\partial\mathcal{T}_h} \\
&+ (\boldsymbol{\tau}_h, \nabla_h \boldsymbol{w}_h)_{\mathcal{T}_h} - \left\langle \frac{\widehat{\boldsymbol{\sigma}}_{\text{vis}}}{\rho_0}\, \boldsymbol{n}, \boldsymbol{w}_h \right\rangle_{\partial\mathcal{T}_h} \\
&+ \left\langle \frac{\widehat{\boldsymbol{\varphi}}_{\text{vis}}}{\rho_0} - \nu \boldsymbol{u}_h, \left(\nabla_h \boldsymbol{w}_h + \nabla_h \boldsymbol{w}_h^T - \frac{2}{3} (\nabla \cdot \boldsymbol{w}_h)\, \mathbb{I} \right) \boldsymbol{n} \right\rangle_{\partial\mathcal{T}_h} \\
&- \frac{1}{2} \left((\nabla_h \cdot \boldsymbol{u}_h)\, \boldsymbol{u}_h, \boldsymbol{w}_h \right)_{\mathcal{T}_h} = (\boldsymbol{f}_u, \boldsymbol{w}_h)_{\mathcal{T}_h}\,,
\end{aligned}
\tag{3.4.3}
$$

Discrete Temperature Equation

$$
\begin{aligned}
&(\partial_t T_h, r_h)_{\mathcal{T}_h} - (T_h \boldsymbol{u}_h, \nabla_h r_h)_{\mathcal{T}_h} + \left\langle \frac{\widehat{\boldsymbol{\phi}}_{\text{inv}}}{\rho_0} \cdot \boldsymbol{n}, r_h \right\rangle_{\partial\mathcal{T}_h} \\
&+ \gamma\alpha \left(\nabla_h T_h, \nabla_h r_h \right)_{\mathcal{T}_h} - \left\langle \frac{\widehat{\boldsymbol{\phi}}_{\text{vis}}}{\rho_0} \cdot \boldsymbol{n}, r_h \right\rangle_{\partial\mathcal{T}_h} + \left\langle \frac{\widehat{\lambda}_{\text{vis}}}{\rho_0} - \gamma\alpha T_h, \nabla_h r_h \cdot \boldsymbol{n} \right\rangle_{\partial\mathcal{T}_h} \\
&- \frac{1}{2} \left((\nabla_h \cdot \boldsymbol{u}_h)\, T_h, r_h \right)_{\mathcal{T}_h} \\
&= -(\gamma - 1) \Big[\left((\nabla \cdot \boldsymbol{u}_h)\, T_h, r_h \right)_{\mathcal{T}_h} + C_{\text{mod}} \left(|\nabla \cdot \boldsymbol{u}_h|\, \nabla_h T_h, \nabla_h r_h \right)_{\mathcal{T}_h} \Big] + (f_T, r_h)_{\mathcal{T}_h}\,,
\end{aligned}
\tag{3.4.4}
$$

where we have set $\alpha := \kappa_0 / C_p \rho_0$, $\boldsymbol{f}_u := \boldsymbol{S}_u / \rho_0$, and $f_T := S_T / \rho_0$. Next, upon substituting $\rho_h = \rho_0 = \text{const}$, $\mu_h = \mu_0 = \text{const}$, and $\kappa_h = \kappa_0 = \text{const}$ into the numerical fluxes (Eqs. (3.3.4)–(3.3.8)) and dividing through the result by ρ_0, we have that

$$\breve{\boldsymbol{\sigma}}_{\text{inv}} := \frac{\widehat{\boldsymbol{\sigma}}_{\text{inv}}}{\rho_0} = \{\{\boldsymbol{u}_h\}\} \otimes \{\{\boldsymbol{u}_h\}\} + \{\{p_h\}\}\,\mathbb{I} + \zeta\,|\boldsymbol{u}_h \cdot \boldsymbol{n}_F|\,[\![\boldsymbol{u}_h \otimes \boldsymbol{n}]\!]\,, \tag{3.4.5}$$

$$\nu\breve{\boldsymbol{\sigma}}_{\text{vis}} := \frac{\widehat{\boldsymbol{\sigma}}_{\text{vis}}}{\rho_0} = \{\{\boldsymbol{\tau}_h\}\} - \frac{\eta\nu}{h_F}\,[\![\boldsymbol{u}_h \otimes \boldsymbol{n}]\!]\,, \tag{3.4.6}$$

$$\breve{\boldsymbol{\phi}}_{\text{inv}} := \frac{\widehat{\boldsymbol{\phi}}_{\text{inv}}}{\rho_0} = \{\{T_h\}\}\,\boldsymbol{u}_h + \delta\,|\boldsymbol{u}_h \cdot \boldsymbol{n}_F|\,[\![T_h\,\boldsymbol{n}]\!]\,, \tag{3.4.7}$$

$$\gamma\alpha\breve{\boldsymbol{\phi}}_{\text{vis}} := \frac{\widehat{\boldsymbol{\phi}}_{\text{vis}}}{\rho_0} = \gamma\alpha\left(\{\{\nabla_h T_h\}\} - \frac{\varepsilon}{h_F}\,[\![T_h\,\boldsymbol{n}]\!]\right), \tag{3.4.8}$$

$$\nu\breve{\boldsymbol{\varphi}}_{\text{vis}} := \frac{\widehat{\boldsymbol{\varphi}}_{\text{vis}}}{\rho_0} = \nu\,\{\{\boldsymbol{u}_h\}\}\,, \qquad \gamma\alpha\breve{\lambda}_{\text{vis}} := \frac{\widehat{\lambda}_{\text{vis}}}{\rho_0} = \gamma\alpha\,\{\{T_h\}\}\,. \tag{3.4.9}$$

We may then substitute Eqs. (3.4.5)–(3.4.9) into Eqs. (3.4.2)–(3.4.4) in order to obtain

$$(\nabla \cdot \boldsymbol{u}_h, q_h)_{\mathcal{T}_h} = 0, \tag{3.4.10}$$

$$\begin{aligned}
&(\partial_t \boldsymbol{u}_h, \boldsymbol{w}_h)_{\mathcal{T}_h} - (\boldsymbol{u}_h \otimes \boldsymbol{u}_h, \nabla_h \boldsymbol{w}_h)_{\mathcal{T}_h} - (p_h, \nabla \cdot \boldsymbol{w}_h)_{\mathcal{T}_h} + \langle \breve{\boldsymbol{\sigma}}_{\text{inv}}\,\boldsymbol{n}, \boldsymbol{w}_h \rangle_{\partial\mathcal{T}_h} \\
&+ (\boldsymbol{\tau}_h, \nabla_h \boldsymbol{w}_h)_{\mathcal{T}_h} - \nu\,\langle \breve{\boldsymbol{\sigma}}_{\text{vis}}\,\boldsymbol{n}, \boldsymbol{w}_h \rangle_{\partial\mathcal{T}_h} \\
&+ \nu\left\langle \breve{\boldsymbol{\varphi}}_{\text{vis}} - \boldsymbol{u}_h, \left(\nabla_h \boldsymbol{w}_h + \nabla_h \boldsymbol{w}_h^T - \frac{2}{3}\,(\nabla \cdot \boldsymbol{w}_h)\,\mathbb{I}\right)\boldsymbol{n} \right\rangle_{\partial\mathcal{T}_h} \\
&- \frac{1}{2}\,((\nabla \cdot \boldsymbol{u}_h)\,\boldsymbol{u}_h, \boldsymbol{w}_h)_{\mathcal{T}_h} = (\boldsymbol{f}_u, \boldsymbol{w}_h)_{\mathcal{T}_h}\,,
\end{aligned} \tag{3.4.11}$$

$$
\begin{aligned}
&\left(\partial_t T_h, r_h\right)_{\mathcal{T}_h} - \left(T_h \boldsymbol{u}_h, \nabla_h r_h\right)_{\mathcal{T}_h} + \left\langle \breve{\boldsymbol{\phi}}_{\text{inv}} \cdot \boldsymbol{n}, r_h \right\rangle_{\partial \mathcal{T}_h} \\
&+ \gamma\alpha \left(\nabla_h T_h, \nabla_h r_h\right)_{\mathcal{T}_h} - \gamma\alpha \left\langle \breve{\boldsymbol{\phi}}_{\text{vis}} \cdot \boldsymbol{n}, r_h \right\rangle_{\partial \mathcal{T}_h} + \gamma\alpha \left\langle \breve{\lambda}_{\text{vis}} - T_h, \nabla_h r_h \cdot \boldsymbol{n} \right\rangle_{\partial \mathcal{T}_h} \\
&- \frac{1}{2} \left(\left(\nabla \cdot \boldsymbol{u}_h\right) T_h, r_h\right)_{\mathcal{T}_h} \\
&= -\left(\gamma - 1\right) \Big[\left(\left(\nabla \cdot \boldsymbol{u}_h\right) T_h, r_h\right)_{\mathcal{T}_h} + C_{\text{mod}} \left(\left|\nabla \cdot \boldsymbol{u}_h\right| \nabla_h T_h, \nabla_h r_h\right)_{\mathcal{T}_h} \Big] + \left(f_T, r_h\right)_{\mathcal{T}_h}.
\end{aligned}
\tag{3.4.12}
$$

The resulting class of methods is identical to the class which was originally introduced in [55], with the caveat that the temperature space R_h is one degree lower than in the original work. The original methods were proven to be inf-sup stable for the incompressible, non-isothermal, Navier-Stokes equations; and furthermore this fact is unaffected by the change in the degree of the temperature space. Therefore, based on the analysis above, we can conclude that the finite element methods in Eqs. (3.3.1)–(3.3.3) are incompressibly stable.

We also note that rigorous error estimates for the original versatile mixed methods were derived in [55]. This analysis (again) holds for the present methods, with the caveat that the temperature converges at a rate of $k+1$, instead of $k+2$, as was shown in [55].

Lastly, we note that our versatile methods maintain stability of the discrete kinetic energy field (for incompressible flows). In particular, if we construct a versatile method with BDM elements, we recover the kinetic-energy-stabilized H(div)-conforming method of Guzman et al. [94].

3.5. Numerical Experiments

In this section, the results from several numerical simulations are presented. These simulations were performed using Taylor-Hood elements with polynomials of degree k, k, and $k+1$ for the density, temperature and velocity respectively, unless otherwise stated. In the following simulations, the convective numerical fluxes were computed using upwind biased parameters $\zeta = \delta = 0.5$, and the viscous numerical fluxes were computed with $\eta = \varepsilon = 3(k+1)(k+2)$. The modeling constant $C_{\text{mod}} = 0$ was used. In addition, a high-order BDF5 scheme was used for the time discretization. The meshes for each simulation were generated with quadrilateral elements split along the diagonal to make triangular elements. In the following sections, mesh dimensions will be reported as $N \times M$, where N and M refer to the number of quadrilaterals in the x and y directions. The actual total number of triangular elements is then $2(N \times M)$. Finally, all computations were carried out using the open-source finite element software package FEniCS [53].

The rest of this section contains four test cases for assessing the proposed versatile finite element methods. In section 3.5.1, we evaluate their order of accuracy using the method of manufactured solutions. In section 3.5.2, we examine the compressible solution behavior at low Mach numbers, and prove that it converges to the correct incompressible solution. In section 3.5.3, we perform a Mach number sweep on a two-dimensional cylinder in cross flow. Finally, in section 3.5.4, we examine the drag forces on a Joukowski airfoil.

3.5.1 Method of Manufactured Solutions

For the first test case, we compared the results of our versatile method equipped with Taylor-Hood elements to an exact manufactured solution. We defined the exact solution for $t \geq 0$ as follows

$$\rho = \sin(x)\sin(y)\exp(-2\nu t),$$

$$T = \frac{1}{2}\sin(x)\sin(y)\exp\left(-2\frac{\kappa}{C_v}t\right),$$

$$u = \sin(x)\cos(y)\exp(-2\nu t),$$

$$v = -\sin(y)\cos(x)\exp(-2\nu t),$$

where $\boldsymbol{u} = (u, v)$. Here, we used $\Omega = [0, 1.25]^2$ as the spatial domain for our solution. In addition, we note that the exact solution (above) was “manufactured” by using the following forcing functions

$$S_\rho = -\frac{2\nu \sin(x)\sin(y)}{\exp(2\nu t)},$$

$$S_T = \Bigg(-4\nu \cos^2(x)\cos^2(y) + \kappa \exp\left(2\left(\nu - \frac{\kappa}{C_v}\right)t\right)\sin(x)\sin(y)\exp(2\nu t)$$
$$- (\kappa + C_v\nu)\sin(x)\sin(y)\Bigg) / \exp(4\nu t),$$

$$S_u = \Bigg(\sin(x)\Big(\cos(x)\cos^2(y)\sin(x)\sin(y)$$
$$+ 2\mu \exp(2\nu t)\cos(y)\exp(2\nu t) - 2\sin(x)\sin(y)$$
$$+ \cos(x)\sin^2(y)(\exp\left(\frac{-2\kappa t}{C_v} + 4\nu t\right)R + \sin(x)\sin(y))\Big)\Bigg) / \exp(6\nu t),$$

$$S_v = \Bigg(\sin(y)\Big(\cos(y)\cos^2(x)\sin(x)\sin(y)$$
$$- 2\mu \exp(2\nu t)\cos(x)\exp(2\nu t) - 2\sin(x)\sin(y)$$
$$+ \cos(y)\sin^2(x)(\exp\left(\frac{-2\kappa t}{C_v} + 4\nu t\right)R + \sin(x)\sin(y))\Big)\Bigg) / \exp(6\nu t),$$

where $\boldsymbol{S}_u = (S_u, S_v)$. We ran the simulation for $t \in [0, 0.25]$, with parameters $C_v = 1$, $R = 1$, $\nu = 3$, and $\kappa = 0.47$. The simulations were performed on a uniform grid with the exact solution specified as a Dirichlet boundary condition on all boundaries. Time stepping was performed with a step-size of $\Delta t = 5 \times 10^{-4}$. In addition, we utilized polynomials of degrees $k = 1$ and 2. We therefore expected to see convergence rates of $k + 2$ for the velocity and $k + 1$ for the temperature and density, as the latter quantities are represented with a polynomial one-degree lower than the velocity. From table 3.1, we can see that the expected rates of convergence are achieved.

k	h	dofs	Velocity		Density		Temperature	
			L^2 error	order	L^2 error	order	L^2 error	order
1	0.44194	212	8.292e-5	-	0.001756	-	0.001954	-
	0.22097	740	1.047e-5	2.984	4.470e-4	1.974	4.974e-4	1.974
	0.11048	2756	1.312e-6	2.996	1.122e-4	1.993	1.249e-4	1.993
	0.05524	10628	1.641e-7	2.999	2.809e-5	1.998	3.126e-5	1.998
2	0.44194	500	3.830e-6	-	9.1878e-5	-	1.022e-4	-
	0.22097	1828	2.392e-7	4.001	1.148e-5	2.999	1.278e-5	2.999
	0.11048	6980	1.494e-8	4.000	1.435-6	2.999	1.597e-6	2.999
	0.05524	27268	9.341e-10	4.000	1.794e-7	2.999	1.997e-7	2.999

Table 3.1: Velocity, density, and temperature L^2 errors for various polynomial degrees k and maximum element diameters h, for the versatile mixed method with Taylor-Hood elements.

3.5.2 Asymptotic Preservation

The second test case involved an isothermal vortex in a box with isothermal no-slip boundary conditions on each wall. The domain was $\Omega \in [0,1] \times [0,1]$, and we tessellated it with a 64×64 triangular mesh. The case was run over the time interval $t \in [0, 0.2]$. The fluid properties were set to $\mu = 0.01$, $C_v = 717.8$, $R = 287$, and $\gamma = 1.4$.

The goal of the test case was to show that compressible simulation solutions converge to the incompressible solution in the presence of decreasing Mach number. In order to facilitate this comparison, we prescribed an initial, divergence-free, velocity field for both cases. The compressible case had the density and velocity specified, while the incompressible case had the velocity and kinematic pressure specified. The initial condition for the compressible case was specified as

$$\rho = \rho_{ref} - \frac{\mathrm{Ma}^2}{2}\tanh(y - 0.5),$$

$$u = \sin^2(\pi x)\sin(2\pi y),$$

$$v = -\sin^2(\pi y)\sin(2\pi x).$$

The initial condition for the incompressible case used the same velocity, but the kinematic pressure was specified as

$$p = (\rho_{ref})^{\gamma}.$$

The incompressible case was simulated with constant density $\rho_{ref} = 1$, and the compressible case was simulated with Ma = 0.1, 0.05, 0.01, 0.005, 0.001, 0.0005, and 0.0001. The incompressible simulation was performed with Taylor-Hood elements of degree $k = 2$, and the compressible simulations were performed with three different methods: i) a versatile mixed method with Taylor-Hood elements of degree $k = 2$, ii) a versatile mixed method with BDM elements of degree $k = 2$, and iii) a standard DG method with $k = 3$ elements. We included the standard DG method in our analysis in order to highlight the difficulty that conventional methods have in the low-Mach-number regime.

The time-steps for each compressible simulation are summarized in table 3.2, and the time-step for the incompressible simulation was 5×10^{-6}. The Δt's were chosen carefully in order to maintain the stability of each finite element method, and to control the amount of temporal error that was generated.

Ma	TH, Δt	BDM, Δt	DG, Δt
0.1	2.0e-6	2.0e-6	2.0e-6
0.05	2.0e-6	2.0e-6	2.0e-6
0.01	2.0e-6	2.0e-6	2.0e-6
0.005	2.0e-6	2.0e-6	2.0e-6
0.001	1.0e-6	5.0e-7	5.0e-7
0.0005	5.0e-7	1.0e-7	5.0e-7
0.0001	1.0e-7	5.0e-8	1.0e-7

Table 3.2: Time-steps Δt for three different finite element methods: a) the versatile mixed method with Taylor-Hood elements of degree $k = 2$, b) the versatile mixed method with BDM elements of degree $k = 2$, and c) the standard DG method with $k = 3$.

At each Mach number, we calculated the differences between the incompressible and compressible approximations for the kinematic pressure and density. In particular, we calculated

$$\|p_{\text{comp}} - p_\star\|_{L^2(\Omega)}, \qquad \|\rho_{\text{comp}} - \rho_\star\|_{L^2(\Omega)},$$

where ρ_{comp} is the density extracted from the compressible simulations at different Mach numbers,

$$p_{\text{comp}} = (\rho_{\text{comp}})^\gamma,$$

and $p_\star$ and $\rho_\star$ are computed as follows

$$p_\star = 1 + \mathrm{Ma}^2 p_{\mathrm{incomp}}, \qquad \rho_\star = \left(1 + \mathrm{Ma}^2 p_{\mathrm{incomp}}\right)^{1/\gamma}.$$

The quantity p_{incomp} is the kinematic pressure which was extracted from the incompressible simulation. Evidently, as $\mathrm{Ma} \to 0$, we expect

$$\|p_{\mathrm{comp}} - p_\star\|_{L^2(\Omega)} \longrightarrow 0, \qquad \|\rho_{\mathrm{comp}} - \rho_\star\|_{L^2(\Omega)} \longrightarrow 0.$$

Ma	TH, L^2-differences		BDM, L^2-differences		DG, L^2-differences	
	Pressure	Density	Pressure	Density	Pressure	Density
0.1	4.269e-3	3.052e-3	4.075e-3	2.913e-3	3.036e-3	2.169e-3
0.05	1.232e-3	8.799e-4	7.938e-4	5.671e-4	7.990e-4	5.708e-4
0.01	3.888e-5	2.777e-5	4.057e-5	2.898e-5	8.965e-2	6.324e-2
0.005	9.471e-6	6.765e-6	8.380e-6	5.986e-6	2.164e-1	1.502e-1
0.001	4.525e-7	3.232e-7	4.017e-7	2.870e-7	1.927e-7	1.376e-7
0.0005	7.900e-8	5.643e-8	8.350e-8	5.965e-8	4.817e-8	3.441e-8
0.0001	5.155e-9	3.682e-9	5.360e-9	3.828e-9	1.927e-9	1.376e-9

Table 3.3: L^2 norms of differences between compressible and incompressible field variables (kinematic pressure and density), for different Mach numbers, and three different finite element methods: a) the versatile mixed method with Taylor-Hood elements of degree $k = 2$, b) the versatile mixed method with BDM elements of degree $k = 2$, and c) the standard DG method with $k = 3$.

We can see in table 3.3 that our mixed methods follow the expected trend, and significantly outperform the standard DG approach at low Mach numbers. In particular, we can see that around $\mathrm{Ma} = 0.01$, the DG method experiences a large spike in error, as the solution stops converging towards the incompressible results. In addition, we can see from figure 3.1 that while our BDM method maintains

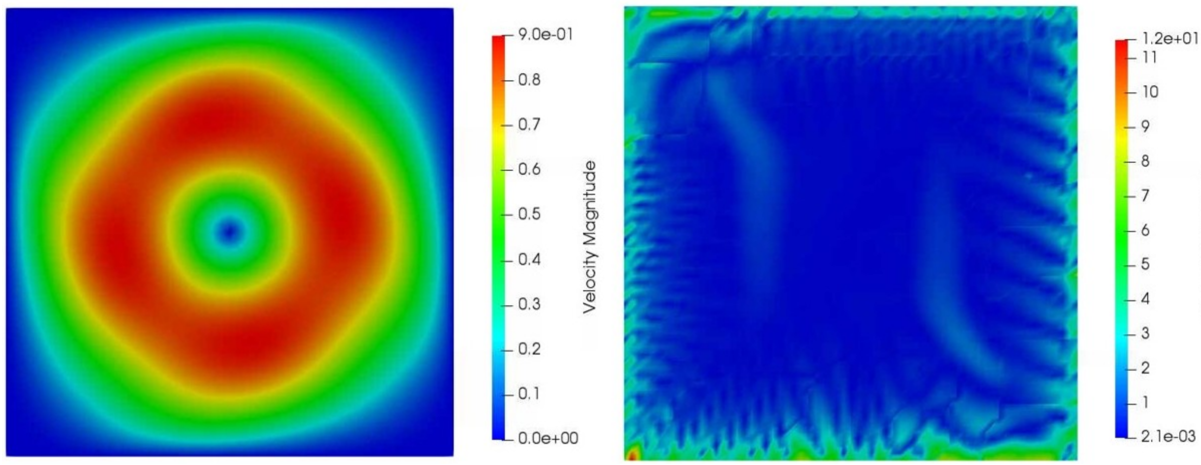

Figure 3.1: Velocity magnitude contours for the versatile mixed method with BDM elements of degree $k = 2$ (left) and the standard DG method with $k = 3$ (right) at $\mathrm{Ma} = 0.005$ and $t = 0.18$.

the initial decaying vortex, the DG solution has become completely unphysical. We note that the DG method does not always produce unphysical results, as it generates accurate results at some lower and higher Mach numbers, ($\mathrm{Ma} \geq 0.05$ and $\mathrm{Ma} \leq 0.0005$). However, generally speaking, the accuracy of the DG method in the low-Mach-number regime is unreliable. Here, we have demonstrated that it is possible for the DG method to converge to a non-physical solution in this regime. In our experience, this phenomenon was not observed for the versatile mixed methods with Taylor-Hood or BDM elements. We believe that this highlights a clear advantage of our approach: namely, since we are using function spaces traditionally associated with incompressible flows, we are successfully able to capture near-incompressible flow, even when solving the compressible equations.

3.5.3 2-D Cylinder in Cross Flow

For the third test case, we simulated a two-dimensional cylinder in cross flow over a range of Mach numbers, at a fixed Reynolds number Re = 100. The simulations were run with a uniform inlet flow, where the Mach number was adjusted over the following range of values: Ma = 0.1, 0.2, 0.3, and 0.4. For these experiments, we utilized an initial density of $\rho = 1.0$ kg/m^3. The viscosity inside of the domain was allowed to change in accordance with Sutherland's law. The fixed Reynolds number at the inlet was maintained by adjusting the inlet viscosity in accordance with the inlet Mach number. In addition, a fixed Prandtl number Pr = 0.72 was used. The following fluid properties were assumed: C_v = 717.8 J/kg-K and γ = 1.4. The boundary condition for the left-most boundary was a subsonic inlet condition, and for the right-most boundary it was an extrapolation condition. The top and bottom boundaries utilized symmetry boundary conditions. The cylinder itself was equipped with adiabatic no-slip walls.

The computational domain was $\Omega = [-20, 40] \times [-20, 20]$. The cylinder had a diameter of 0.1247 m and was centered at the point $(0, 0)$. We used a mesh with $70,000$ unstructured triangular elements. The polynomial order was $k = 2$, and the simulations were run for $t \in [0, 200]$ with a time-step of $\Delta t = 1.5 \times 10^{-5}$. Data for post-processing purposes was sampled over $t \in [150, 200]$.

For this study, the primary quantity of interest was the time-averaged drag coefficient of the cylinder, C_d, defined as

$$C_d = \frac{\overline{F}_d}{\frac{1}{2}\rho_\infty u_\infty^2 d}. \tag{3.5.1}$$

Here, $\overline{F}_d$ is the time-averaged drag force acting on the cylinder, ρ_∞ is the free-stream density, u_∞ is the free-stream flow speed, and d is the diameter of the cylinder.

In what follows, we compare our results against an earlier study performed by [3] on an identical geometry. At the given Reynolds number (100), the reference predicts that the flow will be unsteady with an oscillatory wake structure. This behavior is independent of the Mach number, as long as $\mathrm{Ma} < 0.6$. As such, the flow fields for the various Mach numbers all exhibit similar behavior, which is correctly predicted for the $\mathrm{Ma} = 0.4$ case by our method, (see figure 3.2). In particular, we can see from the figure the previously mentioned oscillatory wake behavior with the sinusoidal streamlines leaving the cylinder. This behavior is consistent across all Mach numbers, and implies that at least qualitatively we are in agreement with the reference solution.

In figure 3.3, we compare our predictions for the drag coefficients with those of the reference solution [3]. The predicted drag coefficient is in good agreement with the reference across the full range of Mach numbers considered.

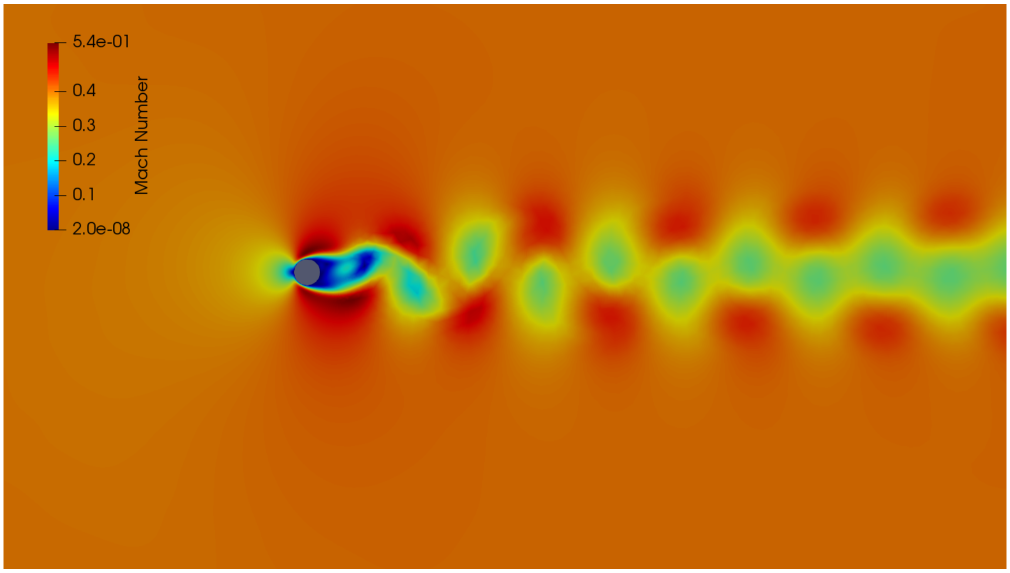

Figure 3.2: A snapshot of Mach number contours for the 2-D cylinder in cross flow at Ma = 0.4. Results were obtained using the versatile mixed method with Taylor-Hood elements of degree $k = 2$.

3.5.4 Joukowski Airfoil

The final test case involved flow over a Joukowski airfoil. This case was introduced at the 4th International Workshop on High-order CFD Methods, (see [125]). Here, an airfoil is simulated at an angle of attack of 0 degrees. The flow has Reynolds and Mach numbers of Re = 1000 and Ma = 0.5. The Prandtl number is again fixed at Pr = 0.72. Fluid properties for all simulations were $C_v = 717.8$ J/kg-K, $\mu = 1.716 \times 10^{-5}$ kg/m-s, and $\gamma = 1.4$. The viscosity was varied via Sutherland's Law. The initial density was prescribed as $\rho = 1$ kg/m^3. The boundary conditions were specified as a subsonic inlet condition on the left-most boundary, and an extrapolation condition on the right-most boundary. The airfoil itself was equipped

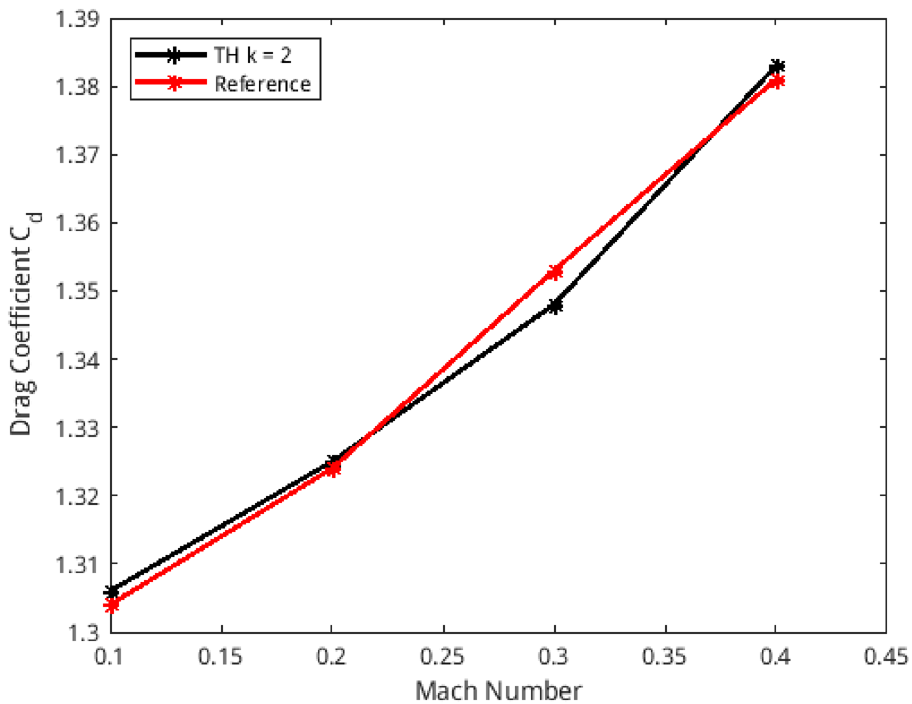

Figure 3.3: A plot of the time-averaged drag coefficient vs. the Mach number. Results were obtained using the versatile mixed method with Taylor-Hood elements of degree $k = 2$, and the reference [3].

with an adiabatic, no-slip condition.

The domain was $\Omega = [-100, 100] \times [-100, 100]$ with the airfoil starting at $(0, 0)$. The length of the airfoil from nose to trailing edge was 1 m. Unstructured meshes with 16,384, 65,536, and 262,144 triangular elements were used to tessellate the domain. These meshes were provided by organizers of the 5th International Workshop on High-order CFD Methods, and are numbered as meshes 2, 3, and 4, (see [126]). The simulations were run with polynomial order $k = 2$ on these meshes until the drag converged to a steady-state value.

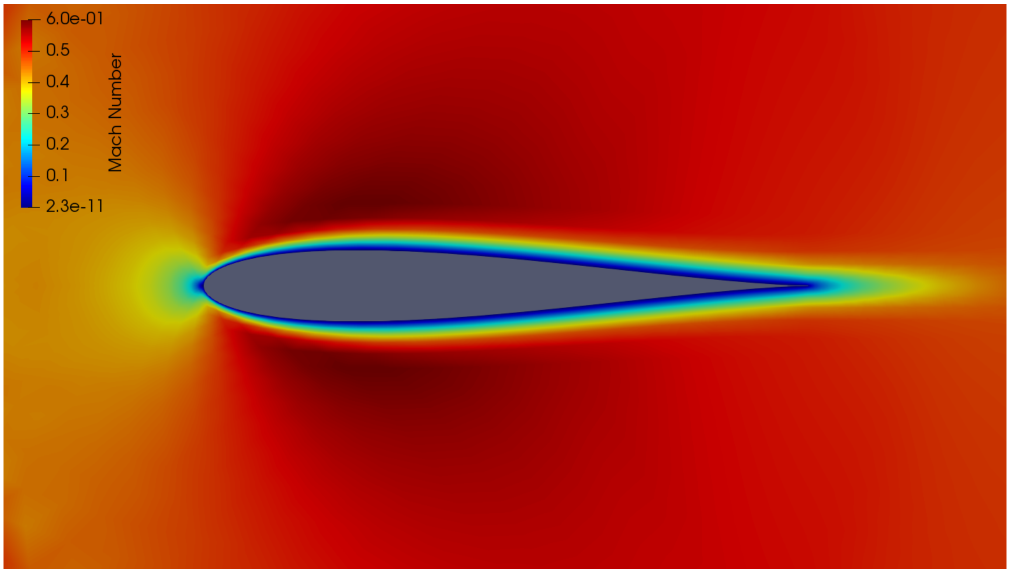

Figure 3.4: Mach number contours for the Joukowski airfoil at Re = 1000 and Ma = 0.5. Results were obtained using the versatile mixed method with Taylor-Hood elements of degree $k = 2$ on the finest mesh.

Mesh No.	DoF Count	C_d
2	16,704	0.1320
3	66,176	0.1273
4	263,424	0.1221

Table 3.4: A table of drag coefficients on the given meshes. Results were obtained using the versatile mixed method with Taylor-Hood elements of degree $k = 2$. The reference value for this case is $C_d = 0.1219$

Our results on mesh 4 are shown in figure 3.4. Here, the flow around the airfoil appears to be laminar, and the wake coming off the trailing edge has reached a steady state.

The primary challenge for this case is to converge to the reference drag coefficient using the meshes provided. In table 3.4, we see that, as we increase the degrees of freedom in the simulation, we move closer to the reference steady-state value of $C_d = 0.1219$. On the final grid, there is reasonable agreement between our predicted value and the reference.

3.6. Conclusion

In this work, we introduce a new class of 'versatile mixed finite element methods' for solving the compressible Navier-Stokes equations. These methods appear to be unique, as they simultaneously leverage multiple stabilization strategies for solving problems in the incompressible and compressible flow regimes. More precisely, our methods leverage numerical-flux-based stabilization, kinetic-energy-based stabilization, and inf-sup-based stabilization strategies.

We note that our philosophy for designing these methods is somewhat unusual. In particular, many numerical methods are only designed to be stable for linear advection and diffusion problems. In contrast, we have created finite element methods which are provably stable for the non-linear, non-isothermal, incompressible Navier-Stokes equations. Therefore, the starting point for our methods is significantly more complex than most, which facilitates their robustness and flexibility, in terms of successful application to increasingly complex problems. This claim has been demonstrated within the present paper, where we have successfully extended our methods to solve weakly- and fully-compressible flows.

The proposed methods are primarily designed to maintain their performance in the incompressible limit. In fact, we have ensured that the methods are 'incompressibly stable', which means they are mathematically guaranteed to maintain stability when the density, dynamic viscosity coefficient, and heat conductivity coefficient assume constant values. We have shown through numerical experiments, that the resulting methods maintain good convergence properties and stability as the Mach number approaches zero. Based on this evidence, we argue that most (if not all) methods designed for weakly-compressible flows should satisfy the 'incompressible stability' property.

Lastly, we note that the new methods perform well, even far away from the incompressible limit, for flows in which the local Mach number exceeds 0.5. Of course, our numerical experiments in this regard are not exhaustive. Therefore, subsequent work will be needed to investigate the properties of these methods at higher Mach numbers (and Reynolds numbers), in an effort to establish their validity in these more challenging contexts.

APPENDICES

A Derivation of the Incompressible Navier-Stokes Equations

In order to obtain the non-isothermal, incompressible Navier-Stokes equations, we start by introducing the fully compressible Navier-Stokes equations

$$\partial_t \rho + \nabla \cdot (\rho \boldsymbol{u}) = 0,$$

$$\partial_t (\rho \boldsymbol{u}) + \nabla \cdot (\rho \boldsymbol{u} \otimes \boldsymbol{u} + P\mathbb{I}) - \nabla \cdot (\rho \boldsymbol{\tau}) = -\beta \rho T \boldsymbol{g} + \boldsymbol{S}_u,$$

$$\partial_t (\rho T) + \nabla \cdot (\rho T \boldsymbol{u}) - \nabla \cdot \left(\frac{\kappa}{C_v} \nabla T \right) = -(\gamma - 1) \rho T (\nabla \cdot \boldsymbol{u}) + \frac{1}{C_v} (\rho \boldsymbol{\tau} : \nabla \boldsymbol{u}) + S_T,$$

where $\boldsymbol{S}_u = \rho \boldsymbol{f}_u$ and $S_T = \rho f_T$ are density-scaled forcing functions. Note: the buoyancy term in the linear momentum equation above has been modeled using the Boussinesq approximation. Next, we can non-dimensionalize these governing equations by using the following normalizations

$$\boldsymbol{x}^\star = \frac{\boldsymbol{x}}{L_{\text{ref}}}, \quad t^\star = \frac{t}{t_{\text{ref}}}, \quad \boldsymbol{u}^\star = \frac{\boldsymbol{u}}{U_{\text{ref}}}, \quad \rho^\star = \frac{\rho}{\rho_{\text{ref}}}, \quad \beta^\star = \frac{\beta}{\beta_{\text{ref}}}, \quad \boldsymbol{g}^\star = \frac{\boldsymbol{g}}{g_{\text{ref}}},$$

$$\boldsymbol{S}_u^\star = \frac{\boldsymbol{S}_u}{S_{u_{\text{ref}}}}, \quad S_T^\star = \frac{S_T}{S_{T_{\text{ref}}}}, \quad T^\star = \frac{T}{T_{\text{ref}}}, \quad P^\star = \frac{P}{P_{\text{ref}}}, \quad \kappa^\star = \frac{\kappa}{\kappa_{\text{ref}}}, \quad \boldsymbol{\tau}^\star = \frac{\boldsymbol{\tau} \rho_{\text{ref}} L_{\text{ref}}}{\mu_{\text{ref}} U_{\text{ref}}},$$

where L_{ref}, t_{ref}, U_{ref}, ρ_{ref}, β_{ref}, g_{ref}, $S_{u_{\text{ref}}}$, $S_{T_{\text{ref}}}$, T_{ref}, P_{ref}, and κ_{ref} are reference quantities. In a natural fashion, these reference quantities can be used to form the following dimensionless numbers

$$St = \frac{L_{\text{ref}}}{t_{\text{ref}} U_{\text{ref}}}, \quad Ma = \frac{U_{\text{ref}}}{\sqrt{\gamma P_{\text{ref}}/\rho_{\text{ref}}}}, \quad Re = \frac{\rho_{\text{ref}} U_{\text{ref}} L_{\text{ref}}}{\mu_{\text{ref}}}, \quad Fr = \frac{U_{\text{ref}}}{\sqrt{g_{\text{ref}} L_{\text{ref}}}},$$
$$Te = \beta_{\text{ref}} T_{\text{ref}}, \quad Pr = \frac{C_p \mu_{\text{ref}}}{\kappa_{\text{ref}}}, \quad Cu = \frac{S_{u_{\text{ref}}} L_{\text{ref}}}{\rho_{\text{ref}} U_{\text{ref}}^2}, \quad Ct = \frac{S_{T_{\text{ref}}} L_{\text{ref}}}{\rho_{\text{ref}} T_{\text{ref}} U_{\text{ref}}},$$

where St is the Strouhal number, Ma is the Mach number, Re is the Reynolds number, Fr is the Froude number, Te is the thermal expansion number, Pr is the Prandtl number, and Cu and Ct are non-dimensional numbers associated with the forcing terms.

Next, upon non-dimensionalizing the governing equations using the reference quantities and the non-dimensional numbers above, we obtain

$$\begin{aligned}
&St\, \partial_{t^\star}(\rho^\star) + \nabla^\star \cdot (\rho^\star \boldsymbol{u}^\star) = 0, \\
&St\, \partial_{t^\star}(\rho^\star \boldsymbol{u}^\star) + \nabla^\star \cdot (\rho^\star \boldsymbol{u}^\star \otimes \boldsymbol{u}^\star) + \frac{1}{\gamma Ma^2} \nabla^\star P^\star - \frac{1}{Re} \nabla^\star \cdot (\rho^\star \boldsymbol{\tau}^\star) \\
&= -\frac{Te}{Fr^2} \beta^\star \rho^\star T^\star \boldsymbol{g}^\star + Cu\, \boldsymbol{S}_u^\star, \\
&St\, \partial_{t^\star}(\rho^\star T^\star) + \nabla^\star \cdot (\rho^\star T^\star \boldsymbol{u}^\star) - \frac{\gamma}{Pr\, Re} \nabla^\star \cdot (\kappa^\star \nabla^\star T^\star) \\
&= -(\gamma - 1)\, \rho^\star T^\star \left(\nabla^\star \cdot \boldsymbol{u}^\star\right) + \gamma\,(\gamma - 1)\, \frac{Ma^2}{Re} \rho^\star \left(\boldsymbol{\tau}^\star : \nabla^\star \boldsymbol{u}^\star\right) + Ct\, S_T^\star.
\end{aligned}$$

We will now consider the case where the density is constant ($\rho^\star = \text{const}$), the Mach number approaches zero ($Ma \to 0$), and the pressure gradient becomes small ($\nabla^\star P^\star \ll 1$). In this case, we obtain

$$
\begin{aligned}
&\nabla^\star \cdot \boldsymbol{u}^\star = 0,\\
&St\,\partial_{t^\star}\boldsymbol{u}^\star + \nabla^\star \cdot (\boldsymbol{u}^\star \otimes \boldsymbol{u}^\star) + \frac{1}{\gamma Ma^2}\nabla^\star p^\star - \frac{1}{Re}\nabla^\star \cdot \boldsymbol{\tau}^\star\\
&= -\frac{Te}{Fr^2}\beta^\star T^\star \boldsymbol{g}^\star + Cu\,\boldsymbol{f}_u^\star,\\
&St\,\partial_{t^\star}T^\star + \nabla^\star \cdot (T^\star \boldsymbol{u}^\star) - \frac{\gamma}{Pr\,Re}\nabla^\star \cdot \left(\frac{\kappa^\star}{\rho^\star}\nabla^\star T^\star\right)\\
&= -\,(\gamma - 1)\,T^\star\,(\nabla^\star \cdot \boldsymbol{u}^\star) + Ct\,f_T^\star.
\end{aligned}
$$

Our governing equations for non-isothermal incompressible flows (Eqs. (2.2.1)–(2.2.3)) immediately follow from these equations by reversing the non-dimensionalization performed above.

B Useful Norm Inequalities for Incompressible Flows

B.1. Supporting Results

In this section, we introduce some technical results which are used in the proofs of the theorems in the main text.

Lemma B.1.1 (Comparison of Gradient Norms)**.** *Suppose that* $\boldsymbol{w} \in \boldsymbol{W}^{1,p}(\mathcal{T}_h)$*. Then, for* $1 \leq q < p < \infty$

$$\|\boldsymbol{w}\|_{\mathrm{grad},q} \leq \varrho_{p,q} \|\boldsymbol{w}\|_{\mathrm{grad},p}, \tag{B.1.1}$$

where $\varrho_{p,q}$ *depends on* p*,* q*,* d*, the size of the domain, and the mesh topology.*

Proof. One may consult [47], p. 189 for a proof of the scalar case. The proof of the vector case follows from applying the scalar result component-wise and using the power-mean inequality. □

Lemma B.1.2 (Inequalities of Broken Sobolev Norms)**.** *Suppose that* $\boldsymbol{w} \in \boldsymbol{W}^{1,p}(\mathcal{T}_h)$ *and* $2 \leq p < \infty$*. Then, the following inequalities hold*

$$\|\nabla_h \cdot \boldsymbol{w}\|_{L^p(\Omega)} \leq d^{(p-1)/p} \|\boldsymbol{w}\|_{\mathrm{grad},p}, \tag{B.1.2}$$

$$\|\nabla_h \boldsymbol{w} : \nabla_h \boldsymbol{w}\|_{L^{p/2}(\Omega)} \leq d^{2(p-2)/p} \|\boldsymbol{w}\|^2_{\mathrm{grad},p}, \tag{B.1.3}$$

where C_{norm} *is a constant that depends on* d *and* p*.*

Proof. Let us begin by noting that

$$
\begin{aligned}
&\|\nabla_h \cdot \boldsymbol{w}\|_{L^p(\Omega)} \\
&= \left(\sum_{K \in \mathcal{T}_h} \int_K \left(\sum_i^d (\partial_i w_i) \right)^p dV \right)^{1/p} \leq \left(\sum_{K \in \mathcal{T}_h} \int_K \left(\sum_i^d |\partial_i w_i| \right)^p dV \right)^{1/p} \\
&\leq d^{(p-1)/p} \left(\sum_{K \in \mathcal{T}_h} \int_K \sum_i^d (\partial_i w_i)^p \, dV \right)^{1/p} \leq d^{(p-1)/p} \left(\sum_{K \in \mathcal{T}_h} \int_K \sum_{i,j}^d (\partial_j w_i)^p \, dV \right)^{1/p} .
\end{aligned}
$$

Here, we have used the power-mean inequality. Upon combining this result with the definition for the norm $\|\cdot\|_{\text{grad},p}$, we obtain the first result (Eq. (B.1.2)).

Next, we expand the L$p/2$-norm

$$
\|\nabla_h \boldsymbol{w} : \nabla_h \boldsymbol{w}\|_{L^{p/2}(\Omega)} = \left\| \sum_{i,j}^d (\partial_j w_i)^2 \right\|_{L^{p/2}(\Omega)} = \left(\sum_{K \in \mathcal{T}_h} \int_K \left(\sum_{i,j}^d (\partial_j w_i)^2 \right)^{p/2} dV \right)^{2/p} . \tag{B.1.4}
$$

Then, by the power-mean inequality, we have

$$
\begin{gathered}
\sum_{K \in \mathcal{T}_h} \int_K \left(\sum_{i,j}^d (\partial_j w_i)^2 \right)^{p/2} dV \leq d^{(p-2)} \left(\sum_{K \in \mathcal{T}_h} \int_K \sum_{i,j}^d |\partial_j w_i|^p \, dV \right) \\
\left(\sum_{K \in \mathcal{T}_h} \int_K \left(\sum_{i,j}^d (\partial_j w_i)^2 \right)^{p/2} dV \right)^{2/p} \leq d^{2(p-2)/p} \left(\sum_{K \in \mathcal{T}_h} \int_K \sum_{i,j}^d |\partial_j w_i|^p \, dV \right)^{2/p} .
\end{gathered} \tag{B.1.5}
$$

Upon combining this result with Eq. (B.1.4), and the definition for the norm

$\|\cdot\|_{\mathrm{grad},p}$, we obtain the inequality in Eq. (B.1.3).

□

Lemma B.1.3 (Comparison of Lebesgue and Gradient Norms)**.** *Suppose that* $\boldsymbol{w}_h \in \boldsymbol{W}_h \subset \boldsymbol{\mathcal{P}}_k(\mathcal{T}_h)$ *for polynomial degree* $k \geq 0$*. Then, for* $1 \leq q < \infty$ *and* $d \leq p < \infty$*, we have*

$$\|\boldsymbol{w}_h\|_{\boldsymbol{L}^q(\Omega)} \leq \sigma_{p,q} \|\boldsymbol{w}_h\|_{\mathrm{grad},p}, \tag{B.1.6}$$

where $\sigma_{p,q}$ *is a constant which depends on* p*,* q*,* d*,* k*, the size of the domain, and the mesh regularity.*

Proof. One may consult [47], p. 190 for a proof of the scalar case. The proof of the vector case follows immediately by applying the scalar result component-wise and using the power-mean inequality. □

Lemma B.1.4 (Discrete Trace Inequalities)**.** *Suppose that* $\boldsymbol{w}_h \in \boldsymbol{W}_h \subset \boldsymbol{\mathcal{P}}_k(\mathcal{T}_h)$ *for polynomial degree* $k \geq 0$*, and* $\mathcal{T}_h$ *is part of a shape- and contact-regular mesh sequence. Then, for interior faces* $\mathcal{F}_h^i$

$$\sum_{F \in \mathcal{F}_h^i} h_F \|[\![\boldsymbol{w}_h]\!]\|^2_{\boldsymbol{L}^2(F)} \leq 2N_\partial C^2_{\mathrm{tr},2} \|\boldsymbol{w}_h\|^2_{\boldsymbol{L}^2(\Omega)}, \tag{B.1.7}$$

$$\sum_{F \in \mathcal{F}_h^i} h_F \|\{\{\boldsymbol{w}_h\}\}\|^2_{\boldsymbol{L}^2(F)} \leq \frac{1}{2}N_\partial C^2_{\mathrm{tr},2} \|\boldsymbol{w}_h\|^2_{\boldsymbol{L}^2(\Omega)}, \tag{B.1.8}$$

$$\sum_{F \in \mathcal{F}_h^i} h_F \|\{\{\boldsymbol{w}_h\}\}\|^4_{\boldsymbol{L}^4(F)} \leq \frac{1}{2}N_\partial C^4_{\mathrm{tr},4} \|\boldsymbol{w}_h\|^4_{\boldsymbol{L}^4(\Omega)}, \tag{B.1.9}$$

where N_∂, $C_{\mathrm{tr},2}$, *and* $C_{\mathrm{tr},4}$, *are parameters that depend on the mesh topology, and the degree* k.

Proof. One may consult [47], p. 273 for a proof of Eq. (B.1.9). The proofs of Eqs. (B.1.7) and (B.1.8) follow similar arguments. $\square$

C Convective Error Derivations for Incompressible Flows

C.1. Convective Terms in the Momentum Equation, Part I

First, we introduce a modified version of the convective operator c_h, neglecting the surface terms because we have assumed that our elements are H1-conforming

$$c_h\left(\boldsymbol{\varrho}_h; \boldsymbol{v}_h, \boldsymbol{w}_h\right) = \frac{1}{2}\left[\left((\boldsymbol{\varrho}_h \cdot \nabla)\boldsymbol{v}_h, \boldsymbol{w}_h\right)_{\mathcal{T}_h} - \left((\boldsymbol{\varrho}_h \cdot \nabla)\boldsymbol{w}_h, \boldsymbol{v}_h\right)_{\mathcal{T}_h}\right]. \tag{C.1.1}$$

Using the modified convective operator along with the definitions of $\boldsymbol{\eta}_{u,h}$ and $\boldsymbol{e}_{u,h}$ from Definition 2.4.3, and integrating by parts, we obtain

$$\begin{aligned}
c_h\left(\boldsymbol{u}_h; \boldsymbol{u}_h, \boldsymbol{e}_{u,h}\right) &= \frac{1}{2}\left(\boldsymbol{u}_h \cdot \nabla \boldsymbol{u}_h, \boldsymbol{e}_{u,h}\right)_{\mathcal{T}_h} - \frac{1}{2}\left(\boldsymbol{u}_h \cdot \nabla \boldsymbol{e}_{u,h}, \boldsymbol{u}_h\right)_{\mathcal{T}_h} \\
&= \frac{1}{2}\left(\boldsymbol{u}_h \cdot \nabla \boldsymbol{u}_h, \boldsymbol{e}_{u,h}\right)_{\mathcal{T}_h} + \frac{1}{2}\left(\boldsymbol{u}_h \cdot \nabla \boldsymbol{e}_{u,h}, \boldsymbol{e}_{u,h}\right)_{\mathcal{T}_h} - \frac{1}{2}\left(\boldsymbol{u}_h \cdot \nabla \boldsymbol{e}_{u,h}, j_u \boldsymbol{u}\right)_{\mathcal{T}_h} \\
&= \left(\boldsymbol{u}_h \cdot \nabla j_u \boldsymbol{u}, \boldsymbol{e}_{u,h}\right)_{\mathcal{T}_h} + \frac{1}{2}\left(\left(\nabla \cdot \boldsymbol{u}_h\right) j_u \boldsymbol{u}, \boldsymbol{e}_{u,h}\right)_{\mathcal{T}_h}.
\end{aligned}$$

Now, we begin the treatment of the convective terms in Eq. (2.4.73)

$$\begin{aligned}
&c_h\left(\boldsymbol{u}; \boldsymbol{u}, \boldsymbol{e}_{u,h}\right) - c_h\left(\boldsymbol{u}_h; \boldsymbol{u}_h, \boldsymbol{e}_{u,h}\right) \\
&= \underbrace{\left(\left(\boldsymbol{u} - \boldsymbol{u}_h\right) \cdot \nabla \boldsymbol{u}, \boldsymbol{e}_{u,h}\right)_{\mathcal{T}_h}}_{\Lambda_1^u} + \underbrace{\left(\boldsymbol{u}_h \cdot \nabla\left(\boldsymbol{u} - j_u \boldsymbol{u}\right), \boldsymbol{e}_{u,h}\right)_{\mathcal{T}_h}}_{\Lambda_2^u} - \underbrace{\frac{1}{2}\left(\left(\nabla \cdot \boldsymbol{u}_h\right) j_u \boldsymbol{u}, \boldsymbol{e}_{u,h}\right)_{\mathcal{T}_h}}_{\Lambda_3^u}.
\end{aligned}$$

Each term can be treated independently. First, we use Young's inequality as follows

$$\begin{aligned}
\Lambda_1^u &\leq \sum_{K\in\mathcal{T}_h} \|\nabla \boldsymbol{u}\|_{L^\infty(K)} \left(\|\boldsymbol{e}_{u,h}\|^2_{L^2(K)} + \|\boldsymbol{\eta}_{u,h}\|_{L^2(K)} \|\boldsymbol{e}_{u,h}\|_{L^2(K)} \right) \\
&= |\boldsymbol{u}|_{W^{1,\infty}(\Omega)} \|\boldsymbol{e}_{u,h}\|^2_{L^2(\Omega)} + \sum_{K\in\mathcal{T}_h} \frac{1}{h_K} |\boldsymbol{u}|_{W^{1,\infty}(K)} \|\boldsymbol{\eta}_{u,h}\|_{L^2(K)} h_K \|\boldsymbol{e}_{u,h}\|_{L^2(K)} \\
&\leq \frac{1}{4\varepsilon} \sum_{K\in\mathcal{T}_h} \frac{1}{h_K^2} \|\boldsymbol{\eta}_{u,h}\|^2_{L^2(K)} + \left(|\boldsymbol{u}|_{W^{1,\infty}(\Omega)} + \varepsilon \max_{K\in\mathcal{T}_h} \{ h_K^2 |\boldsymbol{u}|^2_{W^{1,\infty}(K)} \} \right) \|\boldsymbol{e}_{u,h}\|^2_{L^2(\Omega)} .
\end{aligned} \tag{C.1.2}$$

Next, we expand Λ_2^u via integration by parts

$$\Lambda_2^u = (\boldsymbol{u}_h \cdot \nabla \boldsymbol{\eta}_{u,h}, \boldsymbol{e}_{u,h})_{\mathcal{T}_h} = -(\boldsymbol{u}_h \cdot \nabla \boldsymbol{e}_{u,h}, \boldsymbol{\eta}_{u,h})_{\mathcal{T}_h} - ((\nabla \cdot \boldsymbol{u}_h) \boldsymbol{e}_{u,h}, \boldsymbol{\eta}_{u,h})_{\mathcal{T}_h} =: \Lambda_{2,1}^u + \Lambda_{2,2}^u.$$

Now, focusing on $\Lambda_{2,1}^u$, we introduce the local Reynolds number from Definition 2.4.4, and apply Young's inequality in order to obtain

$$\begin{aligned}
\Lambda_{2,1}^u &= -(\boldsymbol{u}_h \cdot \nabla \boldsymbol{e}_{u,h}, \boldsymbol{\eta}_{u,h})_{\mathcal{T}_h} \\
&\leq \sum_{K\in\mathcal{T}_h} \|\boldsymbol{u}_h\|_{L^\infty(K)} \|\nabla \boldsymbol{e}_{u,h}\|_{L^2(K)} \|\boldsymbol{\eta}_{u,h}\|_{L^2(K)} \\
&\leq \|\nabla \boldsymbol{e}_{u,h}\|_{\boldsymbol{L}^2(\Omega)\times \boldsymbol{L}^2(\Omega)} \left(\left(\sum_{K\in\mathcal{T}_h} \frac{h_K \nu}{h_K \nu} \|\boldsymbol{u}_h\|_{L^\infty(K)} \|\boldsymbol{\eta}_{u,h}\|_{L^2(K)} \right)^2 \right)^{1/2} \\
&\leq C_2^2 \varepsilon \nu \|\boldsymbol{e}_{u,h}\|^2_{\mathrm{sym},2} + \frac{1}{4\varepsilon} \sum_{K\in\mathcal{T}_h} \frac{\nu}{h_K^2} Re_K^2 \|\boldsymbol{\eta}_{u,h}\|^2_{L^2(K)} .
\end{aligned} \tag{C.1.3}$$

Note that, on the last line we have used Lemma 2.4.6. Next, focusing on $\Lambda^u_{2,2}$, we use the fact that $\nabla \cdot \boldsymbol{u} = 0$ along with Assumption 2.4.19 and Young's inequality

$$\begin{aligned}
\Lambda^u_{2,2} &= -\left(\left(\nabla \cdot \boldsymbol{u}_h\right) \boldsymbol{\eta}_{u,h}, \boldsymbol{e}_{u,h}\right)_{\mathcal{T}_h} = \left(\nabla \cdot \left(\boldsymbol{\eta}_{u,h} + \boldsymbol{e}_{u,h} - \boldsymbol{u}\right) \boldsymbol{\eta}_{u,h}, \boldsymbol{e}_{u,h}\right)_{\mathcal{T}_h} \\
&\leq \sum_{K \in \mathcal{T}_h} \|\boldsymbol{\eta}_{u,h}\|_{L^\infty(K)} \|\boldsymbol{e}_{u,h}\|_{L^2(K)} \left(\|\nabla \cdot \boldsymbol{e}_{u,h}\|_{L^2(K)} + \|\nabla \cdot \boldsymbol{\eta}_{u,h}\|_{L^2(K)}\right) \\
&\leq \sum_{K \in \mathcal{T}_h} C h_K \left|\boldsymbol{u}\right|_{W^{1,\infty}(K)} \|\boldsymbol{e}_{u,h}\|_{L^2(K)} \left(\|\nabla \cdot \boldsymbol{e}_{u,h}\|_{L^2(K)} + \|\nabla \cdot \boldsymbol{\eta}_{u,h}\|_{L^2(K)}\right) \\
&\leq \sum_{K \in \mathcal{T}_h} \left[\frac{\varepsilon\nu}{2} \left(\|\nabla \cdot \boldsymbol{e}_{u,h}\|_{L^2(K)} + \|\nabla \cdot \boldsymbol{\eta}_{u,h}\|_{L^2(K)}\right)^2 + \frac{C}{\varepsilon\nu} h_K^2 \left|\boldsymbol{u}\right|^2_{W^{1,\infty}(K)} \|\boldsymbol{e}_{u,h}\|^2_{L^2(K)}\right] \\
&\leq (C_1 C_2)^2 \varepsilon\nu \|\boldsymbol{e}_{u,h}\|^2_{\mathrm{sym},2} + (C_1 C_2)^2 \varepsilon\nu \|\boldsymbol{\eta}_{u,h}\|^2_{\mathrm{sym},2} + \frac{C}{\varepsilon\nu} \max_{K \in \mathcal{T}_h} \{h_K^2 \left|\boldsymbol{u}\right|^2_{W^{1,\infty}(K)}\} \|\boldsymbol{e}_{u,h}\|^2_{L^2(\Omega)}.
\end{aligned} \tag{C.1.4}$$

Here, we have used Lemmas 2.4.5 and 2.4.6 on the last line. Thereafter, we can split Λ^u_3 into two terms as we did previously for the case of Λ^u_2

$$\begin{aligned}
\Lambda^u_3 &= -\frac{1}{2} \left(\left(\nabla \cdot \boldsymbol{u}_h\right) j_u \boldsymbol{u}, \boldsymbol{e}_{u,h}\right)_{\mathcal{T}_h} = \frac{1}{2} \left(\left(\nabla \cdot \boldsymbol{u}_h\right) \boldsymbol{\eta}_{u,h}, \boldsymbol{e}_{u,h}\right)_{\mathcal{T}_h} - \frac{1}{2} \left(\left(\nabla \cdot \boldsymbol{u}_h\right) \boldsymbol{u}, \boldsymbol{e}_{u,h}\right)_{\mathcal{T}_h} \\
&:= \Lambda^u_{3,1} + \Lambda^u_{3,2}.
\end{aligned}$$

We can immediately see that $\Lambda^u_{3,1} = -\frac{1}{2}\Lambda^u_{2,2}$, and therefore, it can be bounded as follows

$$\Lambda^u_{3,1} \leq (C_1 C_2)^2 \varepsilon\nu \|\boldsymbol{e}_{u,h}\|^2_{\mathrm{sym},2} + (C_1 C_2)^2 \varepsilon\nu \|\boldsymbol{\eta}_{u,h}\|^2_{\mathrm{sym},2} + \frac{C}{\varepsilon\nu} \max_{K \in \mathcal{T}_h} \{h_K^2 \left|\boldsymbol{u}\right|^2_{W^{1,\infty}(K)}\} \|\boldsymbol{e}_{u,h}\|^2_{L^2(\Omega)}. \tag{C.1.5}$$

Next, we can use the fact that $\nabla\cdot\boldsymbol{u}=0$ and Young's inequality to bound $\Lambda^u_{3,2}$ as follows

$$
\begin{aligned}
\Lambda^u_{3,2} &\le \frac{1}{2}\left|\left(\nabla\cdot\boldsymbol{u}_h,\boldsymbol{u}\cdot\boldsymbol{e}_{u,h}\right)_{\mathcal{T}_h}\right| = \frac{1}{2}\left|\left(\nabla\cdot\left(-\boldsymbol{\eta}_{u,h}-\boldsymbol{e}_{u,h}+\boldsymbol{u}\right),\boldsymbol{u}\cdot\boldsymbol{e}_{u,h}\right)_{\mathcal{T}_h}\right| \\
&\le \frac{1}{2}\left|\left(\nabla\cdot\boldsymbol{\eta}_{u,h},\boldsymbol{u}\cdot\boldsymbol{e}_{u,h}\right)_{\mathcal{T}_h}\right| + \frac{1}{2}\left|\left(\nabla\cdot\boldsymbol{e}_{u,h},\boldsymbol{u}\cdot\boldsymbol{e}_{u,h}\right)_{\mathcal{T}_h}\right| \\
&\le \frac{1}{2}\sum_{K\in\mathcal{T}_h}\Big(\left\|\boldsymbol{u}\right\|_{L^\infty(K)}\left\|\nabla\cdot\boldsymbol{\eta}_{u,h}\right\|_{L^2(K)}\left\|\boldsymbol{e}_{u,h}\right\|_{L^2(K)} \\
&+\left\|\boldsymbol{u}\right\|_{L^\infty(K)}\left\|\nabla\cdot\boldsymbol{e}_{u,h}\right\|_{L^2(K)}\left\|\boldsymbol{e}_{u,h}\right\|_{L^2(K)}\Big) \\
&\le \frac{1}{2}\sum_{K\in\mathcal{T}_h}\left(\left\|\boldsymbol{u}\right\|_{L^\infty(K)}\left\|\boldsymbol{e}_{u,h}\right\|_{L^2(K)}\left(\left\|\nabla\cdot\boldsymbol{\eta}_{u,h}\right\|_{L^2(K)}+\left\|\nabla\cdot\boldsymbol{e}_{u,h}\right\|_{L^2(K)}\right)\right) \\
&\le \frac{1}{2}\sum_{K\in\mathcal{T}_h}\left(\varepsilon\nu\left(\left\|\nabla\cdot\boldsymbol{\eta}_{u,h}\right\|_{L^2(K)}+\left\|\nabla\cdot\boldsymbol{e}_{u,h}\right\|_{L^2(K)}\right)^2+\frac{1}{4\varepsilon\nu}\left\|\boldsymbol{u}\right\|^2_{L^\infty(K)}\left\|\boldsymbol{e}_{u,h}\right\|^2_{L^2(K)}\right) \\
&\le (C_1C_2)^2\varepsilon\nu\left\|\boldsymbol{\eta}_{u,h}\right\|^2_{\mathrm{sym},2}+(C_1C_2)^2\varepsilon\nu\left\|\boldsymbol{e}_{u,h}\right\|^2_{\mathrm{sym},2}+\frac{1}{8\varepsilon\nu}\left\|\boldsymbol{u}\right\|^2_{L^\infty(\Omega)}\left\|\boldsymbol{e}_{u,h}\right\|^2_{L^2(\Omega)}.
\end{aligned}
\tag{C.1.6}
$$

C.2. Convective Terms in the Momentum Equation, Part II

Using the modified convective operator (Eq. (C.1.1)), and integrating by parts, we obtain

$$\begin{aligned}
c_h(\boldsymbol{u};\boldsymbol{u},\boldsymbol{w}_h) - c_h(\boldsymbol{u}_h;\boldsymbol{u}_h,\boldsymbol{w}_h) &= \frac{1}{2}\left[((\boldsymbol{u}\cdot\nabla)\boldsymbol{u},\boldsymbol{w}_h)_{\mathcal{T}_h} - ((\boldsymbol{u}\cdot\nabla)\boldsymbol{w}_h,\boldsymbol{u})_{\mathcal{T}_h}\right] \\
&\quad - \frac{1}{2}\left[((\boldsymbol{u}_h\cdot\nabla)\boldsymbol{u}_h,\boldsymbol{w}_h)_{\mathcal{T}_h} - ((\boldsymbol{u}_h\cdot\nabla)\boldsymbol{w}_h,\boldsymbol{u}_h)_{\mathcal{T}_h}\right] \\
&= -\underbrace{((\boldsymbol{u}-\boldsymbol{u}_h)\cdot\nabla\boldsymbol{w}_h,\boldsymbol{u}_h)_{\mathcal{T}_h}}_{\Phi_1^u} - \underbrace{((\boldsymbol{u}\cdot\nabla)\boldsymbol{w}_h,\boldsymbol{u}-\boldsymbol{u}_h)_{\mathcal{T}_h}}_{\Phi_2^u} \\
&\quad - \underbrace{\frac{1}{2}(\nabla\cdot(\boldsymbol{u}-\boldsymbol{u}_h),\boldsymbol{u}_h\cdot\boldsymbol{w}_h)_{\mathcal{T}_h}}_{\Phi_3^u}
\end{aligned}$$

We can bound the first term with a substitution of $\boldsymbol{u}-\boldsymbol{u}_h = \boldsymbol{\eta}_{u,h} + \boldsymbol{e}_{u,h}$ and Cauchy-Schwarz inequality

$$\begin{aligned}
\Phi_1^u &\leq \left|((\boldsymbol{\eta}_{u,h}\cdot\nabla)\boldsymbol{w}_h,\boldsymbol{u}_h)_{\mathcal{T}_h}\right| + \left|((\boldsymbol{e}_{u,h}\cdot\nabla)\boldsymbol{w}_h,\boldsymbol{u}_h)_{\mathcal{T}_h}\right| \\
&\leq \left(\|\boldsymbol{\eta}_{u,h}\|_{L^2(\Omega)} + \|\boldsymbol{e}_{u,h}\|_{L^2(\Omega)}\right)\|\boldsymbol{u}_h\|_{L^\infty(\Omega)}\|\boldsymbol{w}_h\|_{\text{grad},2}\,.
\end{aligned}$$

We can also bound the second term with a substitution of $\boldsymbol{u}-\boldsymbol{u}_h = \boldsymbol{\eta}_{u,h} + \boldsymbol{e}_{u,h}$ and Cauchy-Schwarz inequality

$$\begin{aligned}
\Phi_2^u &\leq \left|((\boldsymbol{u}\cdot\nabla)\boldsymbol{w}_h,\boldsymbol{\eta}_{u,h})_{\mathcal{T}_h}\right| + \left|((\boldsymbol{u}\cdot\nabla)\boldsymbol{w}_h,\boldsymbol{e}_{u,h})_{\mathcal{T}_h}\right| \\
&\leq \left(\|\boldsymbol{\eta}_{u,h}\|_{L^2(\Omega)} + \|\boldsymbol{e}_{u,h}\|_{L^2(\Omega)}\right)\|\boldsymbol{u}\|_{L^\infty(\Omega)}\|\boldsymbol{w}_h\|_{\text{grad},2}\,.
\end{aligned}$$

Lastly, we can bound the third term with a substitution of $\boldsymbol{u} - \boldsymbol{u}_h = \boldsymbol{\eta}_{u,h} + \boldsymbol{e}_{u,h}$, Cauchy-Schwarz inequality, a Sobolev norm inequality (Lemma B.1.2), and an embedding inequality (Lemma B.1.3)

$$
\begin{aligned}
\Phi_3^u &\leq \left| \left(\nabla \cdot \boldsymbol{\eta}_{u,h}, \boldsymbol{u}_h \cdot \boldsymbol{w}_h \right)_{\mathcal{T}_h} \right| + \left| \left(\nabla \cdot \boldsymbol{e}_{u,h}, \boldsymbol{u}_h \cdot \boldsymbol{w}_h \right)_{\mathcal{T}_h} \right| \\
&\leq \left(\left\| \nabla \cdot \boldsymbol{\eta}_{u,h} \right\|_{L^2(\Omega)} + \left\| \nabla \cdot \boldsymbol{e}_{u,h} \right\|_{L^2(\Omega)} \right) \left\| \boldsymbol{u}_h \right\|_{L^\infty(\Omega)} \left\| \boldsymbol{w}_h \right\|_{L^2(\Omega)} \\
&\leq d^{1/2} \left(\left\| \boldsymbol{\eta}_{u,h} \right\|_{\mathrm{grad},2} + \left\| \boldsymbol{e}_{u,h} \right\|_{\mathrm{grad},2} \right) \left\| \boldsymbol{u}_h \right\|_{L^\infty(\Omega)} \left\| \boldsymbol{w}_h \right\|_{L^2(\Omega)} \\
&\leq d^{1/2} \sigma_{2,2} \left(\left\| \boldsymbol{\eta}_{u,h} \right\|_{\mathrm{grad},2} + \left\| \boldsymbol{e}_{u,h} \right\|_{\mathrm{grad},2} \right) \left\| \boldsymbol{u}_h \right\|_{L^\infty(\Omega)} \left\| \boldsymbol{w}_h \right\|_{\mathrm{grad},2} .
\end{aligned}
$$

C.3. Convective Terms in the Temperature Equation

We can treat the convective terms in Eq. (2.4.84) in an analogous way to the convective terms in Eq. (2.4.73)

$$
\begin{aligned}
&\underline{c}_h \left(\boldsymbol{u}; T, e_{T,h} \right) - \underline{c}_h \left(\boldsymbol{u}_h; T_h, e_{T,h} \right) \\
&\quad = \underbrace{\left(\left(\boldsymbol{u} - \boldsymbol{u}_h \right) \cdot \nabla T, e_{T,h} \right)_{\mathcal{T}_h}}_{\Lambda_1^T} + \underbrace{\left(\boldsymbol{u}_h \cdot \nabla \left(T - j_T T \right), e_{T,h} \right)_{\mathcal{T}_h}}_{\Lambda_2^T} - \underbrace{\frac{1}{2} \left(\left(\nabla \cdot \boldsymbol{u}_h \right) j_T T, e_{T,h} \right)_{\mathcal{T}_h}}_{\Lambda_3^T} .
\end{aligned}
\tag{C.3.1}
$$

Next, we can bound the first term with a substitution of $\boldsymbol{u} - \boldsymbol{u}_h = \boldsymbol{\eta}_{u,h} + \boldsymbol{e}_{u,h}$ and Young's inequality

$$\begin{aligned}
\Lambda_1^T &\le \sum_{K\in\mathcal{T}_h} \|\nabla T\|_{L^\infty(K)} \left(\|\boldsymbol{e}_{u,h}\|_{L^2(K)} + \|\boldsymbol{\eta}_{u,h}\|_{L^2(K)}\right) \|e_{T,h}\|_{L^2(K)} \\
&= |T|_{W^{1,\infty}(\Omega)} \|e_{T,h}\|_{L^2(\Omega)} \|\boldsymbol{e}_{u,h}\|_{L^2(\Omega)} + \sum_{K\in\mathcal{T}_h} \frac{1}{h_K} |T|_{W^{1,\infty}(K)} \|\boldsymbol{\eta}_{u,h}\|_{L^2(K)} h_K \|e_{T,h}\|_{L^2(K)} \\
&\le \frac{1}{4\varepsilon} \sum_{K\in\mathcal{T}_h} \frac{1}{h_K^2} \|\boldsymbol{\eta}_{u,h}\|^2_{L^2(K)} + \varepsilon \max_{K\in\mathcal{T}_h} \{h_K^2 |T|^2_{W^{1,\infty}(K)}\} \|e_{T,h}\|^2_{L^2(\Omega)} \\
&+ \frac{1}{2} |T|_{W^{1,\infty}(\Omega)} \|e_{T,h}\|^2_{L^2(\Omega)} + \frac{1}{2} |T|_{W^{1,\infty}(\Omega)} \|\boldsymbol{e}_{u,h}\|^2_{L^2(\Omega)} . \qquad \text{(C.3.2)}
\end{aligned}$$

We can split the second term in Eq. (C.3.1) into two new terms via integration by parts

$$\Lambda_2^T = (\boldsymbol{u}_h \cdot \nabla \eta_{T,h}, e_{T,h})_{\mathcal{T}_h} = -(\boldsymbol{u}_h \cdot \nabla e_{T,h}, \eta_{T,h})_{\mathcal{T}_h} - ((\nabla \cdot \boldsymbol{u}_h) e_{T,h}, \eta_{T,h})_{\mathcal{T}_h} := \Lambda_{2,1}^T + \Lambda_{2,2}^T. \qquad \text{(C.3.3)}$$

In accordance with our analysis of $\Lambda^u_{2,1}$, we use Young's inequality and definition 2.4.4 to obtain

$$\begin{aligned}
\Lambda_{2,1}^T &= -(\boldsymbol{u}_h \cdot \nabla e_{T,h}, \eta_{T,h})_{\mathcal{T}_h} \le \left|(\boldsymbol{u}_h \cdot \nabla e_{T,h}, \eta_{T,h})_{\mathcal{T}_h}\right| \\
&\le 7\alpha\gamma\varepsilon \|e_{T,h}\|^2_{\mathrm{grad},2} + \frac{1}{28\varepsilon} \sum_{K\in\mathcal{T}_h} \frac{\alpha}{h_K^2 \gamma} Pe_K^2 \|\eta_{T,h}\|^2_{L^2(K)} . \qquad \text{(C.3.4)}
\end{aligned}$$

Next, we proceed in accordance with our analysis of $\Lambda_{2,2}^u$ in order to obtain

$$\begin{aligned}\Lambda_{2,2}^T &= -\left((\nabla\cdot\boldsymbol{u}_h)\, e_{T,h}, \eta_{T,h}\right)_{\mathcal{T}_h} \leq \left|\left((\nabla\cdot(\boldsymbol{\eta}_{u,h}+\boldsymbol{e}_{u,h}))\, e_{T,h}, \eta_{T,h}\right)_{\mathcal{T}_h}\right| \\ &\leq \sum_{K\in\mathcal{T}_h} \|\eta_{T,h}\|_{L^\infty(K)} \left(\|\nabla\cdot\boldsymbol{e}_{u,h}\|_{L^2(K)} + \|\nabla\cdot\boldsymbol{\eta}_{u,h}\|_{L^2(K)}\right) \|e_{T,h}\|_{L^2(K)} \\ &\leq (C_1C_2)^2\varepsilon\nu\, \|\boldsymbol{e}_{u,h}\|_{\mathrm{sym},2}^2 + (C_1C_2)^2\varepsilon\nu\, \|\boldsymbol{\eta}_{u,h}\|_{\mathrm{sym},2}^2 + \frac{C}{\varepsilon\nu}\max_{K\in\mathcal{T}_h}\{h_K^2\, |T|_{W^{1,\infty}(K)}^2\}\, \|e_{T,h}\|_{L^2(\Omega)}^2 .\end{aligned} \tag{C.3.5}$$

The third term in Eq. (C.3.1) can be partitioned using $j_T T = T - \eta_{T,h}$

$$\begin{aligned}\Lambda_3^T &= -\frac{1}{2}\left((\nabla\cdot\boldsymbol{u}_h)\, j_T T, e_{T,h}\right)_{\mathcal{T}_h} = \frac{1}{2}\left((\nabla\cdot\boldsymbol{u}_h)\, \eta_{T,h}, e_{T,h}\right)_{\mathcal{T}_h} - \frac{1}{2}\left((\nabla\cdot\boldsymbol{u}_h)\, T, e_{T,h}\right)_{\mathcal{T}_h} \\ &:= \Lambda_{3,1}^T + \Lambda_{3,2}^T.\end{aligned}$$

Note that $\Lambda_{3,1}^T = -\frac{1}{2}\Lambda_{2,2}^T$, and therefore

$$\Lambda_{3,1}^T \leq (C_1C_2)^2\varepsilon\nu\, \|\boldsymbol{e}_{u,h}\|_{\mathrm{sym},2}^2 + (C_1C_2)^2\varepsilon\nu\, \|\boldsymbol{\eta}_{u,h}\|_{\mathrm{sym},2}^2 + \frac{C}{\varepsilon\nu}\max_{K\in\mathcal{T}_h}\{h_K^2\, |T|_{W^{1,\infty}(K)}^2\}\, \|e_{T,h}\|_{L^2(\Omega)}^2 . \tag{C.3.6}$$

In addition, using $\nabla \cdot \boldsymbol{u} = 0$ and Young's inequality, we have that

$$
\begin{aligned}
\Lambda_{3,2}^{T} &\leq \frac{1}{2}\left|\left(\left(\nabla \cdot \boldsymbol{u}_h\right) T, e_{T,h}\right)_{\mathcal{T}_h}\right| = \frac{1}{2}\left|\left(\nabla \cdot \left(-\boldsymbol{\eta}_{u,h} - \boldsymbol{e}_{u,h} + \boldsymbol{u}\right) T, e_{T,h}\right)_{\mathcal{T}_h}\right| \\
&\leq \frac{1}{2}\left|\left(\nabla \cdot \boldsymbol{\eta}_{u,h}, T e_{T,h}\right)_{\mathcal{T}_h}\right| + \frac{1}{2}\left|\left(\nabla \cdot \boldsymbol{e}_{u,h}, T e_{T,h}\right)_{\mathcal{T}_h}\right| \\
&\leq \frac{1}{2}\sum_{K \in \mathcal{T}_h}\Big(\|T\|_{L^\infty(K)} \|\nabla \cdot \boldsymbol{\eta}_{u,h}\|_{L^2(K)} \|e_{T,h}\|_{L^2(K)} \\
&+ \|T\|_{L^\infty(K)} \|\nabla \cdot \boldsymbol{e}_{u,h}\|_{L^2(K)} \|e_{T,h}\|_{L^2(K)} \Big) \\
&\leq (C_1 C_2)^2 \varepsilon \nu \|\boldsymbol{\eta}_{u,h}\|_{\mathrm{sym},2}^2 + (C_1 C_2)^2 \varepsilon \nu \|\boldsymbol{e}_{u,h}\|_{\mathrm{sym},2}^2 + \frac{1}{8\varepsilon\nu} \|T\|_{L^\infty(\Omega)}^2 \|e_{T,h}\|_{L^2(\Omega)}^2 .
\end{aligned}
\tag{C.3.7}
$$

D Derivation of the Finite Element Methods for Compressible Flows

D.1. Mass Equation Derivation

One may substitute ρ_h and $\boldsymbol{u}_h$ into Eq. (3.2.1), multiply by a test function q_h, and integrate over the entire domain in order to yield

$$\left(\partial_t\, \rho_h, q_h\right)_{\mathcal{T}_h} + \left(\nabla_h \cdot \left(\rho_h \boldsymbol{u}_h\right), q_h\right)_{\mathcal{T}_h} = \left(S_\rho, q_h\right)_{\mathcal{T}_h} . \tag{D.1.1}$$

This is identical to Eq. (3.3.1).

D.2. Linear Momentum Equation Derivation

One may substitute ρ_h, $\boldsymbol{u}_h$, and T_h into Eq. (3.2.2), compute the dot product with a test function $\boldsymbol{w}_h$, and integrate over the entire domain in order to yield

$$\left(\partial_t \left(\rho_h \boldsymbol{u}_h\right), \boldsymbol{w}_h\right)_{\mathcal{T}_h} + \left(\nabla_h \cdot \left(\left(\rho_h \boldsymbol{u}_h\right) \otimes \boldsymbol{u}_h + P_h \mathbb{I}\right), \boldsymbol{w}_h\right)_{\mathcal{T}_h} - \left(\nabla_h \cdot \left(\rho_h \boldsymbol{\tau}_h\right), \boldsymbol{w}_h\right)_{\mathcal{T}_h} = \left(\boldsymbol{S}_u, \boldsymbol{w}_h\right)_{\mathcal{T}_h} . \tag{D.2.1}$$

Upon integrating the second and third terms on the LHS by parts and inserting numerical fluxes $\widehat{\boldsymbol{\sigma}}_{\text{inv}}$ and $\widehat{\boldsymbol{\sigma}}_{\text{vis}}$, one obtains

$$\begin{aligned}
&\left(\nabla_h \cdot \left((\rho_h \boldsymbol{u}_h) \otimes \boldsymbol{u}_h + P_h \mathbb{I}\right), \boldsymbol{w}_h\right)_{\mathcal{T}_h} \\
&= -\left((\rho_h \boldsymbol{u}_h) \otimes \boldsymbol{u}_h + P_h \mathbb{I}, \nabla_h \boldsymbol{w}_h\right)_{\mathcal{T}_h} + \left\langle \left((\rho_h \boldsymbol{u}_h) \otimes \boldsymbol{u}_h + P_h \mathbb{I}\right) \boldsymbol{n}, \boldsymbol{w}_h \right\rangle_{\partial \mathcal{T}_h} \\
&\equiv -\left((\rho_h \boldsymbol{u}_h) \otimes \boldsymbol{u}_h + P_h \mathbb{I}, \nabla_h \boldsymbol{w}_h\right)_{\mathcal{T}_h} + \left\langle \widehat{\boldsymbol{\sigma}}_{\text{inv}} \boldsymbol{n}, \boldsymbol{w}_h \right\rangle_{\partial \mathcal{T}_h} \\
&= -\left((\rho_h \boldsymbol{u}_h) \otimes \boldsymbol{u}_h, \nabla_h \boldsymbol{w}_h\right)_{\mathcal{T}_h} - \left(P_h, \nabla \cdot \boldsymbol{w}_h\right)_{\mathcal{T}_h} + \left\langle \widehat{\boldsymbol{\sigma}}_{\text{inv}} \boldsymbol{n}, \boldsymbol{w}_h \right\rangle_{\partial \mathcal{T}_h} .
\end{aligned} \tag{D.2.2}$$

$$\begin{aligned}
-\left(\nabla_h \cdot (\rho_h \boldsymbol{\tau}_h), \boldsymbol{w}_h\right)_{\mathcal{T}_h} &= \left(\rho_h \boldsymbol{\tau}_h, \nabla_h \boldsymbol{w}_h\right)_{\mathcal{T}_h} - \left\langle \rho_h \boldsymbol{\tau}_h \boldsymbol{n}, \boldsymbol{w}_h \right\rangle_{\partial \mathcal{T}_h} \\
&\equiv \left(\rho_h \boldsymbol{\tau}_h, \nabla_h \boldsymbol{w}_h\right)_{\mathcal{T}_h} - \left\langle \widehat{\boldsymbol{\sigma}}_{\text{vis}} \boldsymbol{n}, \boldsymbol{w}_h \right\rangle_{\partial \mathcal{T}_h} .
\end{aligned} \tag{D.2.3}$$

Consider substituting the definition of $\boldsymbol{\tau}_h$ (Eq. (3.2.8)) into the first term on the RHS of Eq. (D.2.3)

$$\left(\rho_h \boldsymbol{\tau}_h, \nabla_h \boldsymbol{w}_h\right)_{\mathcal{T}_h} = \left(\mu_h \left(\nabla_h \boldsymbol{u}_h + \nabla_h \boldsymbol{u}_h^T - \frac{2}{3} \left(\nabla \cdot \boldsymbol{u}_h\right) \mathbb{I}\right), \nabla_h \boldsymbol{w}_h\right)_{\mathcal{T}_h} . \tag{D.2.4}$$

One may expand each term in Eq. (D.2.4) by integrating by parts, inserting a numerical flux $\widehat{\boldsymbol{\varphi}}_{\text{vis}}$, and integrating by parts again as follows

$$
\begin{aligned}
\left(\mu_h \nabla_h \boldsymbol{u}_h, \nabla_h \boldsymbol{w}_h\right)_{\mathcal{T}_h} &= \left(\nabla_h \boldsymbol{u}_h, \mu_h \nabla_h \boldsymbol{w}_h\right)_{\mathcal{T}_h} \\
&= -\left(\boldsymbol{u}_h, \nabla_h \cdot \left(\mu_h \nabla_h \boldsymbol{w}_h\right)\right)_{\mathcal{T}_h} + \left\langle \mu_h \boldsymbol{u}_h, \left(\nabla_h \boldsymbol{w}_h\right) \boldsymbol{n}\right\rangle_{\partial\mathcal{T}_h} \\
&\equiv -\left(\boldsymbol{u}_h, \nabla_h \cdot \left(\mu_h \nabla_h \boldsymbol{w}_h\right)\right)_{\mathcal{T}_h} + \left\langle \widehat{\boldsymbol{\varphi}}_{\text{vis}}, \left(\nabla_h \boldsymbol{w}_h\right) \boldsymbol{n}\right\rangle_{\partial\mathcal{T}_h} \\
&= \left(\mu_h \nabla_h \boldsymbol{u}_h, \nabla_h \boldsymbol{w}_h\right)_{\mathcal{T}_h} + \left\langle \widehat{\boldsymbol{\varphi}}_{\text{vis}} - \mu_h \boldsymbol{u}_h, \left(\nabla_h \boldsymbol{w}_h\right) \boldsymbol{n}\right\rangle_{\partial\mathcal{T}_h}.
\end{aligned}
\tag{D.2.5}
$$

$$
\begin{aligned}
\left(\mu_h \nabla_h \boldsymbol{u}_h^T, \nabla_h \boldsymbol{w}_h\right)_{\mathcal{T}_h} &= \left(\nabla_h \boldsymbol{u}_h, \mu_h \nabla_h \boldsymbol{w}_h^T\right)_{\mathcal{T}_h} \\
&= -\left(\boldsymbol{u}_h, \nabla_h \cdot \left(\mu_h \nabla_h \boldsymbol{w}_h^T\right)\right)_{\mathcal{T}_h} + \left\langle \mu_h \boldsymbol{u}_h, \left(\nabla_h \boldsymbol{w}_h^T\right) \boldsymbol{n}\right\rangle_{\partial\mathcal{T}_h} \\
&\equiv -\left(\boldsymbol{u}_h, \nabla_h \cdot \left(\mu_h \nabla_h \boldsymbol{w}_h^T\right)\right)_{\mathcal{T}_h} + \left\langle \widehat{\boldsymbol{\varphi}}_{\text{vis}}, \left(\nabla_h \boldsymbol{w}_h^T\right) \boldsymbol{n}\right\rangle_{\partial\mathcal{T}_h} \\
&= \left(\mu_h \nabla_h \boldsymbol{u}_h^T, \nabla_h \boldsymbol{w}_h\right)_{\mathcal{T}_h} + \left\langle \widehat{\boldsymbol{\varphi}}_{\text{vis}} - \mu_h \boldsymbol{u}_h, \left(\nabla_h \boldsymbol{w}_h^T\right) \boldsymbol{n}\right\rangle_{\partial\mathcal{T}_h}.
\end{aligned}
\tag{D.2.6}
$$

$$
\begin{aligned}
\left(-\frac{2}{3}\mu_h \left(\nabla \cdot \boldsymbol{u}_h\right) \mathbb{I}, \nabla_h \boldsymbol{w}_h\right)_{\mathcal{T}_h} &= -\frac{2}{3}\left(\left(\nabla \cdot \boldsymbol{u}_h\right), \mu_h \nabla \cdot \boldsymbol{w}_h\right)_{\mathcal{T}_h} \\
&= -\frac{2}{3}\left(-\left(\boldsymbol{u}_h, \nabla_h \left(\mu_h \nabla_h \cdot \boldsymbol{w}_h\right)\right)_{\mathcal{T}_h} + \left\langle \mu_h \boldsymbol{u}_h, \left(\nabla \cdot \boldsymbol{w}_h\right) \boldsymbol{n}\right\rangle_{\partial\mathcal{T}_h}\right) \\
&\equiv -\frac{2}{3}\left(-\left(\boldsymbol{u}_h, \nabla_h \left(\mu_h \nabla_h \cdot \boldsymbol{w}_h\right)\right)_{\mathcal{T}_h} + \left\langle \widehat{\boldsymbol{\varphi}}_{\text{vis}}, \left(\nabla \cdot \boldsymbol{w}_h\right) \boldsymbol{n}\right\rangle_{\partial\mathcal{T}_h}\right) \\
&= \left(-\frac{2}{3}\mu_h \left(\nabla \cdot \boldsymbol{u}_h\right) \mathbb{I}, \nabla_h \boldsymbol{w}_h\right)_{\mathcal{T}_h} - \frac{2}{3}\left\langle \widehat{\boldsymbol{\varphi}}_{\text{vis}} - \mu_h \boldsymbol{u}_h, \left(\nabla \cdot \boldsymbol{w}_h\right) \boldsymbol{n}\right\rangle_{\partial\mathcal{T}_h}.
\end{aligned}
\tag{D.2.7}
$$

Upon combining Eqs. (D.2.5) – (D.2.7) along with the definition of $\boldsymbol{\tau}_h$ (Eq. (3.2.8)), one obtains

$$\left(\rho_h \boldsymbol{\tau}_h, \nabla_h \boldsymbol{w}_h\right)_{\mathcal{T}_h} \equiv \left(\rho_h \boldsymbol{\tau}_h, \nabla_h \boldsymbol{w}_h\right)_{\mathcal{T}_h} + \left\langle \widehat{\boldsymbol{\varphi}}_{\text{vis}} - \mu_h \boldsymbol{u}_h, \left(\nabla_h \boldsymbol{w}_h + \nabla_h \boldsymbol{w}_h^T - \frac{2}{3}\left(\nabla \cdot \boldsymbol{w}_h\right)\mathbb{I}\right)\boldsymbol{n}\right\rangle_{\partial\mathcal{T}_h}. \tag{D.2.8}$$

Finally, one may substitute Eqs. (D.2.2), (D.2.3), and (D.2.8), into Eq. (D.2.1), in order to obtain Eq. (3.3.2).

D.3. Internal Energy Equation Derivation

One may substitute ρ_h, $\boldsymbol{u}_h$, and T_h into Eq. (3.2.3), multiply by a test function r_h, and integrate over the entire domain in order to yield

$$\begin{aligned}&\left(\partial_t\left(\rho_h T_h\right), r_h\right)_{\mathcal{T}_h} + \left(\nabla_h \cdot \left(\rho_h T_h \boldsymbol{u}_h\right), r_h\right)_{\mathcal{T}_h} - \left(\nabla_h \cdot \left(\frac{\kappa_h}{C_v}\nabla_h T_h\right), r_h\right)_{\mathcal{T}_h}\\ &= -\left(\gamma-1\right)\left(\rho_h T_h\left(\nabla\cdot\boldsymbol{u}_h\right), r_h\right)_{\mathcal{T}_h} + \frac{1}{C_v}\left(\rho_h \boldsymbol{\tau_h} : \nabla_h \boldsymbol{u}_h, r_h\right)_{\mathcal{T}_h} + \left(S_T, r_h\right)_{\mathcal{T}_h}.\end{aligned} \tag{D.3.1}$$

Upon integrating the second and third terms on the LHS by parts and inserting numerical fluxes $\widehat{\boldsymbol{\phi}}_{\text{inv}}$ and $\widehat{\boldsymbol{\phi}}_{\text{vis}}$, one obtains

$$\begin{aligned}\left(\nabla_h \cdot \left(\rho_h T_h \boldsymbol{u}_h\right), r_h\right)_{\mathcal{T}_h} &= -\left(\rho_h T_h \boldsymbol{u}_h, \nabla_h r_h\right)_{\mathcal{T}_h} + \left\langle\left(\rho_h T_h \boldsymbol{u}_h\right)\cdot\boldsymbol{n}, r_h\right\rangle_{\partial\mathcal{T}_h}\\ &\equiv -\left(\rho_h T_h \boldsymbol{u}_h, \nabla_h r_h\right)_{\mathcal{T}_h} + \left\langle\widehat{\boldsymbol{\phi}}_{\text{inv}}\cdot\boldsymbol{n}, r_h\right\rangle_{\partial\mathcal{T}_h}.\end{aligned} \tag{D.3.2}$$

$$
\begin{aligned}
-\left(\nabla_h \cdot \left(\frac{\kappa_h}{C_v}\nabla_h T_h\right), r_h\right)_{\mathcal{T}_h} &= \left(\frac{\kappa_h}{C_v}\nabla_h T_h, \nabla_h r_h\right)_{\mathcal{T}_h} - \left\langle \left(\frac{\kappa_h}{C_v}\nabla_h T_h\right) \cdot \boldsymbol{n}, r_h \right\rangle_{\partial\mathcal{T}_h} \qquad \text{(D.3.3)} \\
&\equiv \left(\frac{\kappa_h}{C_v}\nabla_h T_h, \nabla_h r_h\right)_{\mathcal{T}_h} - \left\langle \widehat{\boldsymbol{\phi}}_{\text{vis}} \cdot \boldsymbol{n}, r_h \right\rangle_{\partial\mathcal{T}_h}.
\end{aligned}
$$

One may further expand Eq. (D.3.3). Consider integrating by parts, inserting the numerical flux $\widehat{\lambda}_{\text{vis}}$, and integrating by parts again as follows

$$
\begin{aligned}
\left(\nabla_h T_h, \frac{\kappa_h}{C_v}\nabla_h r_h\right)_{\mathcal{T}_h} &= -\left(T_h, \nabla_h \cdot \left(\frac{\kappa_h}{C_v}\nabla_h r_h\right)\right)_{\mathcal{T}_h} + \left\langle \frac{\kappa_h}{C_v} T_h, \nabla_h r_h \cdot \boldsymbol{n} \right\rangle_{\partial\mathcal{T}_h} \qquad \text{(D.3.4)} \\
&\equiv -\left(T_h, \nabla_h \cdot \left(\frac{\kappa_h}{C_v}\nabla_h r_h\right)\right)_{\mathcal{T}_h} + \left\langle \widehat{\lambda}_{\text{vis}}, \nabla_h r_h \cdot \boldsymbol{n} \right\rangle_{\partial\mathcal{T}_h} \\
&= \left(\frac{\kappa_h}{C_v}\nabla_h T_h, \nabla_h r_h\right)_{\mathcal{T}_h} + \left\langle \widehat{\lambda}_{\text{vis}} - \frac{\kappa_h}{C_v} T_h, \nabla_h r_h \cdot \boldsymbol{n} \right\rangle_{\partial\mathcal{T}_h}.
\end{aligned}
$$

Finally, one may combine Eqs. (D.3.1)–(D.3.4) in order to obtain Eq. (3.3.3).

Bibliography

[1] H. Dallmann, Finite element methods with local projection stabilization for thermally coupled incompressible flow, Ph.D. thesis, Niedersächsische Staats- und Universitätsbibliothek Göttingen (2015).

[2] R. Iwatsu, J. M. Hyun, K. Kuwahara, Mixed convection in a driven cavity with a stable vertical temperature gradient, International Journal of Heat and Mass Transfer 36 (6) (1993) 1601–1608.

[3] D. Canuto, K. Taira, Two-dimensional compressible viscous flow around a circular cylinder, Journal of Fluid Mechanics 785 (2015) 349–371.

[4] A. Oberbeck, Über die wärmeleitung der flüssigkeiten bei berücksichtigung der strömungen infolge von temperaturdifferenzen, Annalen der Physik 243 (6) (1879) 271–292.

[5] J. Boussinesq, Théorie analytique de la chaleur mise en harmonic avec la thermodynamique et avec la théorie mécanique de la lumière, Vol. 2, Gauthier-Villars, 1903.

[6] R. K. Zeytounian, Joseph Boussinesq and his approximation: a contemporary view, Comptes Rendus Mecanique 331 (8) (2003) 575–586.

[7] H. Dallmann, D. Arndt, Stabilized finite element methods for the Oberbeck–Boussinesq model, Journal of Scientific Computing 69 (1) (2016) 244–273.

[8] T. E. Laskaris, Finite-element analysis of compressible and incompressible viscous flow and heat transfer problems, The Physics of Fluids 18 (12) (1975) 1639–1648.

[9] D.-L. Young, R. H. Gallagher, J. A. Liggett, Steady stratified circulation in a cavity, Journal of the Engineering Mechanics Division 102 (1) (1976) 1–17.

[10] B. Tabarrok, R. C. Lin, Finite element analysis of free convection flows, International Journal of Heat and Mass Transfer 20 (9) (1977) 945–952.

[11] D. K. Gartling, Convective heat transfer analysis by the finite element method, Computer Methods in Applied Mechanics and Engineering 12 (3) (1977) 365–382.

[12] R. S. Marshall, J. C. Heinrich, O. Zienkiewicz, Natural convection in a square enclosure by a finite-element, penalty function method using primitive fluid variables, Numerical Heat Transfer, Part B: Fundamentals 1 (3) (1978) 315–330.

[13] J. Reddy, A. Satake, A comparison of a penalty finite element model with the stream function-vorticity model of natural confection in enclosures, Journal of Heat Transfer 102 (1980) 859.

[14] T. J. Hughes, L. P. Franca, A new finite element formulation for computational fluid dynamics: VII. The Stokes problem with various well-posed boundary conditions: symmetric formulations that converge for all velocity/pressure spaces, Computer Methods in Applied Mechanics and Engineering 65 (1) (1987) 85–96.

[15] T. J. Hughes, L. P. Franca, G. M. Hulbert, A new finite element formulation for computational fluid dynamics: VIII. the Galerkin/least-squares method for advective-diffusive equations, Computer Methods in Applied Mechanics and Engineering 73 (2) (1989) 173–189.

[16] C. Baiocchi, F. Brezzi, L. P. Franca, Virtual bubbles and Galerkin-least-squares type methods, Computer Methods in Applied Mechanics and Engineering 105 (1) (1993) 125–141.

[17] L. Tang, T. Tsang, A least-squares finite element method for doubly-diffusive convection, International Journal of Computational Fluid Dynamics 3 (1) (1994) 1–17.

[18] L. Q. Tang, T. T. Tsang, Temporal, spatial and thermal features of 3-D Rayleigh-Bénard convection by a least-squares finite element method, Computer Methods in Applied Mechanics and Engineering 140 (3-4) (1997) 201–219.

[19] J. N. Reddy, D. K. Gartling, The Finite Element Method in Heat Transfer and Fluid Dynamics, CRC press, 2010.

[20] J. Boland, W. Layton, Error analysis for finite element methods for steady natural convection problems, Numerical Functional Analysis and Optimization 11 (5-6) (1990) 449–483.

[21] J. Boland, W. Layton, An analysis of the finite element method for natural convection problems, Numerical Methods for Partial Differential Equations 6 (2) (1990) 115–126.

[22] O. Dorok, W. Grambow, L. Tobiska, Aspects of finite element discretizations for solving the Boussinesq approximation of the Navier-Stokes equations, in: Numerical Methods for the Navier-Stokes Equations, Springer, 1994, pp. 50–61.

[23] C. Bernardi, B. Métivet, B. Pernaud-Thomas, Couplage des équations de Navier-Stokes et de la chaleur: le modele et son approximation par éléments finis, ESAIM: Mathematical Modelling and Numerical Analysis-Modélisation Mathématique et Analyse Numérique 29 (7) (1995) 871–921.

[24] R. Codina, J. Principe, M. Ávila, Finite element approximation of turbulent thermally coupled incompressible flows with numerical sub-grid scale modelling, International Journal of Numerical Methods for Heat & Fluid Flow 20 (5) (2010) 492–516.

[25] J. Löwe, G. Lube, A projection-based variational multiscale method for large-eddy simulation with application to non-isothermal free convection problems, Mathematical Models and Methods in Applied Sciences 22 (02) (2012) 1150011.

[26] B. Cockburn, G. Kanschat, D. Schötzau, A locally conservative LDG method for the incompressible Navier-Stokes equations, Mathematics of Computation 74 (251) (2005) 1067–1095.

[27] B. Cockburn, G. Kanschat, D. Schötzau, A note on discontinuous Galerkin divergence-free solutions of the Navier–Stokes equations, Journal of Scientific Computing 31 (1) (2007) 61–73.

[28] R. Oyarzúa, T. Qin, D. Schötzau, An exactly divergence-free finite element method for a generalized Boussinesq problem, IMA Journal of Numerical Analysis 34 (3) (2014) 1104–1135.

[29] H.-G. Roos, M. Stynes, L. Tobiska, Robust numerical methods for singularly perturbed differential equations: convection-diffusion-reaction and flow problems, Vol. 24, Springer Science & Business Media, 2008.

[30] G. Matthies, L. Tobiska, Local projection type stabilization applied to inf–sup stable discretizations of the Oseen problem, IMA Journal of Numerical Analysis 35 (1) (2015) 239–269.

[31] A. N. Brooks, T. J. Hughes, Streamline upwind/Petrov-Galerkin formulations for convection dominated flows with particular emphasis on the incompressible Navier-Stokes equations, Computer Methods in Applied Mechanics and Engineering 32 (1-3) (1982) 199–259.

[32] T. J. Hughes, M. Mallet, M. Akira, A new finite element formulation for computational fluid dynamics: II. Beyond SUPG, Computer Methods in Applied Mechanics and Engineering 54 (3) (1986) 341–355.

[33] T. J. Hughes, Recent progress in the development and understanding of SUPG methods with special reference to the compressible Euler and Navier-Stokes equations, International Journal for Numerical Methods in Fluids 7 (11) (1987) 1261–1275.

[34] L. P. Franca, T. J. Hughes, Two classes of mixed finite element methods, Computer Methods in Applied Mechanics and Engineering 69 (1) (1988) 89–129.

[35] T. C. Rebollo, M. G. Mármol, F. Hecht, S. Rubino, I. S. Muñoz, A high-order local projection stabilization method for natural convection problems, Journal of Scientific Computing 74 (2) (2018) 667–692.

[36] J. de Frutos, B. García-Archilla, J. Novo, Grad-div stabilization for the time-dependent Boussinesq equations with inf-sup stable finite elements, Applied Mathematics and Computation 349 (2019) 281–291.

[37] R. Oyarzúa, P. Zúñiga, Analysis of a conforming finite element method for the Boussinesq problem with temperature-dependent parameters, Journal of Computational and Applied Mathematics 323 (2017) 71–94.

[38] J. A. Almonacid, G. N. Gatica, R. Oyarzúa, A mixed–primal finite element method for the Boussinesq problem with temperature-dependent viscosity, Calcolo 55 (3) (2018) 36.

[39] A. Allendes, G. R. Barrenechea, C. Naranjo, A divergence-free low-order stabilized finite element method for a generalized steady state Boussinesq problem, Computer Methods in Applied Mechanics and Engineering 340 (2018) 90–120.

[40] J. A. Almonacid, G. N. Gatica, R. Oyarzúa, R. Ruiz-Baier, A new mixed finite element method for the n-dimensional Boussinesq problem with temperature-dependent viscosity, Networks & Heterogeneous Media 15 (2) (2020) 215.

[41] X. Chen, D. M. Williams, Versatile mixed methods for the incompressible Navier–Stokes equations, Computers & Mathematics with Applications 80 (6) (2020) 1555–1577.

[42] D. Boffi, F. Brezzi, M. Fortin, Mixed Finite Element Methods and Applications, Vol. 44, Springer, 2013.

[43] P. W. Schroeder, C. Lehrenfeld, A. Linke, G. Lube, Towards computable flows and robust estimates for inf-sup stable FEM applied to the time-dependent incompressible Navier–Stokes equations, SeMA Journal, Boletin de la Sociedad Española de Matemática Aplicada 75 (4) (2018) 629–653.

[44] P. W. Schroeder, Robustness of high-order divergence-free finite element methods for incompressible computational fluid dynamics, Ph.D. thesis, Niedersächsische Staats-und Universitätsbibliothek Göttingen (2019).

[45] V. John, Finite Element Methods for Incompressible Flow Problems, Springer, 2016.

[46] D. Williams, Q. Hong, Generalized Korn's inequalities for piecewise H1 and H2 vector fields, Mathematics of Computation (2024).

[47] D. A. Di Pietro, A. Ern, Mathematical Aspects of Discontinuous Galerkin Methods, Vol. 69, Springer Science & Business Media, Berlin Heidelberg, 2011.

[48] G. Dziuk, Theorie und Numerik partieller Differentialgleichungen, de Gruyter, 2010.

[49] M. Rathmair, On how Poincaré inequalities imply weighted ones, Monatshefte für Mathematik 188 (4) (2019) 753–763.

[50] A. Ern, J.-L. Guermond, Theory and Practice of Finite Elements, Vol. 159, Springer Science & Business Media, 2013.

[51] H. Dallmann, D. Arndt, G. Lube, Local projection stabilization for the Oseen problem, IMA Journal of Numerical Analysis 36 (2) (2015) 796–823.

[52] R. L. Panton, Incompressible Flow, John Wiley & Sons, 2013.

[53] M. S. Alnaes, J. Blechta, J. Hake, A. Johansson, B. Kehlet, A. Logg, C. Richardson, J. Ring, M. E. Rognes, G. N. Wells, The FEniCS project version 1.5, Archive of Numerical Software 3 (100) (2015) 9–23.

[54] J. Löwe, Eine finite-elemente-methode für nicht-isotherme inkompressible strömungsprobleme, Ph.D. thesis, Niedersächsische Staats-und Universitätsbibliothek Göttingen (2011).

[55] E. A. Miller, X. Chen, D. M. Williams, Versatile mixed methods for non-isothermal incompressible flows, Computers & Mathematics with Applications 125 (2022) 150–175.

[56] M. Mallet, A finite element method for computational fluid dynamics, Ph.D. thesis, Stanford University Stanford, CA (1985).

[57] F. Shakib, T. J. R. Hughes, Z. Johan, A new finite element formulation for computational fluid dynamics: X. the compressible Euler and Navier-Stokes equations, Computer Methods in Applied Mechanics and Engineering (1991) 141–219.

[58] T. Hughes, F. Shakib, Computational aerodynamics and the finite element method, in: AIAA 25th Aerospace Sciences Meeting, Reno, Nevada, 1988.

[59] P. B. Bochev, M. D. Gunzburger, Least-squares finite element methods, Vol. 166, Springer Science & Business Media, 2009.

[60] T. J. Hughes, G. R. Feijóo, L. Mazzei, J.-B. Quincy, The variational multiscale method—a paradigm for computational mechanics, Computer Methods in Applied Mechanics and Engineering 166 (1-2) (1998) 3–24.

[61] T. J. Hughes, L. Mazzei, K. E. Jansen, Large eddy simulation and the variational multiscale method, Computing and Visualization in Science 3 (2000) 47–59.

[62] V. John, S. Kaya, A finite element variational multiscale method for the Navier–Stokes equations, SIAM Journal on Scientific Computing 26 (5) (2005) 1485–1503.

[63] T. J. Hughes, G. Sangalli, Variational multiscale analysis: the fine-scale Green's function, projection, optimization, localization, and stabilized methods, SIAM Journal on Numerical Analysis 45 (2) (2007) 539–557.

[64] B. Cockburn, C.-W. Shu, TVB Runge–Kutta local projection discontinuous Galerkin finite element method for conservation laws. II. General framework, Mathematics of Computation 52 (186) (1989) 411–435.

[65] B. Cockburn, S.-Y. Lin, C.-W. Shu, TVB Runge–Kutta local projection discontinuous Galerkin finite element method for conservation laws III: One-dimensional systems, Journal of Computational Physics 84 (1) (1989) 90–113.

[66] B. Cockburn, S. Hou, C.-W. Shu, The Runge–Kutta local projection discontinuous Galerkin finite element method for conservation laws. IV. The multidimensional case, Mathematics of Computation 54 (190) (1990) 545–581.

[67] B. Cockburn, C.-W. Shu, The Runge–Kutta local projection p^1-discontinuous Galerkin finite element method for scalar conservation laws, RAIRO-Modélisation mathématique et analyse numérique 25 (3) (1991) 337–361.

[68] B. Cockburn, C.-W. Shu, The Runge–Kutta discontinuous Galerkin method for conservation laws V: Multidimensional systems, Journal of Computational Physics 141 (2) (1998) 199–224.

[69] F. Bassi, S. Rebay, G. Mariotti, S. Pedinotti, M. Savini, A high-order accurate discontinuous finite element method for inviscid and viscous turbomachinery flows, in: Proceedings of the 2nd European Conference on Turbomachinery Fluid Dynamics and Thermodynamics, Technologisch Instituut, Antwerpen, Belgium, 1997, pp. 99–109.

[70] F. Bassi, S. Rebay, High-order accurate discontinuous finite element solution of the 2D Euler equations, Journal of Computational Physics 138 (2) (1997) 251–285.

[71] F. Bassi, S. Rebay, A high-order accurate discontinuous finite element method for the numerical solution of the compressible Navier–Stokes equations, Journal of Computational Physics 131 (2) (1997) 267–279.

[72] J. Peraire, P.-O. Persson, The compact discontinuous Galerkin (CDG) method for elliptic problems, SIAM Journal on Scientific Computing 30 (4) (2008) 1806–1824.

[73] S. Brdar, A. Dedner, R. Klöfkorn, Compact and stable discontinuous Galerkin methods for convection-diffusion problems, SIAM Journal on Scientific Computing 34 (1) (2012) A263–A282.

[74] Y. Pan, P.-O. Persson, Agglomeration-based geometric multigrid solvers for compact discontinuous Galerkin discretizations on unstructured meshes, Journal of Computational Physics 449 (2022) 110775.

[75] B. Cockburn, J. Gopalakrishnan, R. Lazarov, Unified hybridization of discontinuous Galerkin, mixed, and continuous Galerkin methods for second order elliptic problems, SIAM Journal on Numerical Analysis 47 (2) (2009) 1319–1365.

[76] P. Fernandez, N. C. Nguyen, J. Peraire, The hybridized discontinuous Galerkin method for implicit large-eddy simulation of transitional turbulent flows, Journal of Computational Physics 336 (2017) 308–329.

[77] P. Fernández, Entropy-stable hybridized discontinuous Galerkin methods for large-eddy simulation of transitional and turbulent flows, Ph.D. thesis, Massachusetts Institute of Technology (2019).

[78] B. Cockburn, J. Guzmán, S.-C. Soon, H. K. Stolarski, An analysis of the embedded discontinuous Galerkin method for second-order elliptic problems, SIAM Journal on Numerical Analysis 47 (4) (2009) 2686–2707.

[79] N. C. Nguyen, J. Peraire, B. Cockburn, A class of embedded discontinuous Galerkin methods for computational fluid dynamics, Journal of Computational Physics 302 (2015) 674–692.

[80] N. V. Roberts, L. Demkowicz, R. Moser, A discontinuous Petrov–Galerkin methodology for adaptive solutions to the incompressible Navier–Stokes equations, Journal of Computational Physics 301 (2015) 456–483.

[81] T. Ellis, L. Demkowicz, J. Chan, Locally conservative discontinuous Petrov–Galerkin finite elements for fluid problems, Computers & Mathematics with Applications 68 (11) (2014) 1530–1549.

[82] T. E. Ellis, Space-time discontinuous Petrov-Galerkin finite elements for transient fluid mechanics, Ph.D. thesis, University of Texas at Austin (2016).

[83] W. Rachowicz, A. Zdunek, W. Cecot, A discontinuous Petrov-Galerkin method for compressible Navier-Stokes equations in three dimensions, Computers & Mathematics with Applications 102 (2021) 113–136.

[84] A. C. Huang, H. A. Carson, S. R. Allmaras, M. C. Galbraith, D. L. Darmofal, D. S. Kamenetskiy, A variational multiscale method with discontinuous subscales for output-based adaptation of aerodynamic flows, in: AIAA Scitech 2020 Forum, 2020, p. 1563.

[85] A. Huang, An adaptive variational multiscale method with discontinuous subscales for aerodynamic flows, Ph.D. thesis, Massachusetts Institute of Technology (2020).

[86] H. A. Carson, Provably convergent anisotropic output-based adaptation for continuous finite element discretizations, Ph.D. thesis, Massachusetts Institute of Technology (2020).

[87] T. J. Hughes, L. P. Franca, M. Mallet, A new finite element formulation for computational fluid dynamics: I. Symmetric forms of the compressible Euler and Navier-Stokes equations and the second law of thermodynamics, Computer Methods in Applied Mechanics and Engineering 54 (2) (1986) 223–234.

[88] A. Harten, On the symmetric form of systems of conservation laws with entropy, Journal of Computational Physics 49 (1983).

[89] E. Tadmor, Skew-selfadjoint form for systems of conservation laws, Journal of Mathematical Analysis and Applications 103 (2) (1984) 428–442.

[90] T. J. Barth, Numerical methods for gasdynamic systems on unstructured meshes, An Introduction to recent developments in theory and numerics for conservation laws. Springer Berlin Heidelberg (1999) 195–285.

[91] T. J. Barth, On discontinuous Galerkin approximations of Boltzmann moment systems with Levermore closure, Computer Methods in Applied Mechanics and Engineering 195 (25) (2006) 3311–3330.

[92] D. Williams, An entropy stable, hybridizable discontinuous Galerkin method for the compressible Navier-Stokes equations, Mathematics of Computation 87 (309) (2018) 95–121.

[93] D. M. Williams, An analysis of discontinuous Galerkin methods for the compressible Euler equations: entropy and L2 stability, Numerische Mathematik 141 (4) (2019) 1079–1120.

[94] J. Guzmán, C.-W. Shu, F. A. Sequeira, H-(div) conforming and DG methods for incompressible Euler's equations, IMA Journal of Numerical Analysis 37 (4) (2016) 1733–1771.

[95] G. J. Gassner, A kinetic energy preserving nodal discontinuous Galerkin spectral element method, International Journal for Numerical Methods in Fluids 76 (1) (2014) 28–50.

[96] S. Ortleb, Kinetic energy preserving DG schemes based on summation-by-parts operators on interior node distributions, PAMM 16 (1) (2016) 857–858.

[97] S. Ortleb, A kinetic energy preserving DG scheme based on Gauss–Legendre points, Journal of Scientific Computing 71 (2017) 1135–1168.

[98] D. Flad, G. Gassner, On the use of kinetic energy preserving DG-schemes for large eddy simulation, Journal of Computational Physics 350 (2017) 782–795.

[99] B. F. Klose, G. B. Jacobs, D. A. Kopriva, Assessing standard and kinetic energy conserving volume fluxes in discontinuous Galerkin formulations for marginally resolved Navier-Stokes flows, Computers & Fluids 205 (2020) 104557.

[100] A. Jameson, The construction of discretely conservative finite volume schemes that also globally conserve energy or entropy, Journal of Scientific Computing 34 (2) (2008) 152–187.

[101] A. Jameson, Formulation of kinetic energy preserving conservative schemes for gas dynamics and direct numerical simulation of one-dimensional viscous compressible flow in a shock tube using entropy and kinetic energy preserving schemes, Journal of Scientific Computing 34 (2008) 188–208.

[102] Y. Allaneau, A. Jameson, Kinetic energy conserving discontinuous galerkin scheme, in: 49th AIAA Aerospace Sciences Meeting including the New Horizons Forum and Aerospace Exposition, 2011, p. 198.

[103] P. W. Schroeder, G. Lube, Pressure-robust analysis of divergence-free and conforming FEM for evolutionary incompressible Navier–Stokes flows, Journal of Numerical Mathematics (2017).

[104] P. W. Schroeder, G. Lube, Divergence-free H(div)-FEM for time-dependent incompressible flows with applications to high Reynolds number vortex dynamics, Journal of Scientific Computing (2018) 1–29.

[105] J. Schütz, G. May, A hybrid mixed method for the compressible Navier–Stokes equations, Journal of Computational Physics 240 (2013) 58–75.

[106] J. Schütz, G. May, An adjoint consistency analysis for a class of hybrid mixed methods, IMA Journal of Numerical Analysis 34 (3) (2014) 1222–1239.

[107] J. R. Kweon, Optimal error estimate for a mixed finite element method for compressible Navier–Stokes system, Applied Numerical Mathematics 45 (2-3) (2003) 275–292.

[108] R. B. Kellogg, B. Liu, A finite element method for the compressible Stokes equations, SIAM Journal on Numerical Analysis 33 (2) (1996) 780–788.

[109] L. Zhang, Z. Chen, et al., A stabilized mixed finite element method for single-phase compressible flow, Journal of Applied Mathematics 2011 (2011).

[110] H. Egger, A robust conservative mixed finite element method for isentropic compressible flow on pipe networks, SIAM Journal on Scientific Computing 40 (1) (2018) A108–A129.

[111] Y.-H. Choi, C. L. Merkle, The application of preconditioning in viscous flows, Journal of Computational Physics 105 (2) (1993) 207–223.

[112] E. Turkel, Review of preconditioning methods for fluid dynamics, Applied Numerical Mathematics 12 (1-3) (1993) 257–284.

[113] D. Lee, B. Van Leer, Progress in local preconditioning of the Euler and Navier-Stokes equations, in: 11th Computational Fluid Dynamics Conference, 1993, p. 3328.

[114] J. M. Weiss, W. A. Smith, Preconditioning applied to variable and constant density flows, AIAA Journal 33 (11) (1995) 2050–2057.

[115] E. Turkel, Preconditioning techniques in computational fluid dynamics, Annual Review of Fluid Mechanics 31 (1) (1999) 385–416.

[116] H. Guillard, C. Viozat, On the behaviour of upwind schemes in the low Mach number limit, Computers & Fluids 28 (1) (1999) 63–86.

[117] A. Meister, Asymptotic based preconditioning technique for low Mach number flows, ZAMM-Journal of Applied Mathematics and Mechanics/Zeitschrift für Angewandte Mathematik und Mechanik: Applied Mathematics and Mechanics 83 (1) (2003) 3–25.

[118] P. Birken, A. Meister, Stability of preconditioned finite volume schemes at low Mach numbers, BIT Numerical Mathematics 45 (3) (2005) 463–480.

[119] P. Birken, A. Meister, On low Mach number preconditioning of finite volume schemes, PAMM: Proceedings in Applied Mathematics and Mechanics 5 (1) (2005) 759–760.

[120] P.-O. Persson, J. Peraire, Newton-GMRES preconditioning for discontinuous Galerkin discretizations of the Navier–Stokes equations, SIAM Journal on Scientific Computing 30 (6) (2008) 2709–2733.

[121] F. Bassi, C. De Bartolo, R. Hartmann, A. Nigro, A discontinuous Galerkin method for inviscid low Mach number flows, Journal of Computational Physics 228 (11) (2009) 3996–4011.

[122] A. Nigro, C. De Bartolo, R. Hartmann, F. Bassi, Discontinuous Galerkin solution of preconditioned Euler equations for very low Mach number flows, International Journal for Numerical Methods in Fluids 63 (4) (2010) 449–467.

[123] B. Klein, B. Müller, F. Kummer, M. Oberlack, A high-order discontinuous Galerkin solver for low Mach number flows, International Journal for Numerical Methods in Fluids 81 (8) (2016) 489–520.

[124] A. Gouasmi, S. M. Murman, K. Duraisamy, Entropy-stable schemes in the low-Mach-number regime: Flux-preconditioning, entropy breakdowns, and entropy transfers, Journal of Computational Physics 456 (2022) 111036.

[125] M. Galbraith, C. Ollivier-Gooch, 4th International Workshop on High-Order Methods. Laminar Joukowski airfoil at Re=1000, https://how4.cenaero.be/sites/how4.cenaero.be (2016).

[126] M. Galbraith, 5th International Workshop on High-Order Methods. Laminar Joukowski airfoil at Re=1000, https://how5.cenaero.be/sites/how5.cenaero.be (2018).

Vita

Education

B.S., Pennsylvania State University, Mechanical Engineering, May 2016

Professional Experience

Research Assistant, Pennsylvania State University, Advisor David M. Williams, August 2016–May 2024

Publications

1. Miller, Edward A., Williams, David M., Cave, Michael J., Thayalakhandan, Khandan. "A comparison of unsteady RANS and DES for simulating an axial compressor stage." Turbo Expo: Power for Land, Sea, and Air 84065, (2020).

2. Williams, David M., Frontin, Cory V., Miller, Edward A., Darmofal, David L. "A family of symmetric, optimized quadrature rules for pentatopes." Computers and Mathematics with Applications 80 (2020): 1405-1420.

3. Miller, Edward A., Chen, Xi, and Williams, David M. "Versatile mixed methods for non-isothermal incompressible flows." Computers and Mathematics with Applications 125 (2022): 150-175.

4. Miller, Edward A., and Williams, David M. "Versatile mixed methods for compressible flows." arXiv preprint arXiv:2402.18660 (2024).